Flexural fatigue of pre-cracked fibre reinforced concrete: experimental study and numerical modelling

DOCTORAL THESIS

Doctoral thesis by:

Débora Martinello Carlesso

Directed by:

Albert de la Fuente Antequera

Sergio Henrique Pialarissi Cavalaro

Doctoral programme:

Construction Engineering

Barcelona, December 2019

UNIVERSITAT POLITÈCNICA DE CATALUNYA
BARCELONATECH

Department of Civil and Environmental Engineering

ACKNOWLEDGEMENTS

I would like to thank Prof. Dr Albert de la Fuente for his support during the development of this doctoral thesis. Also, I would like to thank Prof. Dr Sergio Cavalaro and Prof. Dr Wellington Repette (Department of Civil Engineering, Federal University of Santa Catarina – UFSC) for the opportunity and assistance.

I would like to thank the Brazilian National Council for Scientific and Technological Development for the scholarship granted (233980/2014-8). This research was enabled by funds provided by the SAES project (BIA2016-78742-C2-1-R) of Spanish Ministerio de Economía, Industria y Competitividad. Likewise, this work was only possible thanks to the support from the Laboratory of Technology of Structures and Materials "Lluis Agulló" of Polytechnic University of Catalonia, specially to Carlos Hurtado.

Also, I would like to thank Leandro Nandi (Central de análises – EQA – UFSC) for his support and data analysis and Francisco Mena for the support and knowledge during the experimental campaign.

A special thanks to my mother Dirce Martinello, my father Orlando Carlesso, my “anjos peludos” and Jose Antonio Cruz. It wouldn’t have been possible without their efforts.

ABSTRACT

Fibre reinforced concrete (FRC) is recognized as a suitable material for structural applications. The number of national codes that have approved it is evidence. Structures where FRC is generally used can be subjected to fatigue loads and are expected to resist millions of cycles during their service life. Cyclic loads affect significantly the characteristics of materials and can cause fatigue failures. The most demanded cross-sections being cracked under tensile stresses due to direct loads or imposed deformations. Commonly, publications report fatigue behaviour of concrete under compression and are valid for uncracked sections. Imprecision in fatigue prescriptions are reflected through formulation of models that contemplate a probabilistic approach, or an introduction of high safety coefficients within construction codes. The aim of the present doctoral thesis is to perform a structural design oriented analysis on the behaviour of pre-cracked FRC subjected to flexural fatigue loads. FRC with steel and polypropylene fibre with different volume content were investigated by means of three-point bending tests, considering an initial crack width accepted in the service limit state. The mechanical behaviour of FRC was analysed in terms of applied load level, crack opening displacement (CMOD) and fatigue life. The residual flexural tensile strength was assessed after these tests to estimate the impact of the cycles in the remaining resistant capacity of the specimens. Results suggest that the mechanism of crack propagation is independent of the fibre type and content and the monotonic load-crack opening displacement curve might be used as deformation failure criterion for FRC under flexural fatigue loading. The conducted probabilistic approach allows predicting the fatigue strength of concrete reinforced with steel fibres. The findings postulate the proposal of a model to predict the evolution of the crack-opening and the remaining resistant capacity. An optimisation procedure is proposed to derive the model parameters using a limited number of initial load cycles. This doctoral thesis provides knowledge and data that may aid further research and contribute to the future development of design recommendations.

Keywords: fatigue; fibre reinforced concrete; pre-cracking; steel fibre; polypropylene fibre

RESUMEN

El hormigón reforzado con fibra (FRC) se reconoce como material adecuado para aplicaciones estructurales. El número de normativas que lo han aprobado es una evidencia. Las estructuras donde generalmente se usa FRC pueden estar sujetas a cargas de fatiga y se espera que resistan millones de ciclos durante su vida útil. Las cargas cíclicas afectan significativamente a las características de los materiales y pueden causar roturas por fatiga. Las secciones transversales más demandadas se fisuran bajo tensión debido a cargas directas o deformaciones impuestas. Comúnmente, las publicaciones informan del comportamiento de fatiga del hormigón bajo compresión y son válidas para secciones no fisuradas. La imprecisión de las recomendaciones se refleja a través de la formulación de modelos que contemplan un enfoque probabilístico o la introducción de altos coeficientes de seguridad dentro de los códigos de construcción. El objetivo de la presente tesis doctoral es realizar un análisis orientado al diseño estructural sobre el comportamiento del FRC pre-fisurado sometido a cargas de fatiga por flexión. Se investigaron FRC con fibras de acero y polipropileno con diferentes contenidos de fibras mediante pruebas de flexotracción a tres puntos, considerando un ancho de fisura inicial aceptado en el estado límite de servicio. El comportamiento mecánico del FRC se analizó en términos de nivel de carga aplicada, desplazamiento de apertura de fisura (CMOD) y vida útil bajo fatiga. La resistencia residual a flexotracción se evaluó después de los ciclos de fatiga para estimar el impacto de los ciclos en la capacidad de resistencia restante de las muestras. Los resultados sugieren que el mecanismo de propagación de fisuras es independiente del tipo y contenido de fibra y la curva monotónica de CMOD podría ser utilizada como criterio de falla de deformación para FRC bajo carga de fatiga por flexotracción. El enfoque probabilístico realizado permite predecir la resistencia a la fatiga del hormigón reforzado con fibras de acero. Los resultados postulan la propuesta de un modelo para predecir la evolución de la apertura de fisura y la capacidad resistente remanente. Se propone un procedimiento de optimización para derivar los parámetros del modelo utilizando un número limitado de ciclos de carga inicial. Esta tesis doctoral proporciona conocimiento y datos que pueden ayudar a futuras investigaciones y contribuir al desarrollo futuro de recomendaciones de diseño.

Palabras clave: fatiga; hormigón reforzado con fibra; pre-fisura; fibra de acero; fibra de polipropileno

LIST OF FIGURES

LIST OF TABLES

TABLE OF CONTENTS

1. INTRODUCTION

1.1. Introduction

Concrete is widely used in civil engineering construction and the number of structural applications in which fibre reinforced concrete (FRC) is used is continuously growing due to its improved properties, such as toughness, ductility and brittle performance (Huang et al. 2018; Di Prisco and Plizzari 2004). These enhanced properties are achieved by the added fibres into the cementitious matrix, which are able to act as stress transfer elements to control cracking, giving greater ductility, increasing post-cracking tensile strength, toughness, resistance to fatigue, impact and other properties of engineering.

The continuous research for better-quality performance FRC that meet the needs of the complexity of new structures, led to special curing technologies, lower water/cement ratio, fine and chemical admixtures, and high volume content of fibres. The most common of reinforcement is steel fibre reinforced concrete, which is known for enhanced post-cracking tensile resistance and the toughness (Singh 2017). Polypropylene fibres are other type of widely used fibre for structural applications in concrete, only behind steel fibres. The use of polypropylene fibres has increased significantly in recent years due to their contribution to post-cracking strength and their inert, non-corrosive nature. Another of these achieves is the high performance fibre reinforced concrete (HPFRC), which represents a class of cement

composites whose stress-strain response in tension undergoes strain hardening behaviour accompanied by multiple cracking and leading to a high failure strain capacity (Naaman and Reinhardt 2007).

During the last decades, FRC and HPFRC have been recognized as a promising material for several structural applications such as tunnel linings (de la Fuente et al. 2017), pavements (Belletti et al. 2008), highway or bridge decks overlays (Brugeaud 2013; Graybeal 2013), wind energy towers (Sritharan and Schmitz 2013; Tapsoba et al. 2017), offshore structures (Holmen 1984; Waagaard 1982) seismic resistant structures (Germano et al. 2016; Yoo and Banthia 2017) and for the repair of old structures and infrastructure facilities (Lappa et al. 2006). Most of these structures are constantly subjected to cyclic loads and are expected to resist millions of cycles during their service life. Cyclic load may cause structural fatigue failure and affect significantly the characteristics of materials (strength, stiffness, toughness, durability, etc.) even under service loads (Banjara and Ramanjaneyulu 2018; Zhang et al. 1999). Therefore, the performance of structures under fatigue loading has to be considered to ensure their safety.

Traditionally, the fatigue of concrete has been analysed through S-N curves, which correlate the applied fatigue load and the fatigue life of concrete, allowing to predict its fatigue performance. Numerous researches have been conducted to investigate the influence of different fatigue parameters such as stress level, stress ratio and loading frequency, as well as material properties, either in compression (Cachim et al. 2002; Huang et al. 2018; Medeiros et al. 2015; Sparks and Menzies 1973), tension (Kessler-Kramer et al. 2001; Makita and Brühwiler 2014; Plizzari et al. 1997; Reinhardt and Cornelissen 1984) or flexure (Bazant and Schell 1993; Chanvillard et al. 2004; Johnston and Zemp 1991; Naaman and Hammoud 1998; Parant et al. 2007; Sohel et al. 2018; Zhang et al. 1996), but just a few have done fatigue tests on pre-cracked concrete specimens (Chanvillard et al. 2004; Germano et al. 2016; González et al. 2018; Naaman and Hammoud 1998).

It is known that fatigue experiments display a considerable scatter (Fib 2013; Fib 2008) and are random in nature (Oh 1986), for this reason, probabilistic concepts procedures are often applied to insure the adequate evaluation of fatigue behaviour of concrete structures. This approach leads to either the formulation of models that take into account logical basis for analysing design uncertainties and evaluating the failure probability (Oh 1986) or introduce high safety coefficients to assess the uncertainty in fatigue prescriptions within construction codes (Tarifa et al. 2018).

Recommendations, technical reports and guidelines on fatigue in concrete are available, such as the State-of-art report from the American Federal Highway Administration (Russell and Graybeal 2013), the Japan Recommendations for Design and Construction of High Performance Fiber Reinforced Cement Composites (Japan Society of Civil Engineers 2008), the *fib* Model Code 2010 (Fib 2013), which covers concrete up to 120 MPa, the DNV GL standard (DNV GL AS 2016), the French standards (AFNOR 2016a; AFNOR 2016b), the Det Norske Veritas (DNV GL AS 2017), the ACI Considerations for Design of Concrete Structures Subjected to Fatigue Loading, the draft of the German guideline (Schmidt et al. 2017), the European Committee for Standardization (EN1992-1-1 2005) and the *fib* Model Code 2010 (Fib 2013). Most of these publications report the fatigue behaviour of concrete under compression, just a few account the flexural behaviour and there are no clear conclusions on flexural fatigue behaviour of pre-cracked cross-sections, that is, an established crack prior to fatigue loading.

The interest in industry increases about fibre reinforced concrete because it has proven to be more adequate to employ in some elements in comparison to normal concrete. Since cyclic load on cracked cross-sections can be crucial to some concrete structures where the fatigue phenomena can be a governing design parameter, it must be investigated not only in terms of applied fatigue load and respective fatigue life, but also how the deformation process until its failure affects the load-bearing capacity of the element. This doctoral thesis provides valuable information about the fatigue behaviour of FRC, contributing with a database containing representative flexural fatigue test results that can be used for generating specific models for fatigue consideration in structures to be introduced in future codes.

1.2. Motivations

The growing uses of FRC with structural applications, the lack of information, the importance of a correct evaluation and models to predict the fibre reinforced concrete performance subject to cyclic loads led to the delimitation of the main topics of this doctoral thesis. First, the material was defined considering the increasing demand of knowledge due to growing structural applications of steel and plastic fibre reinforced concrete. Then, a method that could assess the fatigue performance regardless fibre type, content or type of concrete was established. To define the method, the differences between fibre responses, the capability of FRC to work in a cracked condition and the post-crack strength was contemplated. For those specimens that did not fail, the post-fatigue strength “recover” and the influence of previous

cyclic loads were evaluated through quasi-static reload. After all, the experimental results were compared to the Model Code 2010 (Fib 2013) directives and design limitations could be proposed. Finally, constitutive equations and conceptual model were drawn allowing to predict the behaviour of the investigated FRC under flexural fatigue loading.

1.3. Objectives

Considering the motivations that led to the development of this doctoral thesis, objectives were drawn to respond issues. The main objective of this thesis is to perform a structural design oriented analysis and to recommend design limitations on the behaviour of pre-cracked FRC sections subjected to flexural fatigue loads, considering the points below:

- Analyse the main issues of the literature regarding FRC subjected to cyclic loading and perform an experimental campaign that could contribute with the database containing representative flexural fatigue test results of FRC;
- Study the influence of different fibre type and fibre volume in reinforced concretes subjected to similar fatigue evaluation in concern with each individual static response;
- Propose constitutive equations for the investigated concretes, design limitations comparing experimental findings and guideline directives and a conceptual model to predict the fatigue behaviour of FRC elements, regardless fibre type or content.

To attend the general objectives, several specific objectives are proposed according to the presented chapters of this thesis.

Steel fibre reinforced concrete

- Analyse the fatigue response of a steel fibre reinforced concrete (SFRC) and a high performance steel microfibre reinforced concrete (HPFRC) under flexure for different levels of applied dynamic load and their fatigue life;
- Analyse the development of the crack opening displacement under cyclic loads and the influence of different load levels;
- Compare the static response with the fatigue behaviour of the concretes and identify potential correlations to elucidate and predict the fatigue behaviour;

- Perform probabilistic methods for different probabilities of failure to clarify which method is more satisfactory to predict the fatigue life.

Plastic fibre reinforced concrete

- Assess the influence of the fibre type and fibre content on the mechanical response of three different polypropylene fibre reinforced concrete (PFRC) during dynamic loading;
- Characterize fibre properties through differential scanning calorimetry (DSC) and dynamic mechanical analysis (DMA);
- Analyse the effects of cyclic loads on the stiffness degradation considering for different fibre types and contents in terms of damage evolution and dissipated energy;
- Evaluate the influence of the fatigue cycles on the remaining residual flexural strength and correlate with the quasi-static behaviour;
- Propose a common regression equation that is able to predict the crack-opening displacement evolution of pre-cracked PFRC during fatigue cycles.

Fatigue conceptual model for crack evolution

- Describe the theoretical basis and requirements of design concepts guidelines of Model Code (Fib 2013);
- Suggest design instructions based on the experimental results in terms of crack opening and applied fatigue load;
- Propose a model of crack opening prediction under fatigue flexural loading and validate the results of the experimental campaign through the model.

1.4. Outline of the Thesis

The methodology to assess the fatigue performance was able to consider differences between steel and polypropylene fibre, different fibre content and type of concrete under cyclic loading. The fatigue response of all five investigated concretes showed similarities notwithstanding the inert properties of fibres. Consequently, a model was proposed to

conceptually interpreted and predict the FRC performance under cyclic load regardless fibre type and volume.

This thesis is divided into six chapters, shown in Figure 1. First, an introduction of the subject (chapter 1) and a state of the art (chapter 2) are presented to situate the reader about the knowledge developed and the points that need further research, focusing on pre-cracked FRC in view of the points stated before. Subsequently, the experimental campaign and results conducted on HPFRC and SFRC (chapter 3) and PFRC (chapter 4) are presented. From that, the developed conceptual model and proposed design limitations are shown in chapter 5. Finally, conclusions drawn from this doctoral thesis and future perspectives are shown in chapter 6.

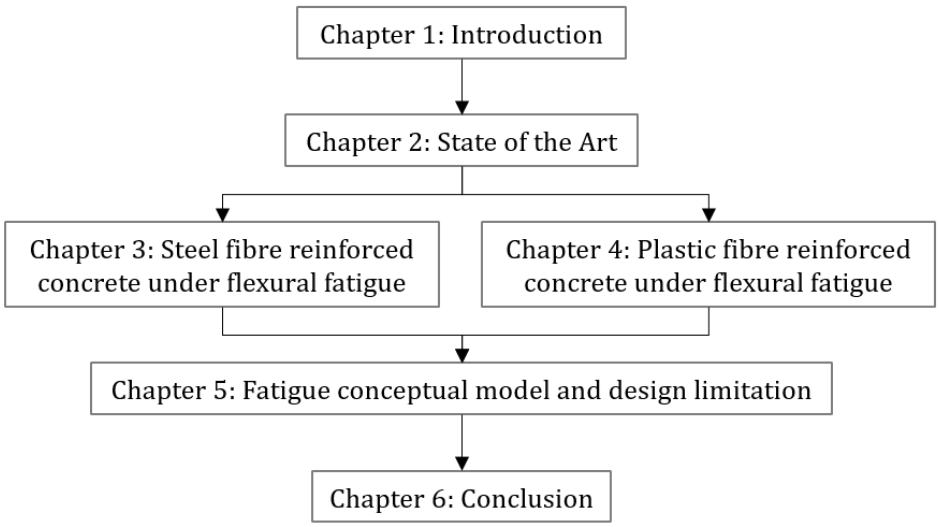

Figure 1 – Schematic representation of research strategy

2. STATE OF THE ART

2.1. Introduction

Fibre reinforced concrete (FRC) has been recognized as suitable material for many structural applications such as tunnel linings (de la Fuente et al. 2017), pavements (Belletti et al. 2008), highway or bridge decks overlays (Brugeaud 2013; Graybeal 2013), wind energy towers (Sritharan and Schmitz 2013; Tapsoba et al. 2017), offshore structures (Holmen 1984; Waagaard 1982) seismic resistant structures (Germano et al. 2016; Yoo and Banthia 2017) and for the repair of old structures and infrastructure facilities (Lappa et al. 2006). These structures can be subjected to cyclic loads and these are expected to resist millions of cycles during their service life. Also, the development of new concrete technologies, like high or ultra-high performance fibre reinforced concrete ((U)HPFRC) (the first considers concretes with characteristic strength from 50 to 120 MPa and the second characteristic strengths higher than 120 MPa (Fib 2013)), enable slender structures that can be more susceptible to cyclic loads (Lee and Barr 2004; Lohaus et al. 2012; Plizzari et al. 1997). Cyclic load may cause structural fatigue failure and affect significantly the characteristics of materials (strength, stiffness, toughness, durability, etc.) even under service loads (Banjara and Ramanjaneyulu 2018; Zhang et al. 1999). Therefore, the performance of structures under fatigue loading has to be considered to ensure their safety.

It is known that fatigue experiments display a considerable scatter (Fib 2013; Fib 2008). This characteristic leads to either the formulation of models that take into account logical basis for analysing design uncertainties to ensure adequate evaluation of failure probability (Oh 1986) or introduce high safety coefficients to assess imprecision in fatigue prescriptions within construction codes (Tarifa et al. 2018). Recommendations, technical reports and guidelines on fatigue in concrete are available mainly directed to the compressive fatigue behaviour of uncracked sections of concrete. Since cyclic load on cracked cross-sections can be crucial to structures, it must be investigated in terms of applied fatigue load, fatigue life, deformation development with correspondent load-bearing capacity.

This chapter presents theoretical concepts of fibre reinforced concrete and its fatigue behaviour, summarizing investigations performed in FRC cracked cross sections. The presented concepts delimited the investigation of this doctoral thesis.

2.2. Fibre reinforced concrete

The number of structural applications in which fibre reinforced concrete (FRC) is used is continuously growing due to its improved properties, such as toughness, ductility and brittle performance (Huang et al. 2018; Di Prisco and Plizzari 2004). These enhanced properties are achieved by the added fibres into the cementitious matrix, which are able to act as stress transfer elements to control cracking, giving greater ductility, increasing post-cracking tensile strength, toughness, resistance to fatigue, impact and other properties of engineering. This mechanism provides the basis for prediction of the stress-strain curve of the composite and its type of fracture. Such understanding and quantitative prediction support the development of composites of improved performance through modifications of fibre-matrix interactions, e.g. the bond to the matrix can be enhanced by mechanical anchorage or surface roughness (Bentur and Mindess 2007).

Currently, there is a wide range of fibres of different mechanical, physical and chemical properties made steel, glass, carbon, polypropylene, sisal, etc. each one designated for improving a desired property of the concrete, effectiveness and cost. The most common type used and investigated are steel fibres, although the use of polypropylene fibres has increased significantly in recent years. The post-cracking contribution provided by polypropylene fibres are particularly important for those cases in which variations in the mechanical properties depend on time are of paramount importance (e.g., sewerage buried pipelines (De La Fuente et

al. 2016; De La Fuente et al. 2013) and metro tunnels (Behfarnia and Behravan 2014; Conforti et al. 2017; de la Fuente et al. 2017)) due to their inert, non-corrosive nature. The mechanical characteristic are the principal properties that influence on the reinforcement ability of the fibres. Cifuentes et al. (2013) investigated the influence of the polypropylene fibres' properties on quasi-static fracture mechanisms of different compressive FRC strength classes proving that both ductility and crack control can be enhanced.

In brittle matrix composites the stress transfer effects are different in both pre- and post- cracking stage. Before cracking, the stress transfer mechanism is elastic and the longitudinal displacement of the fibre and the matrix are proportional. Transition from elastic stress transfer to frictional stress transfer occurs when the interfacial shear stresses due to loading surpass the fibre–matrix shear strength and debonding initiates governed by the fibre–matrix adhesional shear bond strength and on the tensile strength of the matrix. Large number of short fibres are responsible to bridge great number of microcracks in the composite and to avoid localized strain under load. Small number of long fibres can bridge discrete macrocracks at higher loads (Bentur and Mindess 2007).

Fibres volume (V_f) up to 1% do not particularly influence the compressive strength of the concrete, therefore recommendations for plain concrete are accepted (Fib 2013; di Prisco et al. 2009). The mechanical property that is mainly influenced by fibres is the residual post-cracking tensile strength, and that represents an important design parameter for FRC structures. Regulations and guidelines recommend FRC classification based on the post-crack tensile strength from bending tests.

2.2.1. Classification of FRC

Material classification of fibre reinforced concrete consider the post-cracking tensile strength response under bending tests. Depending on the increasing deformation or crack opening, the post-cracking strength can be distinguished by "hardening" or "softening". Strain-softening is a progressive loss in the strength capacity of the matrix after its rupture, related to a single crack opening. Strain-hardening is the increase in its strength capacity after the matrix rupture and it is associated to the formation of multiples cracks until it reaches the maximum post-crack stress. The response can be also categorised between two behaviours under flexure: deflection-softening where, after the matrix rupture, the resisted load of the composite is lower

than the peak load; and deflection-hardening, when the resisted load increases after the matrix rupture.

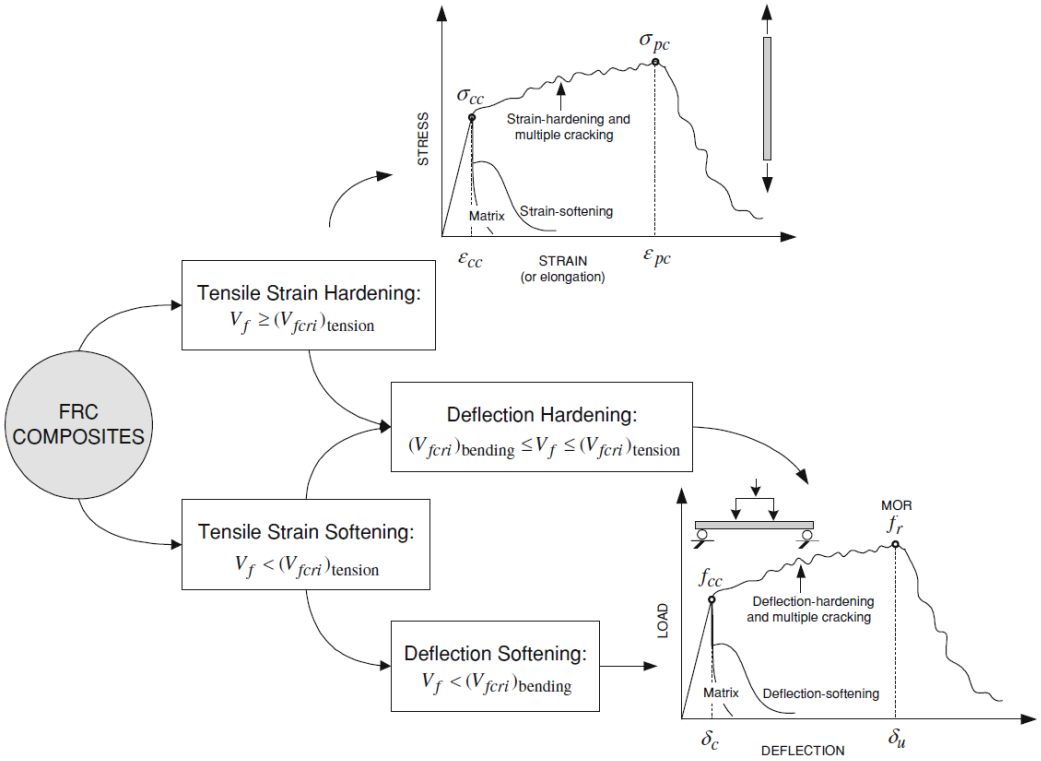

Figure 2 – Softening and hardening concepts for the classification of FRC (Naaman and Reinhardt 2007; di Prisco et al. 2009)

The most common method to characterize post-cracking behaviour of FRC is the three-point test on prismatic specimens. The four values of residual strength f_{R1}, f_{R2}, f_{R3}, f_{R4} corresponds to values of the crack mouth opening displacement (CMOD) of 0.5, 1.5, 2.5 and 3.5 mm, respectively. Two deformation values were adopted to characterize the FRC residual strength: f_{R1k} stands for SLS conditions, while f_{R3k} stands for ULS conditions. Model Code 2010 (Fib 2013) suggests a simplify classification: FRC strength class is specified using f_{R1k} to represent the strength interval and a letter (*a, b, c, d* or *e*) to represent the f_{R3k}/f_{R1k} ratio. The strength interval f_{R1k} is defined by using a number (1.0, 1.5, 2.0, 2.5, 3.0, 4.0, 4.5, 5.0, 6.0, 7.0, 8.0, … (MPa)) and the f_{R3k}/f_{R1k} ratio according to a particular range: *a* if $0.5 < f_{R3k}/f_{R1k} < 0.7$; *b* if $0.7 \leq f_{R3k}/f_{R1k} < 0.9$; *c* if $0.9 \leq f_{R3k}/f_{R1k} < 1.1$; *d* if $1.1 \leq f_{R3k}/f_{R1k} < 1.3$; and *e* if $f_{R3k}/f_{R1k} \geq 1.3$. In addition, Model Code 2010 (Fib 2013) establishes that if $f_{R1k}/f_{Lk} > 0.4$ and $f_{R3k}/f_{R1k} > 0.5$ are satisfied, fibre reinforcement can substitute conventional reinforcement and can be considered as a structural material.

2.3. Fatigue in fibre reinforced concrete

Fatigue is a process of progressive, permanent internal structural changes in the material subjected to repeated loading, attributed to the gradual growth of internal microcracks, resulting in an increase of irrecoverable strain and loss of mechanical properties (Lee and Barr 2004; Lenschow 1984). Each cycle is responsible for a crack increment until CMOD reaches a critical size exceeding the fracture toughness and CMOD grows rapidly and usually leads to structural failure. The corresponding fatigue strength of concrete depends on the applied stress range, structural detail geometry, material characteristics and on the environment (Nussbaumer et al. 2018).

Fatigue loading is categorised by range of number of cycles. Usually, low-cycle loading implicates in few load cycles at high stress levels and high-cycle loading in a large number of cycles at lower stress levels. Examples of structures by rage of number of cycles are shown in Table 1 (Isojeh 2017; Lee and Barr 2004).

Table 1 – Fatigue cycles spectrum with corresponding structures

Low-Cycle Fatigue ($0 – 10^3$ cycles)	High-Cycle Fatigue ($10^3 – 10^7$ cycles)	Super-High-Cycle Fatigue ($10^7 – 5 \times 10^8$ cycles)
Structures subjected to earthquakes Structures subjected to storm	Bridges Airport pavement Wind power plants Highway pavement Concrete railroad ties	Mass rapid transit structures Sea structures Machine foundations

Different methods have been proposed to predict the fatigue failure in concrete. The most frequent is by S-N curves, also known as Wöhler curve, which correlate various stress ranges (S) and the corresponding number of cycles to failure (N). Specimens are subjected to an upper and lower percentage of a determinate stress (usually, the static reference strength). The fatigue life is characterised by plotting the stress and the number of load cycles in logarithm scale. In addition, the effects of minimum stress in the loading cycle may be represented in so-called Goodman diagrams or Smith diagrams.

Another method is a strain-based which involves the deformation evolution at the upper load level plotted as a function of the number of cycles and is known as cyclic creep curve (Plizzari et al. 1997). These curves can be classified into three stages, representing three phases of cracking (illustrated in Figure 3). Phase I involves a large increase of deformation caused by

pre-existing microcracks. The secondary branch, or phase II, is characterized by a stable linear ascent and the slope denotes the crack increment per cycle (dCMOD/dn). Phase III is represented by the rapidly expand of the deformations at the end of the semi-stabilized curve until failure. The first stage represents, approximately, 10% of the total curve, the second stage approximately 80% and the third stage approximately the final 10% of the total curve (Fib 2008).

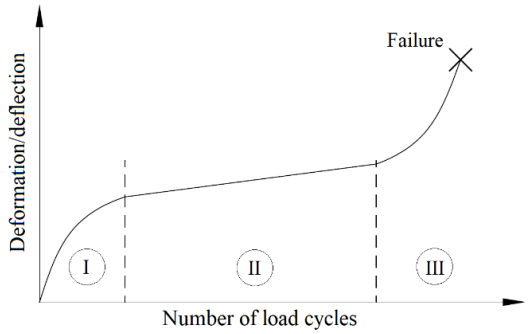

Figure 3 – Schematic representation of deformation with increasing number of load cycles

Also, a crack growth approach can be used and it adopts a crack growth equation such as the Paris' law which give the rate of growth of the fatigue crack correlated to a stress intensity factor as functions of crack depth, shape factor and stress range, shown in Eq. (2.1).

$$\frac{da}{dN} = C(\Delta K_{tip})^n \tag{2.1}$$

where a is the crack length, N the number of load cycles, ΔK_{tip} the crack tip stress intensity factor amplitude, and C and n are Paris constants that depend on the material, environment and stress ratio, where C is the value of *y-axis* intercept and n the slope of the curve. It has been shown that the Paris law coefficients are dependent on the material composition (Bazant and Schell 1993), thus explaining the differences in values of the Paris law coefficients reported by different authors (Kolluru et al. 2000).

Until now, there is no agreement if (fibre reinforced) concrete has an endurance limit to cyclic loads, this is, a maximum non-reversing load that can be sustained that concrete can endure without failure. Different endurance limits can be found in literature: 500,000 (Shen and Carpenter 2007), 1,000,000 (de Andrade Silva et al. 2010; Breña et al. 2005; Chanvillard et al. 2004; Farhat et al. 2007; Nanni 1991; Tarifa et al. 2015) or 2,000,000 (Arora and Singh 2016; Johnston and Zemp 1991; Ramakrishnan et al. 1989; Zhang and Tian 2011). However, Johnston and Zemp (1991) proposes that tests up to 10,000,000 cycles need to be carried out to confirm

whether or not the failure stress remains constant regardless of the number of loading cycles. Lee and Barr (2004) affirm that further experimental work beyond 1,000,000 cycles is required before drawing firm conclusions regarding an endurance limit. From the numerous reported findings, it is not possible to conclude if concrete has a fatigue limit. Delimiting an endurance limit would make fibre-reinforced cementitious composites much more attractive for many applications than plain concrete, which seems to have no fatigue strength (Lee and Barr 2004).

It has been observed that the addition of fibres can significantly improve the bending performance of concrete elements subjected to fatigue load (Germano et al. 2016; Johnston and Zemp 1991; Lee and Barr 2004; Morris and Garrett 1981; Spadea and Bencardino 1997). FRC structures can work in the cracked condition during their service life either because they were designed to do so or because accidental, transient or thermal-hygrometric actions induce cracks. The action of fibre bridging and fibre pull-out dissipates energy playing a dominant role in inhibiting crack growth. Improvements on the fatigue capacity of FRC depend on the fibre volume content, fibre type and geometry (Johnston and Zemp 1991; Naaman and Hammoud 1998). Fatigue crack growth is governed by three main factors: matrix crack growth specific to the matrix microstructure system, crack bridging by fibres and fatigue damage in the fibre and/or fibre-matrix interface (Li and Matsumoto 1998). The first microcracks formed during the preparation of the beams (prior to the cyclic loading test) create a damaged area where the tensile stresses cannot cross through the matrix and must be conducted by the fibres that bridge the cracked plane. During the application of the cyclic load, additional microcracks may develop in the fibre-matrix interface, increasing over cycles and may merge into macrocracks (Malek et al. 2018). The accumulated crack opening displacement is associated to the degradation of the fibre-matrix interface bond (Li and Matsumoto 1998; Müller and Mechtcherine 2017) and fatigue response of the fibre itself and eventually leading to noncompliance with service or limit state requirements (Banjara and Ramanjaneyulu 2018; Blasón et al. 2019; Zhang et al. 1999).

Numerous researches have been conducted to investigate the influence of different fatigue parameters such as stress level, stress ratio, loading frequency, and material properties, but just a few have done fatigue tests on pre-cracked concrete specimens. Most of recommendations, technical reports and guidelines on concrete under fatigue loading available report the fatigue behaviour under compression and just a few take into consideration the flexural tensile response. Nevertheless, reports dealing with flexural tensile fatigue are valid for uncracked sections while only a few give recommendations for post-cracking fatigue response.

Since before cracking the behaviour of FRC can be compared to plain concrete, the role of fibres in an element subjected to fatigue load should be evaluated in a post-cracking stage. Assumptions and conclusions from studies about SFRC cannot be directly generalised to plastic fibre reinforced concrete (PFRC) due to the significant differences between the properties of these fibres. High modulus fibre composites have superior fatigue resistance (Fib 2013).

The addition of fibre reinforcement has been found to have a dual effect on the cyclic behaviour of concrete. An optimum fibre content has been suggested by some authors (Germano et al. 2016; Johnston and Zemp 1991; Zhang et al. 1999). Higher fibre volume could increase the pore and initial microcrack density, resulting in strength decrease. Zhang and Stang (1998) reported an optimum fibre volume concentration of 1% by volume. Johnston and Zemp (1991) suggest that a fibre volume up to 1% improves fatigue life, while for 1.5% diminishes the fatigue performance. Germano et al. (2006) states that the optimized fibre content for fatigue performance was of 0.5 % of steel fibres, guarantying a higher number of cycles at failure with respect to 1.0 % of fibres.

The perception of damage evolution of a material provides a conceptual basis by which the degradation of the mechanical properties of concrete and the corresponding physical deformation can be correlated. After the damage localisation, the continuous damage accumulation controls the stress–strain behaviour in the damage zone (Mu et al. 2004). Considering pre-cracked specimens at the beginning of the fatigue test, damage localisation will be located so that only damage accumulation occurs. The internal propagation of the damage in the concrete leads to a decrease of the secant modulus, which may reach 60% of its initial value as the material approaches failure (Destrebecq 2013; Federation Internacionale du beton 2000). This condition may serve as a criterion for predicting the proximity to fatigue failure in concrete.

Since cyclic load in cracked cross sections can be a governing design parameter, this must be investigated in terms of both applied fatigue load and respective number of cycles and of damage accumulation process since crack widths and loading bearing capacity evolution until failure are affected. Validation of the structural safety should consider values of crack opening correspondent to the expected fatigue life of the element during its service life (González et al. 2018). The understanding of the fatigue damage propagation and the failure mechanism of concrete are the basis for the proposal of numerical models to estimate the loss of performance over the load cycles, which enable the prediction of the fatigue life in concrete

structures (González et al. 2018; Isojeh et al. 2017; Shah 1984; Xu et al. 2018) and should be particularly important in pre-cracked elements reinforced only with fibres.

2.3.1. Literature review of pre-cracked FRC

Table 2 shows the investigations in fatigue with steel and polypropylene fibre reinforced concrete. As summarised, the literature provides limited information about post-cracking and post-fatigue residual FRC response. The "fatigue numerical analysis" can be either constitutive equations or numerical models.

Chanvillard et al. (2004) investigated the three-point bending fatigue tests on an ultra-high performance fibre reinforced concrete (UHPFRC), the pre-crack width being 0.3 mm. Fatigue test was load-controlled, between 10% and 90% of the first crack load, which was approximately half of the ultimate flexural strength. Fatigue test was stopped at 1,200,000 cycles. No specimen failed under these conditions and little damage was observed. After fatigue testing, the specimens were subjected to static flexural load and there was no influence of preceding cyclic loading process on the ultimate strength of the specimens. An endurance limit at 1,000,000 cycles was estimated to be at about 54 % of the elastic limit strength.

Naaman and Hammoud (1998) carried out an experimental program on fatigue of HPFRC. Three different target load ranges were applied: maximum load of 70%, 80%, 90% of the ultimate flexural capacity, and minimum load was kept constant of 10%. The ultimate flexural capacity was obtained from the corresponding static test made with control specimens. The beams were pre-cracked prior cyclic loading with two to three visible cracks. The relation between maximum fatigue stress and number of cycles to failure suggested a fatigue endurance limit of 2,000,000 cycles of the order of 65% of ultimate load. The specimens that resisted the dynamic load were subjected to a static bending test up to failure. Results showed that preceding cyclic load may lead to an improvement in post-fatigue strength.

Table 2 – Research about the fatigue of FRC

Fibre type	Reference	Compressive load cycles	Tension load cycles	Flexural load cycles	Pre-cracked specimens	Post-fatigue residual behaviour	Fatigue numerical analyisis
Steel	(Medeiros et al. 2015)	x			x		
	(Cachim et al. 2002)	x				x	
	(Cangiano et al. 1996; Makita and Brühwiler 2014; Plizzari et al. 1997; Zhang et al. 2000)		x		x		
	(Johnston and Zemp 1991; Nanni 1991; Parant et al. 2007; Ramakrishnan et al. 1989)			x		x	
	(Banjara and Ramanjaneyulu 2018; Farhat et al. 2007; Ganesan et al. 2013; Goel et al. 2012a; Graeff et al. 2012; Lappa 2007; Singh et al. 2005; Singh and Kaushik 2003)			x			x
	(Germano et al. 2016)			x	x		
	(González et al. 2018)			x	x		x
	(Chanvillard et al. 2004; Naaman and Hammoud 1998)			x	x	x	
	(Carlesso et al. 2019)[1]			x	x	x	x
Plastic	(Xu et al. 2018)	x			x		x
	(Medeiros et al. 2015)	x			x		
	(de Alencar Monteiro et al. 2018)			x			
	(Bedi et al. 2014; Li et al. 2007; Mohamadi et al. 2013; Zhang and Tian 2011)			x			
	(Nagabhushanam et al. 1989; Ramakrishnan et al. 1989)			x		x	
	This thesis – chapter 4			x	x	x	x

[1] Carlesso et al. 2019 corresponds to the publication "Fatigue of cracked high performance fiber reinforced concrete subjected to bending" (doi: 10.1016/j.conbuildmat.2019.06.038) and partial results are presented in chapter 3 of this thesis.

Germano et al. (2016) studied the fatigue behaviour of FRC on notched beams under three point bending test. It was adopted two volume fractions of fibres (0.5 and 1.0 %) and three fatigue load levels: load amplitude was kept constant (50%) and cyclic load varied between 15 – 65%, 25 – 75% and 35 – 85% of the maximum applied load. The pre-crack was done considering a drop of 5% of the referred beam peak load. Dynamic cycles were imposed until the CMOD reached the equivalent width of the static curve bound failure. After that, it was monotonically loaded. Results showed that the fatigue deformations at failure match the monotonic stress–strain curves and these, in consequence, can be used to express fatigue failure. Crack opening range and crack opening increment per cycle are the two parameters that govern the fatigue life.

González et al. (2018) analysed the residual tensile strength of steel fibre reinforced concretes following cyclic flexural loading. Pre-crack was considered effective either if the applied load fell to 90% of the maximum load applied during the test or if vertical deflection of the specimen was over 0.125 mm. The maximum applied stress was 65% of its post-cracking flexural tensile strength, obtained in the earlier pre-cracking tests and the minimum applied stress was 5%. Weibull fitting was used to obtain the characteristic fatigue life, considered to be 2,260 cycles. Results showed that cyclic loads cause a progressive reduction in the stiffness of the specimens. The reduction is attributable to the cracking in the fibre-matrix interface, causing a reduction of fibre–concrete bond, which results in a reduction of the residual strength. The numerical models derived from these studies are generally based on regressions of the experimental results and could hardly be generalised to other conditions

Cangiano et al. (1996) investigated the fatigue behaviour of cracked normal and high strength concrete with steel and carbon fibres (0.38% by volume of both) were conducted on notched cylindrical specimens under direct tension and the response compared to the structural response measured in bending tests. Fatigue tests were under displacement control: after reaching the peak load, the load dropped to 85%, 90%, 95%, or 98% and unloaded, subsequently, subjected to a cyclic loading in the range of 25% to 75% of the maximum load. Results showed the fatigue failure matches the quasi-static envelope curve for both concretes.

Makita and Brühwiler (2014) investigated the tensile fatigue performance of ultra-high performance fibre reinforced concrete (3.0 vol.% content of 13 mm long steel fibre) up to a maximum of 10 million cycles to verify the occurrence of an endurance limit. Strains between 0.5 and 6 ‰ was imposed prior to starting the fatigue test. Results revealed that UHPFRC shows a fatigue endurance limit with respect to 10 million cycles at a stress levels of 0.6 in a strain-

hardening domain, S of 0.45 in the strain softening domain, and S od 0.7 in the elastic domain (specimens without previous load-crack). Tensile fatigue crack propagation was categorised by a smooth surface while final fracture led to rough surface. Large differences in local deformation suggest that variations in material properties may dictate the final fatigue performance by redistributing stress and deformation capacity. UHPFRC fatigue failure showed different fracture surface such as matrix spalling, fibre pull-out and abrasion of fibres with the matrix, due to fretting and grinding. Smooth areas showed rust-coloured powdery products due to tribocorrosion.

Zhang et al. (2000) studied the crack bridging in SFRC under deformation-controlled uniaxial fatigue tension with constant amplitude between maximum and minimum crack opening with straight and hooked-end steel fibres. Maximum crack widths were 0.05, 0.10, 0.20, 0.30, 0.40, and 0.50 mm and pre-crack was determined by the deformation corresponding to a loading-unloading test. Experimental results revealed that the bridging stress decreases with the number of load cycles, known as bridging degradation which is correlated to the crack width. Increase the elastic slippage of fibres during fatigue loading and, consequently faster bridging degradation was found in hooked-end fibres reinforced concrete compared to straight fibres, with the same maximum crack width and minimum load condition.

Xu et al. (2018) carried out an experimental investigation on the stress–strain behaviour and the damage mechanism of polypropylene fibre reinforced concrete (PFRC) under cyclic compression. A pre-load was applied following displacement-controlled load cycles with increasing displacement. Incorporation of polypropylene fibres displayed a positive effect on the cyclic behaviour of concrete, especially for the post-cracking branch by improving energy dissipation, compressive toughness and ultimate strain, which increased with increasing volume fraction of fibres.

Medeiros et al. (2015) analysed the influence of the loading frequency on the compressive fatigue behaviour of concrete reinforced with polypropylene (0.56% vol.) and steel (0.64% vol.) fibres. Four different loading frequencies, 4 Hz, 1 Hz, 1/4 Hz and 1/16 Hz, were employed. The maximum stress applied was 85% of its compressive strength and the stress ratio was kept constant as 0.3. A preload was applied with the rate of 100 kN/min until the corresponding mean stress was reached. Frequency of cyclic load seemed to affect the fatigue response: lower frequencies generated smaller fatigue life than high frequencies. However, fibres enhanced the fatigue life by improving fibre bridging and preventing the crack extension under cyclic loads.

Considering the different responses of the fibre reinforced in a pre- or post- cracked concrete, the fundamental role of the fibre reinforcement in the concrete system subjected to cyclic loads should be evaluated after the matrix crack. The literature review reveals a lack of knowledge not only on pre-cracked FRC under fatigue loads, but also of its post-fatigue behaviour and numerical models to predict the material performance. After analysing the available literature review on the fatigue response of FRC, it was possible to identify missing points, which delimited the experimental campaign of this thesis. Applying percentages of actual resisted load of each specimen instead of using mean results from flexural test, can help reducing the scatter, providing concise information. Wider ranges of applied cyclic load, controlled pre-crack widths, tests up to 2,000,000 cycles, post-fatigue behaviour and probabilistic approach should be taken into consideration aiming at generating design-oriented constitutive models. In this regard, the presented results urge to contribute with the database containing representative flexural fatigue test results, constitutive equations and a conceptual model of pre-cracked FRC.

2.4. Concluding remarks

The literature review has evidenced some of the main issues regarding the characterization and design of FRC. The most relevant conclusions that can be drawn from this analysis are presented as follows:

- Owing to the lack of experimental results and accepted models, codes and guidelines for the design of FRC structures are unclear on how to account for the fatigue in the design. This poses a potential hazard for users of FRC structures subjected to a significant number of load cycles;
- The limited studies on flexural fatigue on pre-cracked concrete reveals that a broader understanding of the overall behaviour is necessary. Applying percentages of actual resisted load of each specimen instead of using mean results from flexural test, can help reducing the scatter, providing concise information. Wider ranges of applied cyclic load, controlled pre-crack widths, tests up to 2,000,000 cycles, post-fatigue behaviour and probabilistic approach should be taken into consideration aiming at generating design-oriented constitutive models;

Considering the surge in FRC application with structural responsibility and the likelihood of finding elements with cracks in service, additional studies are needed to grasp the

implications of the flexural fatigue of pre-cracked FRC in terms of crack-opening evolution and residual flexural strength. Likewise, models are needed to predict the material performance in terms of the evolution of crack-opening and residual resistant capacity after the cycles.

3. FATIGUE OF CONVENTIONAL AND HIGH PERFORMANCE CONCRETE REINFORCED WITH STEEL FIBRE

3.1. Introduction

Traditionally, the fatigue of concrete has been analysed through S-N curves, which correlate the applied fatigue load and the fatigue life of concrete, allowing to predict its fatigue performance. It is known that fatigue experiments display a considerable scatter (Fib 2013; Fib 2008) and are random in nature (Oh 1986), for this reason, probabilistic concepts procedures are often applied to insure the adequate evaluation of fatigue behaviour of concrete structures. This approach leads to either the formulation of models that take into account logical basis for analysing design uncertainties and evaluating the failure probability (Oh 1986).

The limited studies on flexural fatigue on pre-cracked concrete reveals that a broader understanding of the overall behaviour is necessary. Applying percentages of actual resisted load of each specimen instead of using mean results from flexural test, can help reducing the scatter, providing concise information. Wider ranges of applied cyclic load, controlled pre-crack widths, tests up to 2,000,000 cycles, post-fatigue behaviour and probabilistic approach should be taken into consideration aiming at generating design-oriented constitutive models. This chapter presents results of an extensive experimental campaign on two types of steel fibre

reinforced concrete, allowing to predict the fatigue response of these materials, a comparison between their flexural static and fatigue behaviour and contributing with the database.

3.1.1. Objectives

The main objective of this chapter is to perform a structural design oriented analysis on the behaviour of pre-cracked steel fibre reinforced concrete sections subjected to flexural fatigue loads. For this purpose, several specific objectives are defined:

- Analyse the fatigue response of the two studied concrete under flexure for different levels of applied dynamic load and their fatigue life;
- Analyse the development of the crack opening displacement under cyclic loads and the influence of different load levels in the evolution;
- Compare the static with the fatigue response of the concretes and identify potential correlations to elucidate and predict the fatigue behaviour;
- Perform probabilistic methods for different probabilities of failure that are able to predict the fatigue life.

3.1.2. Outline of the chapter

This chapter on materials and experimental procedures adopted to characterize the response of concretes under a wide range of assessments. The experimental campaign was carried out at Laboratorio de Estructuras Luis Agulló at the Universidad Polictécnica de Cataluña – BarcelonaTech.

Two cementitious composites were produced: one high performance steel microfibre reinforced concrete, and one hooked-end steel fibre reinforced concrete. Both experimental and theoretical studies were conducted on the flexural fatigue behaviour of pre-cracked specimens. The experimental program was carried out on monotonic and cyclic three-point bending notched beam tests. Different load levels were applied with a constant amplitude ratio and the cyclic dynamic response was evaluated in terms of evolution of crack mouth opening displacement (CMOD) throughout fatigue cycles and the fatigue life. Specimens that survived the maximum prescribed number of cycles were re-loaded under quasi-static condition to study the influence of the cyclic loading on the mechanical performance. Thereafter, the cross section of samples was examined with 80-times magnifying glass.

3.2. Experimental procedures

3.2.1. Mix design, casting and curing procedures

High performance fibre reinforced concrete (HPFRC) specimens were cast with Portland cement CEM I-52R, a rounded shape fine siliceous aggregate, steel microfibre and a polycarboxylate based superplasticizer. An ultrafine calcium carbonate and a water-based amorphous nanosilica (nano-SiO_2) dispersion were used to achieve optimum packing, flowability and lower porosity. The effective water/cement ratio was 0.20. Steel fibre reinforced concrete (SFRC) were cast with Portland cement CEM I-52.5 R, limestone aggregate, hooked-end steel fibre and a sodium polycarboxylate ether-based superplasticizer admixture. The water/cement ratio was 0.40. Table 3 shows both concrete mix compositions.

Table 3 – Mix composition of HPFRC and SFRC

HPFRC		SFRC	
Materials (kg/m^3)	Mix proportion	Material (kg/m^3)	Mix proportion
Cement content	909	Cement content	390
Water	83	Water	156
Silica sand (0.3 – 0.7 mm)	1,103	Sand (0 – 4 mm)	1050
Calcium carbonate	100	Coarse aggregate (4 – 10 mm)	470
Nano-SiO_2	65	Coarse aggregate (10 – 20 mm)	250
Superplasticizer	64	Superplasticizer	4.8
Steel microfibre	150	Hooked-end steel fibre	50

Table 4 shows the geometrical and mechanical properties of both fibres. The volume fraction of steel microfibres in HPFRC corresponds to, approximately, 2.0% (150 kg of fibres per m^3 of concrete) and the volume fraction of fibres used in SFRC corresponds to 0.65% (50 kg of fibres per m^3 of concrete). Mixtures were chosen based on previous tests and respond to applications with structural responsibility, mainly oriented to precast concrete elements for wind towers, rail-track sleepers and industrial floors. Different type of fibres also allowed the comparison between the effect of the geometry in the overall response.

Table 4 – Geometrical and mechanical properties of both steel fibres

Characteristics	Steel microfibre		Hooked-end steel fibre	
Length (mm)	13		50	
Diameter (mm)	0.16		1.05	
Aspect ratio	82		48	
Tensile strength (MPa)	3,000		1,115	
Mod. of elasticity (GPa)	200		200	

First, all dry components were mixed together (cement, sand/aggregates and calcium carbonate). In the case of HPFRC, after mixing dry components, nanosilica, superplasticizer admixture and water were added and mixed for five minutes. Subsequently, fibres were added and the concrete mixed until the total mixing time reached 18 minutes. For SFRC, after mixing dry components, water and superplasticizer were added to the mixture and lastly, fibres were incorporated in the mixing machine, ensuring to be well-spread. After casting, specimens were left to cure at room temperature for 24 hours, covered with a thin plastic sheet; then, demoulded and stored in a humid chamber (approximately 20 °C, 95% – 100% relative humidity) until the day of the test. Beam specimens were notched at midspan. Static tests were performed at 28 days. Fatigue tests were performed between 30 to 120 days after cast. The flexural strength evolution in time for materials with low water/cement ratio is considered negligible within this timeframe (Lappa 2007).

3.2.2. Experimental procedures

3.2.2.1. Control tests

Mechanical tests were conducted in both HPFRC and SFRC for quality control and characterization of the behaviour. Compressive strength tests followed the Standard EN 12390-3:2009, under a constant rate of loading of 0.5 MPa/s. Elastic modulus was conducted in accordance with EN 12390-13:2014, with loading cycles up to 30% of the mean compressive strength value and measuring the corresponding strain by LVDT transducers. Static monotonic three-point bending test (3PBT) were carried out following the procedures of Standard EN 14651:2007 in an INSTRON hydraulic servo-controlled testing machine with MTS control. The capacity of the machine is 200 kN for static tests and 100 kN for dynamic tests. The crack mouth opening displacement (CMOD) was measured through a clip gauge placed on the notch at midspan. Figure 4 shows the test set-up. The beam size was chosen pondering a reduction of material and ease of handling.

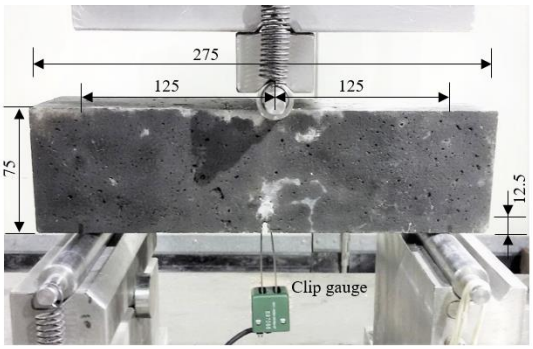

Figure 4 – Three-point bending test set-up in 75 x 75 x 275 mm beam

Barcelona test was also performed according to UNE 83515:2010 as an alternative method to evaluate the static behaviour of the fibres in the post-cracking stage. Compressive strength, elastic modulus and Barcelona test were performed in a universal compression testing machine IBERTEST MEH-3000 with maximum load capacity of 3,000 kN. Table 5 shows the dimensions of specimens by type of concrete and test. In addition, slump-flow test, density and air content in the fresh state were characterized for SFRC according to EN 12350-8:2011, EN 12350-6:2009 and EN 12350-7:2010, respectively.

Table 5 – Summary of tests

Test	Dimension (mm)	HPFRC	SFRC
Compressive strength	Φ 100 x 200	4	–
	Φ 150 x 300	–	4
Elastic modulus	Φ 100 x 200	3	–
	Φ 150 x 300	–	3
Barcelona test	Φ 150 x 150	4	4
Three-point bending test	75 x 75 x 275	3	3
Fatigue test	75 x 75 x 275	21	21

3.2.2.2. Dynamic tests

Twenty-one beams were tested under fatigue loading adopting the same configuration of the static 3PBT (Figure 4). The temperature and relative humidity of testing room were 25 °C and 65%-70%, respectively. Fatigue tests were load-controlled with the purpose of monitoring the crack opening in the beam and its fatigue life. As an attempt to reduce the scatter, it was performed a method of individual fatigue life evaluation of each beam. This experimental procedure also allowed to determine the contribution of the fibres in a cracked cross section.

First, a constant deformation rate (0.05 mm/min) was imposed up to a CMOD of 0.5 mm (considered as service limit value according to *fib* Model Code 2010 (Fib 2013)); therefore, the fatigue assessment would consider the fibre strength and the fibre-matrix interface within a pre-cracked cross section. Then, to each specimen, the corresponding load to a crack opening of 0.5 mm ($f_{R,1}$) was obtained in the first loading stage and set as maximum load ($P_{0.5mm}$). Once $P_{0.5mm}$ is known, percentages of $P_{0.5mm}$ were chosen as cycle's upper limit of applied load (P_{upp}) being 0.65, 0.70, 0.75, 0.80, 0.85, 0.90 and 1 (S). The lower load (P_{low}) was determined as a function of the load amplitude which was kept constant ($R = P_{low}/P_{upp} = 0.3$). The cyclic load follows a sinusoidal wave with a frequency of 6 Hz. The test was registered in terms of a complete cycle at each predetermined time interval. Parameters were chosen based on previous studies and on the literature (Ganesan et al. 2013; Goel et al. 2012b; Huang et al. 2018; Kim and Kim 1996; Lappa 2007).

Specimens that reached a maximum prescribed number of cycles were, then, tested monotonically (deformation rate of 0.2 mm/min) until its complete failure (CMOD > 4.0 mm). It was verified the maximum flexural load after the applied fatigue cycles ($P_{res,cycl}$). These specimens are named "run-out". Figure 5 illustrates the loading pattern.

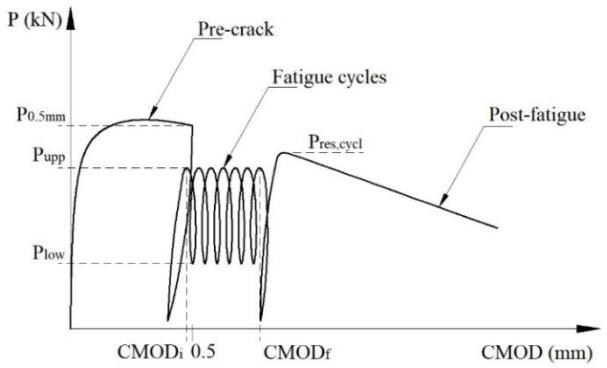

Figure 5 – Fatigue loading history of HPFRC and SFRC

Fatigue life of HPFRC and SFRC was evaluated in terms of total number of cycles until rupture of specimen (N) for each S. The progressive fatigue failure process and the evolution of cracks were recorded, as well as the crack opening at the upper load of first cycle ($CMOD_i$), the crack opening of the last registered cycle ($CMOD_f$) and the crack opening range ($\Delta CMOD = CMOD_f - CMOD_i$).

The adopted criterion of incrementing the individual load was an approach to observe the tendency in a S-N relationship. This criterion also evaluates each fatigue response whilst considering a homogeneous loading criterion for all tested beams and, therefore, reducing the

scatter sources. For the analysis, all specimens were included. This decision was made on the fact that specimens were pre-crack and the P_{upp} was an individual representation of each case. Omitting "run-out" specimens would underestimate the real number of cycles up to failure.

3.3. Results and discussion

3.3.1. Mechanical characterization

Average compressive strength and elastic modulus of HPRFC were 105.7 MPa (CV = 1.9%) and 44.0 GPa (CV = 1.8%), respectively. For SFRC, average compressive strength was 46.8 MPa (CV = 5.3%) and elastic modulus was 28.8 GPa (CV = 1.6%). Figure 6 shows the axil displacement vs load curves of the Barcelona test of HPFRC (a) and SFRC (b).

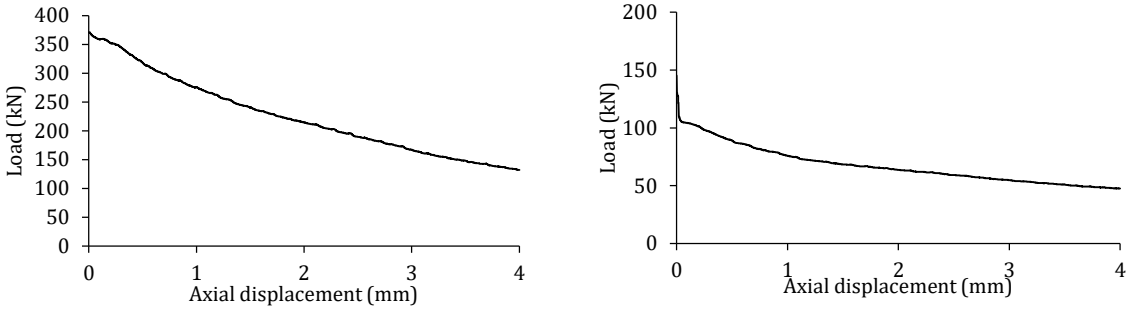

(a) (b)

Figure 6 – Results of Barcelona tests of HPFRC (a) and SFRC (b)

Barcelona test results suggest that these concretes have different cracking mechanisms. After reaching the peak load, HPFRC showed small and continuous load drops and many visible microcracks were formed (Figure 7(a)). In contrast, SFRC showed a sharp load drop of, approximately, 10% of the peak load and the development of a few macrocracks (Figure 7(b)). The different response is attributed mainly to the fibre content employed.

(a) (b)

Figure 7 – Specimens subjected to Barcelona test of HPFRC (a) and SFRC (b)

Average results of slump-flow test, density, air content and the corresponding coefficient of variation (CV) of SFRC are shown in Table 6. Elevated value of air content can be attributed to high quantity of superplasticizer admixture adopted.

Table 6 – Average results of fresh state properties of SFRC

Test	Result	CV
Slump-flow test	61 cm	10.4%
Density	2,140 kg/m3	1.7%
Air content	12.7%	24.9%

Table 7 presents the average residual flexural strengths (f_{R1m}, f_{R2m}, f_{R3m}, f_{R4m}, corresponding to CMOD values of 0.5, 1.5, 2.5 and 3.5 mm, respectively), limit of proportionality (f_{LOPm}), maximum post-crack strength (MOR) and the corresponding CMOD ($CMOD_{MOR}$) and the respective coefficient of variation (CV) measured in the 3PBT. The table also includes the characteristic values of f_{LOP} (f_{LOPk}) and of the flexural residual strengths f_{R1} (f_{R1k}) and f_{R3} (f_{R3k}) related respectively to the service and ultimate limit states (Fib 2013). Figure 8 shows the 3PBT response and the mean curve of HPFRC (a) and SFRC (b).

Table 7 – Average and characteristic 3PBT results and respective CV

	HPFRC	SFRC
f_{LOPm} (MPa)	19.64 (CV = 5.8%)	5.74 (CV = 8.4%)
MOR (MPa)	29.62 (CV = 5.1%)	6.67 (CV = 20.6%)
$CMOD_{MOR}$ (mm)	0.558 (CV = 14.2%)	0.806 (CV = 55.2%)
f_{R1m} (MPa)	29.30 (CV = 6.9%)	6.65 (CV = 18.7%)
f_{R2m} (MPa)	26.65 (CV = 2.8%)	6.12 (CV = 27.7%)
f_{R3m} (MPa)	21.48 (CV = 4.4%)	5.25 (CV = 18.5%)
f_{R4m} (MPa)	17.30 (CV = 2.6%)	4.42 (CV = 13.3%)
f_{LOPk} (MPa)	17.79	5.12
f_{R1k} (MPa)	26.08	4.61
f_{R3k} (MPa)	19.98	3.65
f_{R3k}/f_{R1k}	0.77b*	0.79b*
f_{R1k}/f_{LOPk}	1.47	0.9

* Classification of the post-cracking strength based on Model Code 2010 (Fib 2013)

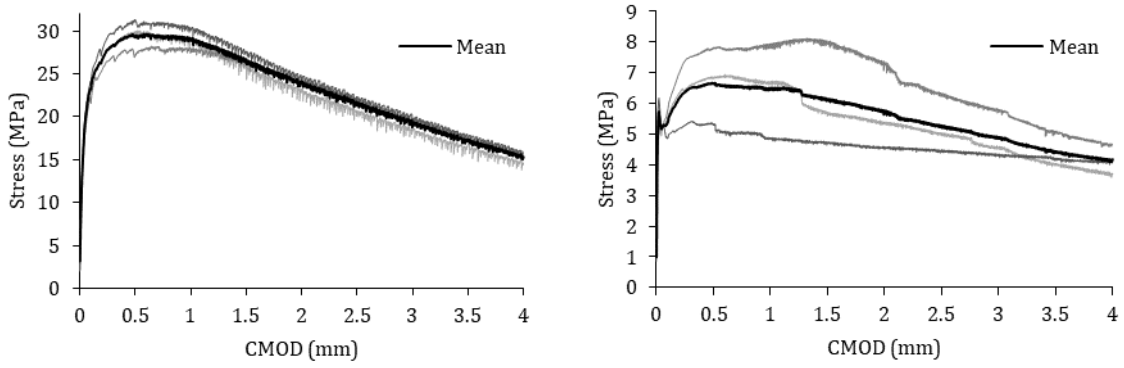

(a) (b)

Figure 8 – Results of 3PBT and the mean curve of HPFRC (a) and SFRC (b)

HPFRC and SFRC show similar flexural response. The performance presented by both concretes reveals a deflection-hardening behaviour with high energy absorption capacity. After the first discontinuity of the static flexural strength curve, corresponding to the matrix crack, the fibres are activated and the strength increases, surpassing the cracking load. In the case of SFRC, it shows a sudden drop of, approximately, 10% of f_{LOPm} immediately after cracking, indicating loss of stiffness. The ductile behaviour and strength recover are attributable to the contribution of the fibres and the adhesion forces between fibre and matrix (de Alencar Monteiro et al. 2018; Oh et al. 2007). The further reduction of the strength after a maximum is reached arises from the progressive fibre debonding and slipping in the cross section. Additionally, flexural response curves exhibited several load drops, representing fibre pull-out. Differences in load drops profile are attributable to steel fibre type and content.

According to the classification proposed by the Model Code 2010 (Fib 2013) for the post-cracking strength, both HPFRC and SFRC can be considered as a structural material and reach enough ductility to be used in the substitution of traditional reinforcement ($f_{R1k}/f_{LOPk} > 0.4$ and $f_{R3k}/f_{R1k} > 0.5$).

3.3.2. Fatigue test

Table 8 summarizes the results of fatigue test on HPFRC and Table 9 on SFRC pre-cracked specimens under bending.

Table 8 – Results from fatigue tests on HPFRC specimen

S	P0.5mm (kN)	Cycles (N)	CMODi (mm)	CMODf (mm)	ΔCMOD (mm)	Pres,cycl (kN)
0.65	20.41	2,000,000+	0.391	0.417	0.026	22.77
0.65	17.71	2,000,000+	0.402	0.495	0.093	18.45
0.65	17.50	2,000,000+	0.432	0.536	0.104	17.27
0.70	15.45	137,230	0.448	1.409	0.96	–
0.70	15.88	1,000,000+	–	–	–	16.45
0.70	16.33	1,581,049	0.432	1.804	1.372	–
0.70	13.06	2,000,000+	0.429	0.663	0.234	13.46
0.75	18.23	3,888	0.406	1.699	1.293	–
0.75	17.75	4,821	0.417	2.723	2.306	–
0.75	15.40	25,821	0.426	1.620	1.194	–
0.80	15.88	238	0.45	5.607	5.158	–
0.80	16.03	421	0.461	3.632	3.171	–
0.80	14.64	1,103	0.441	–	–	–
0.80	17.60	32,569	0.431	5.398	4.967	–
0.85	13.96	176	0.473	3.193	2.719	–
0.85	14.77	380	0.468	4.494	4.026	–
0.85	14.78	448	0.473	3.497	3.024	–
0.90	17.14	84	0.494	4.728	4.234	–
0.90	16.08	86	0.496	4.455	3.959	–
0.90	16.78	129	0.491	5.392	4.901	–
1	16.87	49	0.549	5.334	4.785	–

[+] "Run-out"

Table 9 – Results from fatigue tests on SFRC specimens

S	$P_{0.5mm}$ (kN)	Cycles (N)	$CMOD_i$ (mm)	$CMOD_f$ (mm)	ΔCMOD (mm)	$P_{res,cycl}$ (kN)	Fibre/cm²
0.65	4.23	655,576	0.412	2.498	2.086	–	0.30
0.65	3.87	865,807	0.427	3.298	2.871	–	0.17
0.65	4.03	1,232,969	0.413	–	–	–	0.18
0.65	4.67	1,250,000[+]	0.413	0.593	0.180	6.41	0.22
0.70	5.05	284,037	0.427	2.444	2.018	–	0.34
0.70	4.82	454,816	0.441	3.378	2.937	–	0.21
0.70	5.17	662,702	0.436	2.969	2.533	–	0.22
0.75	3.03	138,590	0.437	5.037	4.600	–	0.29
0.75	4.07	799,830	0.439	1.620	1.181	–	0.27
0.80	4.98	21,490	0.426	2.048	1.622	–	0.34
0.80	6.18	214,800	0.466	3.936	3.470	–	0.31
0.80	3.65	233,727	0.439	2.386	1.946	–	0.30
0.80	4.82	450,070	0.445	3.113	2.668	–	0.27
0.90	4.37	480	0.469	6.752	6.283	–	0.28
0.90	5.51	710	0.505	6.347	5.842	–	0.21
0.90	5.27	2,501	0.490	5.848	5.358	–	0.29
0.90	5.63	3,737	0.501	4.761	4.260	–	0.23
1	5.63	250	0.525	9.178	8.654	–	0.25
1	3.14	874	0.471	9.715	9.244	–	0.16
1	5.05	1,832	0.532	9.141	8.609	–	0.23
1	4.83	4,507	0.527	6.447	5.920	–	0.25

[+] "Run-out"

There were relevant differences when comparing numbers of cycle to failure of a series (same percentage of applied load) in both cases. Both concretes showed the same average value of coefficient of variation (72%) when analysing the number of cycles to failure of each S. For S of 0.70 series of HPFRC, the difference of number of cycles to failure varied from 137,230 cycles to 2,000,000 cycles (run-out), and for S of 0.80, N varied from 238 to 32,569 cycles. In the case of SFRC, specimens with applied load level of 0.65 diverged in failure after 655,576 cycles or withstood 1,2500,000 cycles with no visual sign of damage and for S equal to 1, N differed from 250 to 4,507 cycles. Considering the adopted fatigue evaluation (applied dynamic load as a percentage of a specific $P_{0.5mm}$), this variation suggests that the fatigue life on pre-cracked specimens is a result of probabilistic difference in fibre orientation and distribution, imprecision of test equipment and set-up and a reflection of the fatigue scatter itself.

3.3.2.1. Cyclic creep curves

Figure 9 shows the average cyclic creep curves for each load level, in terms of normalized cycles (the ratio between the actual number of cycle *n* and the number of cycles to failure *N*) versus the maximum CMOD ($CMOD_{upp}$) for HPFRC (a) and SFRC (b). Since all specimens were pre-cracked, only phase II and phase III can be observed. Cyclic creep curve of "run-out" specimens (S = 0.65 of HPFRC) were included for comparison.

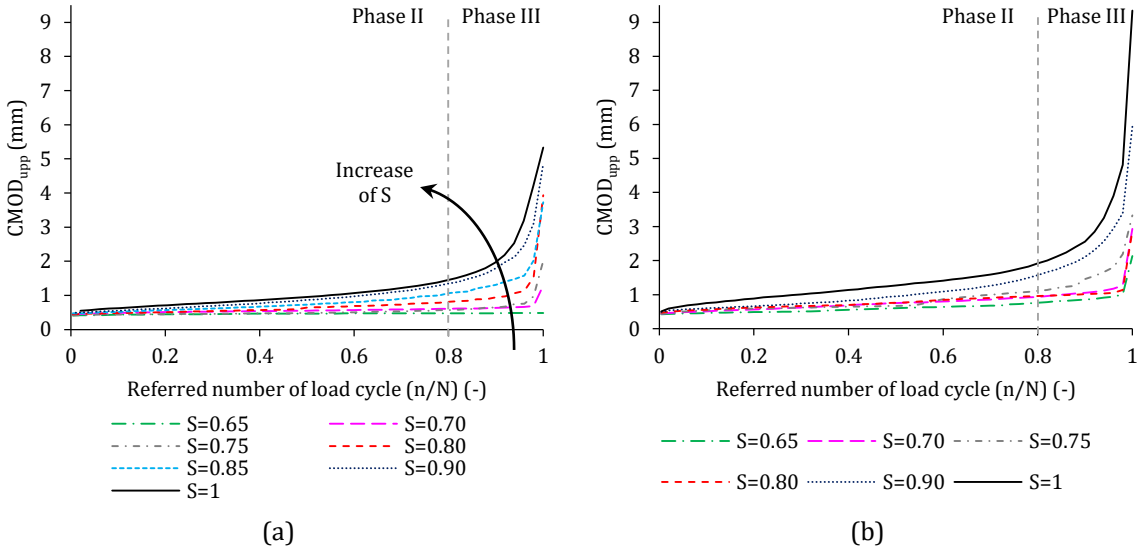

Figure 9 – Average cyclic creep curve for each load level of HPFRC (a) and SFRC (b)

In both cases, the evolution of CMOD seems to depend on the applied load level: as the load level increases, the slope of the crack increment per cycle becomes steeper and the crack

opening wider. Yet, SFRC displayed higher crack opening displacements most likely due to longer fibres bridging the fractured zone and load level of 0.80 curve showed an unexpected behaviour, similar to the CMOD of S = 0.70 set.

Considering the mean fatigue life of HPFRC set for each S (1,179,570 cycles (S = 0.70); 11,510 cycles (S = 0.75); 8,583 cycles (S = 0.80); 335 cycles (S = 0.85); 100 cycles (S = 0.90); 49 cycles (S = 1)) the slope of phase II becomes steeper with smaller fatigue life. On the other hand, SFRC mean fatigue life (1,001,088 cycles (S = 0.65); 467,185 cycles (S = 0.70); 469,210 cycles (S = 0.75); 230,022 cycles (S = 0.80); 1,857 cycles (S = 0.90); 1,866 cycles (S = 1)) between load level 0.70 – 0.75 and 0.90 – 1 showed the opposite behaviour. Since the values were similar, Welch's *t*-test (α equal to 0.05) was performed and revealed that there was not enough evidence to conclude that the differences between the means were statistically significant (p-value equal to 0.996 and 0.995 for S 0.70 – 0.75 and 0.90 – 1, respectively). Considering this statement, cyclic creep curves of HPFRC and SFRC suggest that the dCMOD/dn appears to be correlated to the N: lowering the secondary crack increment rate, the fatigue life increases.

Figure 10(a) and Figure 10(b) show a comparison between ΔCMOD and number of cycles to failure of HPFRC and SFRC, respectively. Higher load levels show greater upper crack opening at the last cycle ($CMOD_f$) and consequently crack opening range (ΔCMOD), than lower load cycles.

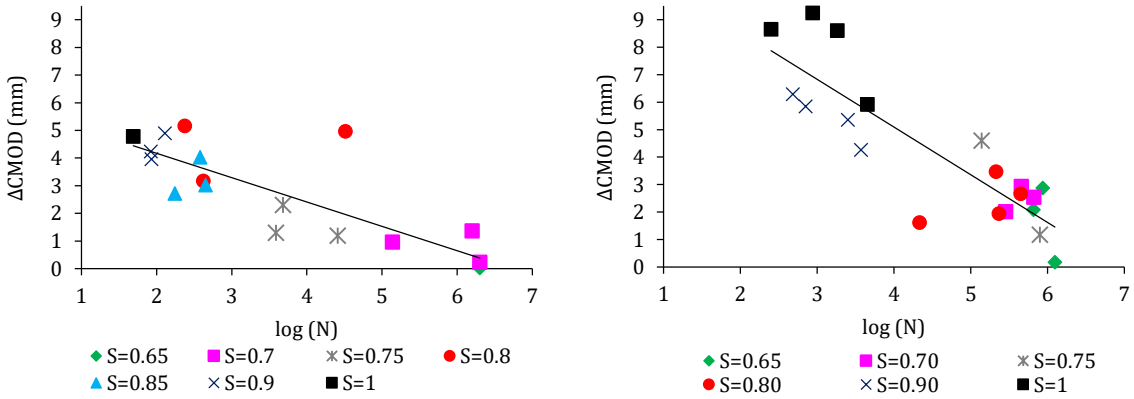

(a) (b)

Figure 10 – Relation between crack opening range and number of cycles to failure

At higher S, the bend at phase III (Figure 9) displays smoother shape. Also, the failure occurs at higher $CMOD_{upp}$. This suggests that lower load levels seem to produce a more brittle failure. This behaviour is in agreement with the observed in other investigations in fibre reinforced concrete in flexure (Korte et al. 2014; Lappa 2007; Leung et al. 2007; Li et al. 2018;

Suthiwarapirak et al. 2002). Higher S may failure through a continuous pull-out of the fibres, generating the ductile profile. Smaller load level can be responsible for the progressive weakening of the fibre-matrix interface through micro-cracks.

3.3.2.2. Failure point under cyclic loading

The concept of envelope curve provides a bound for the load and the crack opening values, establishing a failure criterion (Cachim et al. 2002; Kim and Kim 1996; Plizzari et al. 1997; Zhang et al. 1999). The envelope curve is generally approximated by the monotonic loading curve and it is schematically represented in Figure 11. Although most authors agree that the envelope curve concept is applicable for concrete subject to fatigue in compression, there is no agreement for fatigue in flexure or tension.

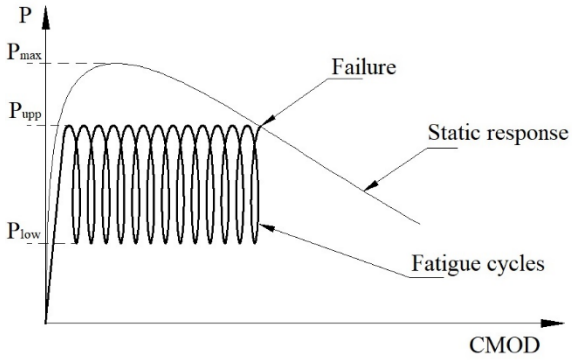

Figure 11 – Schematic representation of envelope curve in terms of applied load and CMOD

Throughout the fatigue loading test, the specimens could no longer reach the imposed load (P_{upp}), but the test did not stop until complete failure. This fact could have occurred because of the combined effect of high amount of fibres, high frequency of the cycles and intrinsic ductility of the steel. In order to associate the fatigue loading bearing capacity with the envelope curve, it was adopted as "fatigue limit of failure" a 2% loss of the reached load in a cycle when compared to P_{upp}. Figure 12(a) and Figure 12(b) exhibits the normalized load, taking as reference $P_{0.5mm}$, versus the point where this loss is first detected ($CMOD_e$) for each tested beam of HPFRC and SFRC, respectively. The corresponding static curve is plotted for comparison and a complete cyclic test response of a specimen (in the case of HPFRC subjected to S = 1 and N = 49, and of SFRC, S = 1 and N = 250) to illustrate the gradual loss of stiffness. The mean relative vertical distance between the fatigue limit of failure points and the static curve of each S is emphasized.

The frequency that the fatigue-data of a test was registered was set considering the expected fatigue life of each specimen, due to data storage limitations. For this reason, the point where HPFRC specimens tested at S of 0.70 and 0.75 start to lose stiffness where estimated considering the trend observed in the graph with sufficient precision that the imposed load (P_{upp}) would be achieved.

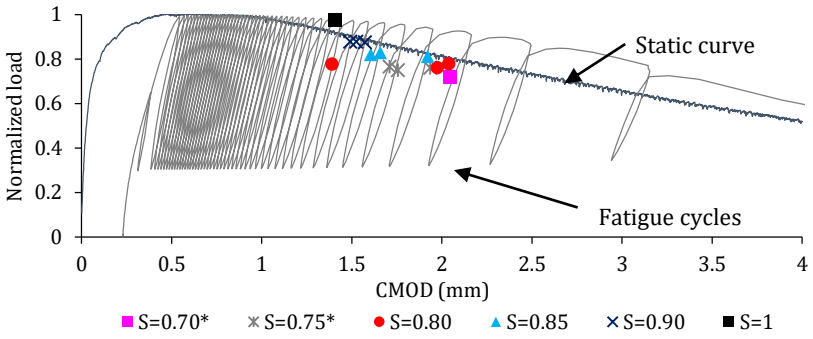

(a)

S	Mean vertical difference
0.70*	-8.1%
0.75*	-8.7%
0.80	-7.4%
0.85	-3.7%
0.95	-1.8%
1	+6.1%

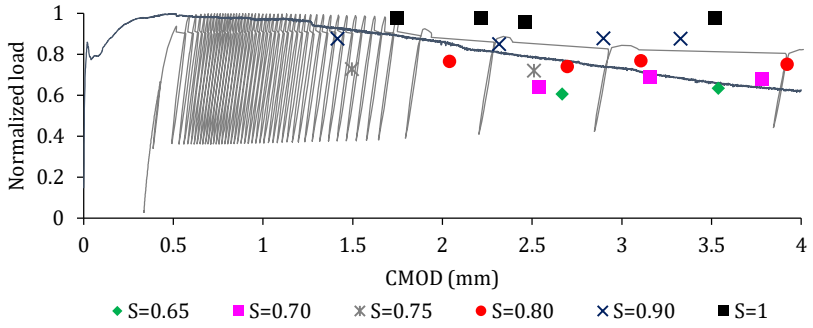

(b)

S	Mean vertical difference
0.65	-9.3%
0.70	-3.8%
0.75	-13.0%
0.80	+1.6%
0.90	+8.2%
1	+18.3%

Figure 12 – Failure points of fatigue test, CMOD evolution, monotonic response in terms of normalized load and CMOD; and the mean vertical difference between the static curve and failure points of HPFRC (a) and SFRC (b) (*stands for estimated points)

Good agreement was found between the bearing capacity of specimens and the static curve of HPFRC, taking into account the typical dispersion. On the hand, SFRC failure points during fatigue test exhibited high dispersion when compared to the monotonic curve. The higher dispersion can be a consequence of the lower number of fibres present in the cross section bridging the damage zone and, consequently, minor variations in fibre orientation and distribution can have great influence in the overall behaviour.

Figure 13(a) and Figure 14(a) illustrate a comparison between the cyclic creep curve and Figure 13(b) and Figure 14(b) the correspondent CMOD versus load curve with switched axis to facilitate the interpretation of results of a HPFRC specimen subjected to S of 0.90 and N of 129 cycles and a SFRC specimen subjected to S of 0.90 and N of 710 cycles, respectively.

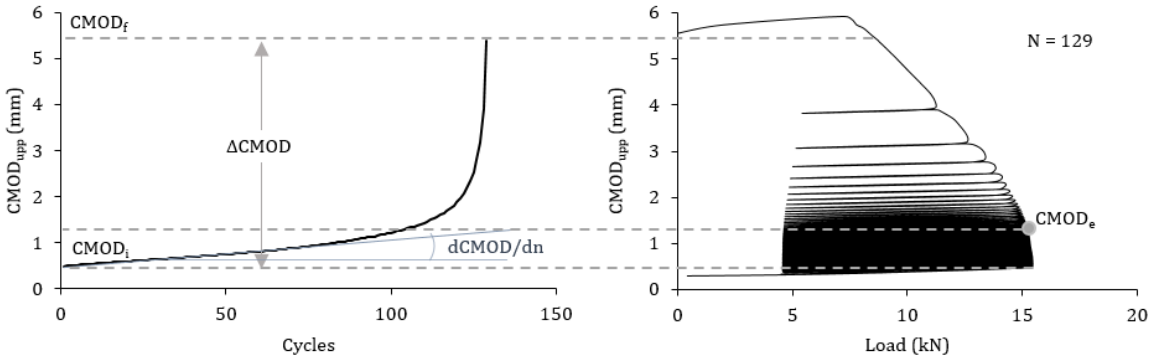

(a) (b)

Figure 13 – Comparison between diagrams of cyclic creep curve (a) and CMOD vs load curve (b) of a HPFRC specimen

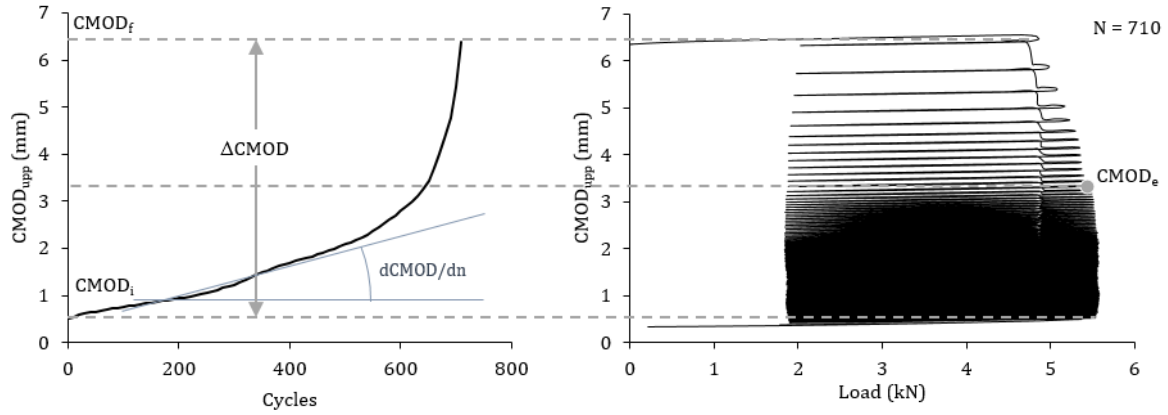

(a) (b)

Figure 14 – Comparison between diagrams of cyclic creep curve (a) and CMOD vs load curve (b) of a SFRC specimen

Initially, the dCMOD/dn (slope of the CMOD-n relationship) is nearly constant and corresponds to the crack opening displacement ratio before reaching the envelope curve ($CMOD_e$, point highlighted in the $CMOD_{upp}$-load curve). The dynamic cycles induce progressive damage in the cross section, causing growth of the CMOD and loss of load bearing capacity. Once the load reaches the envelope curve, the damage process is accelerated until failure ($CMOD_f$). The load at failure is proportionally higher than the applied initial load regarding the distribution of the section.

The envelope curve also suggests that the $CMOD_e$ depends predominantly on the upper load level (P_{upp}). The lower load level (P_{low}) dictates the amplitude ($P_{upp} - P_{low}$), which is strongly related to the number of cycles to failure. Higher amplitude indicates a higher increment per cycle resulting in a smaller number of cycles to failure (Germano et al. 2016; Kolluru et al. 2000).

Analysing the response, the envelope curve for the HPFRC can be approximated to the static monotonic curve and might be used as a deformation failure criterion for HPFRC under flexural fatigue loading. For a given P_{upp} and constant amplitude loading, the $CMOD_e$ can be predicted. Considering the subsequent behaviour, the continuous loss of stiffness in terms of evolution of CMOD, for the majority of the cases studied, seemed to proportionally respect the static curve.

3.3.2.3. Fatigue life

The most common way to evaluate the fatigue behaviour of concrete is the number of load cycle to failure. The results are shown by plotting the relative load level (S) versus the logarithm of the number of cycles to failure (N). This curve is known as S–N curve, or Wöhler curve and from that, it can be obtained the fatigue strength. Figure 15(a) and Figure 15(b) show the number of cycles to failure and the corresponding regression coefficient of determination (R^2) of HPFRC and SFRC, respectively.

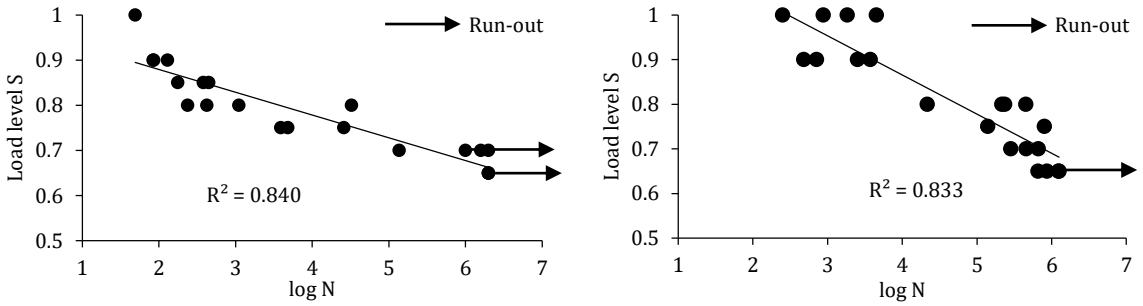

Figure 15 – Load level vs logarithm of cycles curve for HPFRC (a) and SFRC (b)

The corresponding S–N equation which can be used for prediction purposes of pre-cracked specimens of HPFRC or SFRC considered within the experimental program is given by Eq. (3.1) and Eq. (3.2), respectively.

$$S = 0.9801 - 0.0504\, log\, N \quad (3.1)$$

$$S = 1.2168 - 0.0878\, log\, N \quad (3.2)$$

It is still not clear if concrete presents a fatigue limit, but it generally defined as maximum flexural fatigue load at which the beam can withstand 2,000,000 cycles of nonreversed fatigue loading (Johnston and Zemp 1991; Naaman and Hammoud 1998; Ramakrishnan et al. 1989). Through the presented regression, both HPFRC and SFRC pre-

cracked specimens seem to exhibit a fatigue endurance limit of 2,000,000 cycle of the order of 0.66 of $P_{0.5mm}$.

3.3.2.4. Post-fatigue analysis

Specimens that survived the maximum prescribed number of cycles were monotonically reloaded to find the post-fatigue residual strength, respecting the same configurations of the flexural test. Considering the results presented in Table 8, Figure 16 shows the pre-crack loading, the first and the last cycle of the fatigue test, and the post-fatigue load for the four HPFRC specimens that reached 2,000,000 cycles.

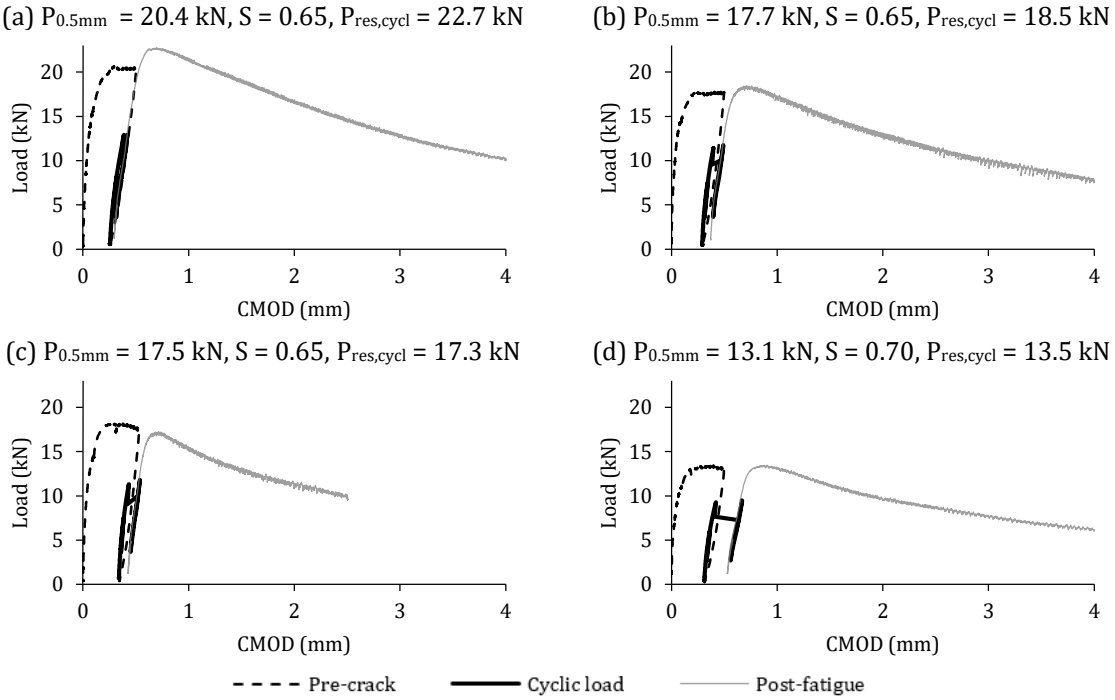

Figure 16 – Post-fatigue behaviour of run-out specimens

Observing the overall behaviour of the specimens, as cycles induce damage, they affect the crack opening, conducting to a displacement of the post-fatigue curve. However, the induced damage does not seem to affect the post-fatigue load bearing capacity, as the post-fatigue curve tends to follow the shape expected for a static loading. In most of the cases, the maximum load of the post-fatigue peak ($P_{res,cycl}$) was higher than $P_{0.5mm}$: the average value of $P_{res,cycl}$ was around 4% higher than $P_{0.5mm}$. According to other studies (Chanvillard et al. 2004; Naaman and Hammoud 1998; Parant et al. 2007; Ramakrishnan et al. 2014), when FRC is subjected to a

fatigue loading below the endurance limit value, there is an increase in the potential flexural strength.

It seems to have a correlation between the load at $P_{0.5mm}$, $CMOD_f$, and, consequently, ΔCMOD. Figure 16 (a), (b) and (c) shows samples subject to the same load level (0.65). Specimens with higher strength ($P_{0.5mm}$) show smaller crack opening range (ΔCMOD). The beam subjected to S of 0.70 (Figure 16 (d)) appears to follow this assumption.

In the case of SFRC, it was possible to manually count the fibres in the cross section after failure. Figure 17 shows the relationship between the number of fibres in the cross-section and strength at CMOD of 0.5mm ($F_{CMOD\ 0.5mm}$) and the respective R^2.

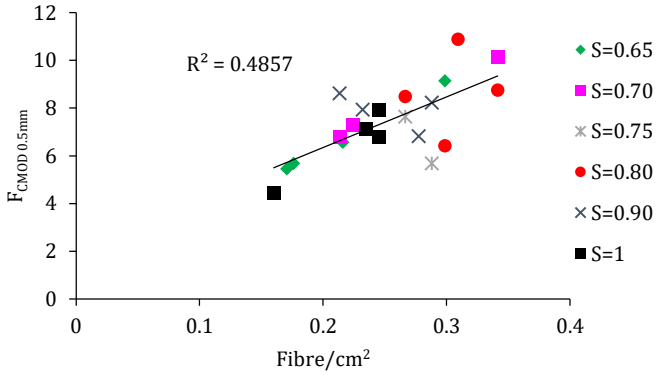

Figure 17 – Relation between number of fibres in the cross section and strength at CMOD of 0.5 mm

The flexural strength increases with the more number of fibres bridging the damaged zone (Pająk and Ponikiewski 2013) hence, the linear regression supports the high dispersion found within the SFRC results.

Lastly, the cross section of specimens subjected to different S were examined with 80-times magnifying glass. In all HPFRC cases, steel microfibre did not break (Figure 18), suggesting that fatigue failure of HPFRC occurs through a continuous fibre pull-out (Figure 18(c)) rather than a fatigue failure of the fibres due to their high-strength (3,000 N/mm²). The fatigue failure in HPFRC specimens is attributable to damage at the matrix-fibre contact interface that progressively reduces the anchorage capacity.

(a) (b) (c)

Figure 18 – Steel microfibres in the HPFRC cementitious matrix: (a) cross section of failure; (b) fibre profile; (c) identification of cavities of fibre pull-out

Contrastingly, fatigue failure in SFRC specimens suggest two failure modes: one case was macrofibres that did not break but showed deformed section (Figure 19(a)) , probably due to fibre pull-out (Figure 19(b)) since the end was flatten and indicates fibre-matrix interface damage. The other mode was fibres with sharped tip suggesting rupture of section (Figure 19(c)).

(a) (b) (c)

Figure 19 – Steel macrofibres of SFRC: (a) cross section of failure; (b) fibre profile and pull-out surface; (c) different fibres' sections

3.3.3. Probabilistic approach

Fatigue test data are normally presented as S–N curves. The need of guaranteeing the target structural reliability level fixed when considering the limit state safety format (Standard 2008) in a substantial scatter system, requires a probabilistic approach to ensure a consistent prediction of fatigue life (Do et al. 1993).

To estimate the probability of fatigue failure (P_f) of both investigated concretes, two different approaches were adopted. Frequently, the logarithmic-normal (lognormal)

distribution function is employed because of the mathematical convenience. However, the hazard function of the lognormal distribution decreases with increasing life (Freudenthal and Gumbel 1953). This violates the physical phenomenon of progressive deterioration of materials resulting from the fatigue process. Because of it, the Weibull distribution is utilized for the statistical description of fatigue data. The other approach used to describe the S–N–P_f relationship is by the mathematical model proposed by McCall (McCall 1958) and slightly modified by Singh et al. (Singh et al. 2005). The McCall model was used successfully to predict the fatigue life of various types of concretes (Do et al. 1993; Goel et al. 2012a; Graeff et al. 2012; McCall 1958; Singh et al. 2006). Lastly, the Wöhler curve is compared with the Weibull distribution and the McCall model.

3.3.3.1. Weibull distribution

The cumulative distribution function (C.D.F.) $F_N(n)$ for the Weibull probability law may be expressed according to Eq. (3.3).

$$F_N(n) = 1 - exp\left[\left(\frac{n}{u}\right)^{\alpha}\right] \tag{3.3}$$

in which n is the specific value of the random variable N; α is shape parameter or Weibull slope; and u is the scale parameter or characteristic life.

First, a graphical method was employed to verify if the fatigue-life data of the two concretes can be modelled by the two-parameter Weibull distribution. Subsequently, three different methods were used to estimate the parameters of the distribution, α and u. These methods are the graphical method, method of moments and method of maximum likelihood.

Graphical method of analysis

Eq. (3.4) express the survivorship function $L_N(n)$ of the two-parameter Weibull distribution (Mohammadi and Kaushik 2005; Oh 1986; Singh and Kaushik 2001).

$$L_N(n) = exp\left[-\left(\frac{n}{u}\right)^{\alpha}\right] \tag{3.4}$$

Taking the logarithm twice on both sides of Eq. (3.4), gives Eq. (3.5):

$$ln\left[ln\left(\frac{1}{L_N}\right)\right] = \alpha\, ln(n) - \alpha\, ln(u) \tag{3.5}$$

Eq. (3.5) represents a linear relationship between *ln[ln(1/L_N)]* and *ln(N).* To obtain a graph from Eq. (3.4), the fatigue-life data corresponding to each load level S was arranged in ascending order of cycles to failure. The empirical survivorship function L_N for each fatigue-life data is obtained from Eq. (3.6).

$$L_N = 1 - \frac{i}{k+1} \tag{3.6}$$

where *i* denotes the failure order number and *k* represents the number of data points.

There was a large variability in the fatigue-life data at the studied load levels and no definite trend was observed, indicating that the load levels selected for testing were probably too close together (Singh and Kaushik 2000). This inconveniency was mitigated by using the average value of the load levels 0.75 and 0.80 (0.78) and 0.90 and 1 (0.93) for HPFRC and the average between 0.70, 0.75 and 0.80 (0.76) and 0.9 and 1 (0.95) for SFRC (Figure 20(a) and Figure 20(b), respectively). The approximate straight-line plot indicates that the two-parameter Weibull distribution is a reasonable assumption for the statistical distribution of the fatigue life. The parameters α and *u* for the load levels were estimated from the regression analysis. Results are presented in Table 10.

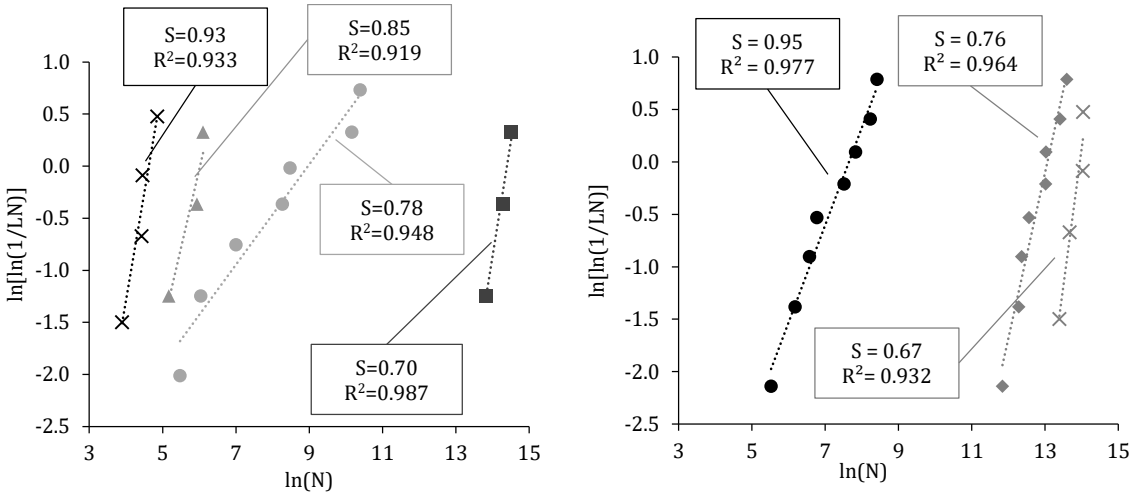

(a) (b)

Figure 20 – Determination of coefficients of the fatigue equation

Parameters from method of moments

The estimation of parameters of the Weibull distribution by the method of moments requires sample moments, such as sample mean and sample variance. The moments of a two-parameter Weibull distribution can be expressed by Eq. (3.7) and (3.8).

$$E(N) = u\Gamma\left(1 + \frac{1}{\alpha}\right) \tag{3.7}$$

$$E(N^2) = u^2\Gamma\left(1 + \frac{2}{\alpha}\right) \tag{3.8}$$

where E denotes expectation. Since the mean $\mu = E(N)$ and the variance $\sigma = E(N^2) - \mu^2$, Eq. (3.7) and (3.8) can be expressed by Eq. (3.9) (Oh 1986; Singh and Kaushik 2000; Tanaka and Ichikawa 1983).

$$CV^2 = \left(\frac{\sigma}{\mu}\right)^2 = \frac{\Gamma(1+{}^2/_\alpha)}{\Gamma^2(1+{}^1/_\alpha)} - 1 \tag{3.9}$$

where μ is the sample mean of the fatigue-life data at a given load level; CV (= σ/μ, σ is standard deviation of sample) is the coefficient of variation of the data. Eq. (3.9) can be approximately reduced to Eq. (3.10) (Oh 1986; Singh and Kaushik 2000).

$$\alpha = (CV)^{-1.08} \tag{3.10}$$

The characteristic life u can be estimated from Eq. (3.10) by substituting μ for $E(n)$, giving Eq. (3.11) (Singh and Kaushik 2000).

$$u = \frac{\mu}{\Gamma\left(\frac{1}{\alpha}+1\right)} \tag{3.11}$$

Equation (3.10) and (3.11) can be used to estimate the values of the parameters of the Weibull distribution. Results are presented in Table 10.

Parameters from method of maximum likelihood estimate

The probability density function of the Weibull distribution is given by Eq. (3.12).

$$f_N(n) = \frac{\alpha}{\theta} n^{\alpha-1} \exp\left[-\frac{n^\alpha}{\theta}\right] \tag{3.12}$$

where $\theta = u^\alpha$. Eq. (3.13) and Eq. (3.14) express the maximum likelihood equations (Mohammadi and Kaushik 2005; Oh 1986; Singh and Kaushik 2001).

$$\theta^* = \frac{1}{k}\sum_{i=1}^{k} n_i^{\alpha^*} \tag{3.13}$$

$$\frac{\sum_{i=1}^{k}\left(n_i^{\alpha^*} \ln n_i\right)}{\sum_{i=1}^{k}\left(n_i^{\alpha^*}\right)} - \frac{1}{\alpha^*} = \frac{1}{k}\sum_{i=1}^{k} \ln n_i \tag{3.14}$$

where α^* and θ^* are the maximum likelihood estimates of α and θ, respectively. The parameter α was obtained from Eq. (3.14) by an iterative procedure. The values of α and u are

shown in Table 10. The differences obtained within the preceding calculations may be due to the relatively few number of samples tested at each S.

Table 10 – Parameters α and u for fatigue-life data for all calculation methods

Type	S	Parameter	Graphical method	Method of moments	Maximum likelihood estimate	Average
HPFRC	0.70	α	2.2209	3.3237	4.4104	3.3186
		u	1,779,624.93	1,701,716.77	1,683,053.13	1,721,473.90
	0.78	α	0.4816	0.7117	0.6329	0.6088
		u	7,830.17	7,893.60	7,010.31	7,578.15
	0.85	α	1.5144	2.5327	3.4926	2.5139
		u	412.21	377.06	374.27	387.86
	0.93	α	2.0540	2.8723	3.3978	2.7751
		u	102.12	97.61	97.07	98.98
SFRC	0.65	α	2.6312	3.8027	4.8085	3.7475
		u	1,145,588.46	1,107,614.88	1,098,819.32	1,117,340.89
	0.76	α	1.5802	1.8214	1.9988	1.8001
		u	472,629.75	455,470.43	459,418.75	462,506.31
	0.95	α	0.9278	1.1842	1.2211	1.1110
		u	2,096.42	1,971.94	1,990.74	2,019.70

Goodness-of-fit test

The Kolmogorov-Smirnov test was applied as goodness-of-fit to the fatigue-life data at each load level. It is given by Eq. (3.15).

$$D_n = \max|F^*(x_i) - F_N(x_i)| \tag{3.15}$$

in which $F^*(x_i) = \frac{i}{k}$ is the observed cumulative histogram and $F_N(x_i)$ is the hypothesized cumulative distribution function given by Eq. (3.3). The critical value D_c is taken from the Kolmogorov–Smirnov table for a 5% significance level. As $D_c > D_n$ (Table 11), the present model is accepted.

Table 11 – Kolmogorov-Smirnov test

Type	Load level	$D_n = \max \|F^* - F_N\|$	Critical value D_c
HPFRC	0.70	0.1983	0.7076
	0.78	0.3269	0.4834
	0.85	0.2239	0.7076
	0.93	0.2608	0.6239
SFRC	0.65	0.2277	0.6239
	0.76	0.1822	0.4543
	0.95	0.1935	0.4543

Flexural fatigue performance

Load level 0.78 of HPFRC revealed $\alpha < 1.0$ (Table 10), which leads to a decreasing hazard function with number of cycles. Although the graphical method as well as the goodness-of-fit test show that the Weibull distribution is a valid model in this situation, it violates the expected fatigue behaviour. For this reason, the value of $\alpha = 1.0$ can assumed (Singh and Kaushik 2000) and the value of u recalculated to 9.837,29. Figure 21(a) and Figure 21(b) show the HPFRC and SFRC C.D.F. curve vs the cycles, respectively.

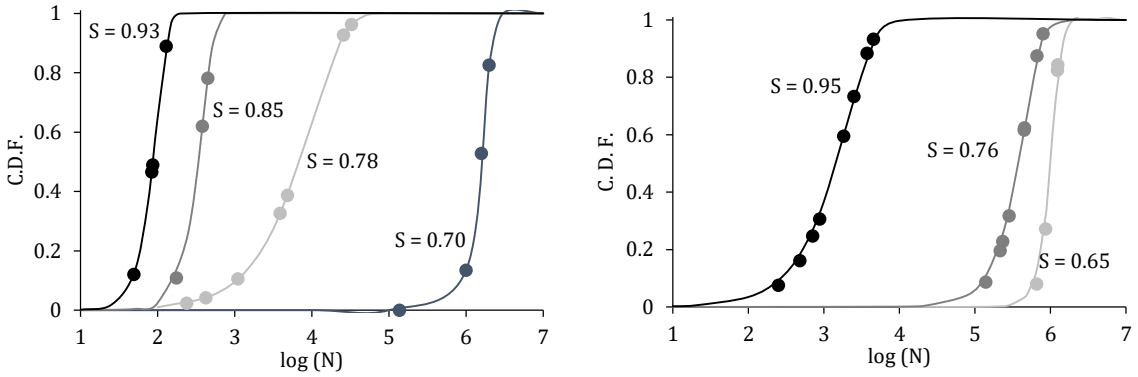

(a) (b)

Figure 21 – Cumulated distribution function for HPFRC (a) and SFRC (b)

Since the flexural fatigue-life data of HPFRC indicates to follow the two-parameter Weibull distribution at different load levels, it can be used to calculate the fatigue lives corresponding to different failure probabilities P_f. Substituting $L_N = 1 - P_f$ and rearranging Eq. (3.5) gives Eq. (3.16).

$$ln\,N = \frac{ln\left[ln\left(\frac{1}{1-P_f}\right)\right] + \alpha\, ln\, u}{\alpha} \tag{3.16}$$

Using the mean values of the parameters of the Weibull distribution, Eq. (3.16) express the fatigue life N for a particular P_f. Figure 22 shows the fatigue life with a corresponding failure probability of 5%, 50% and 95%. of HPFRC (a) and SFRC (b).

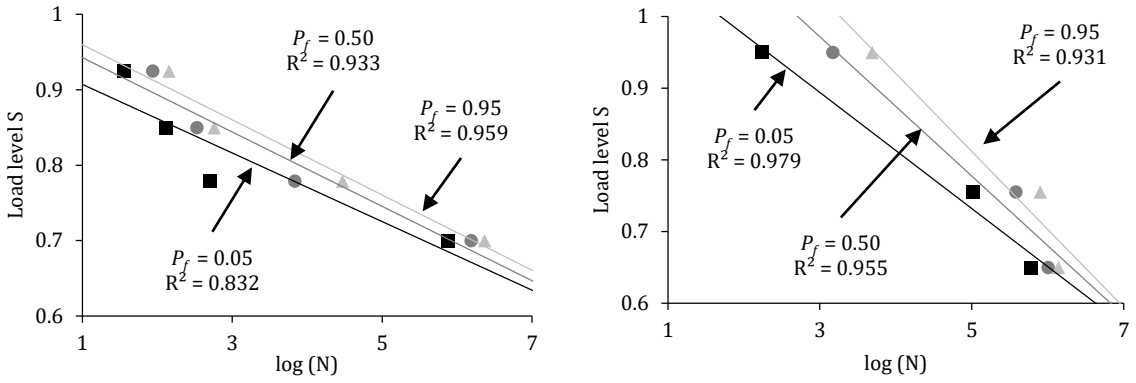

(a) (b)

Figure 22 – Fatigue life of HPFRC calculated through the Weibull distribution

3.3.3.2. Mathematical method: McCall model

The McCall model (McCall 1958) is based on a nonlinear relationship between S and logarithm of N given by Eq. (3.17).

$$L = 10^{-a(S)^b (\log N)^c} \tag{3.17}$$

in which L = 1 – P_f is the survival probability; a, b and c are the experimental constants. Taking logarithms twice of the both sides of Eq. (3.17) gives Eq. (3.18) (Singh et al. 2005).

$$\log(-\log L) = \log a + b \cdot \log S + c \cdot \log(\log N) \tag{3.18}$$

Eq. (3.18) can be rearranged in *Y = A + b.X + c.Z* form, where *Y = log (-log L), A = log a, X = log S, and Z = log (log N).* The experimental data was ranked in an increasing order (i) of cycle to failure at each load level. The probability of failure (P_f) is calculated by dividing i by (1 + n_s), where n_s equals to the total number of specimens tested at each S. Since all series of different S need to comprise the same number of specimens, Grubbs' test for outliers was used to discard additional samples. Specimens that survived the maximum prescribed number of cycles were included in the analysis because generated logical S–N regression curves. The calculated values of probability of failure are shown in Table 12 (HPFRC) and Table 13 (SFRC). The ratio i / (1 + n_s) is accepted to give best estimate of P_f (Do et al. 1993; Singh et al. 2005).

Table 12 – Fatigue-life data for HPFRC according to load level S and the respective probability of failure

i	Load level S						$P_f = i/(1 + n_s)$
	0.65	0.70	0.75	0.80	0.85	0.90	
1	2,000,000	137,230	3,888	238	176	84	0.25
2	2,000,000	1,000,000	4,821	421	380	86	0.50
3	2,000,000	1,581,049	25,821	1,103	448	129	0.75

Table 13 – Fatigue-life data for SFRC according to load level S and the respective probability of failure

i	Load level S					$P_f = {}^{i}/_{(1+n_s)}$
	0.65	0.71	0.80	0.90	1	
1	655,576	138,590	21,490	480	250	0.20
2	865,807	284,037	214,800	710	874	0.40
3	1,232,969	454,816	233,727	2,501	1,832	0.60
4	1,250,000	662,702	450,070	3,737	4,507	0.80

A multiple linear regression analysis was performed in order to fit the experimental data with the analytical model, resulting in Eq. (3.19) for HPFRC and Eq. (3.20) for SFRC.

$$L = 10^{-1.83\times10^{-2}(S)^{40.25}(log\,N)^{10.56}} \tag{3.19}$$

$$L = 10^{-2.69\times10^{-5}(S)^{15.23}(log\,N)^{8.53}} \tag{3.20}$$

The S–N–P_f curve (HPFRC in Figure 23(a)) and SFRC in Figure 23(b)) for different values of P_f are presented and compared to the experimental data. Almost all of the experimental points fall between the curves for P_f = 5% and 95%.

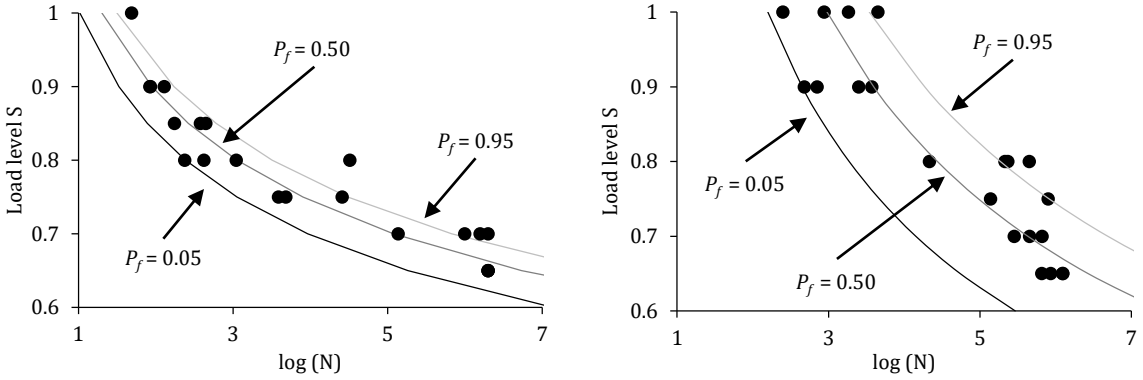

Figure 23 – S–N curves considering various probabilities of failure

3.3.3.3. Comparison between probabilistic methods

To compare the investigates methods, the Wöhler curve considered the average values of N, which corresponds to a 50% of fatigue life survival (Do et al. 1993). Similarly, both probabilistic approaches were calculated to a probability of failure of 50%. Figure 24 shows the S–N–P_f curves of Weibull distribution, McCall model, Wöhler curve and experimental data points and the respective calculated R^2 for HPFRC (a) and SFRC (b).

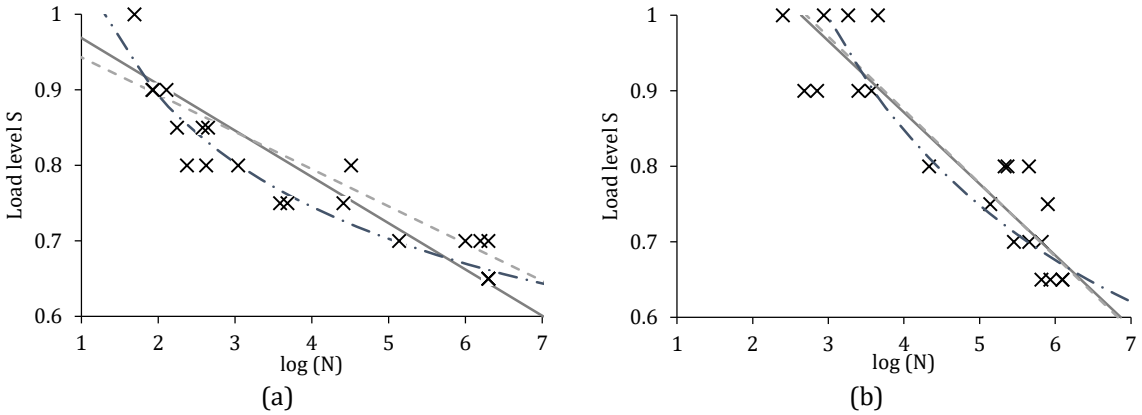

	Wöhler curve	Weibull distribution	McCall model
(a) HPFRC	0.766	0.809	0.889
(b) SFRC	0.849	0.852	0.814

Figure 24 – Comparison between methods considering a probability of failure of 50% and the experimental data and calculated values of R^2 for HPFRC (a) and SFRC (b)

Even though the scope of this research presents low number of results for each load level, the McCall mathematical method predicts reasonably well the flexural fatigue life of pre-cracked HPFRC for a desired probability of failure. Through the presented values of R^2, the fatigue life of pre-cracked SFRC is better predicted by the curve given by the Weibull distribution. Although HPFRC and SFRC showed similar post-crack 3PBT response, fatigue results of SFRC had higher dispersion. This difference may be explained by variations in orientation and distribution of fibre which have more impact in the overall behaviour of the specimen.

3.4. Concluding remarks

The main findings of this research are outlined below.

- Static and dynamic tests indicate higher dispersion of SFRC results compared to HPFRC most likely due to considerable lower number of fibres bridging the damaged zone, consequently minor variations in fibre orientation and distribution can have great influence in the overall behaviour;
- Applied load level plays an important role on the CMOD development through cycles and the equivalent CMOD at failure. As the load level increases, the slope of the crack increment per cycle becomes steeper and the crack opening displacement grows as well. At higher S, the bend at phase III displays smoother shape and the failure

occurs at higher $CMOD_{upp}$. This suggests that lower load levels can cause a reduction of the ductility. Higher S may lead to failure through a continuous pull-out of the fibres, this generating a more ductile response. Smaller S can be responsible for the progressive weakening of the fibre-matrix interface through micro-cracks;

- Good agreement was found between the bearing capacity of specimens and the envelope curve for HPFRC. This result suggests that the monotonic load-CMOD curve might be used as failure criterion under flexural fatigue loading, at least for the adopted load levels (S = 0.65, 0.70, 0.75, 0.80, 0.85, 0.90, 1) and frequency (6 Hz);
- The S–N curve obtained allows affirming that HPFRC and SFRC pre-cracked specimens have a fatigue endurance limit of 2,000,000 cycle of the order of 66% of $P_{0.5mm}$;
- Monotonic tests done on run-out specimens showed that the cyclic loads seem to act on the crack opening width, but not on the post-fatigue load capacity, regardless load level. In fact, in most of the cases, the maximum load of the post-fatigue peak was around 4% higher than $P_{0.5mm}$. Such behaviour confirms that the fatigue was done under the endurance limit;
- Looking into the cross section of specimens, it suggests that fatigue failure of HPFRC occurs due to damage at the matrix-fibre contact interface that progressively reduces the anchorage capacity. No damage on the steel microfibre was observed. In contrast, fatigue failure of SFRC occurs in two failure modes: fibre pull-out similar to HPFRC and steel macrofibre breakage since the tip was sharpen. The second failure mode can be attributable to the longer length of macrofibres;
- The McCall mathematical method predicts reasonably well the flexural fatigue strength of pre-cracked HPFRC, and the Weibull distribution of pre-cracked SFRC, for a desired probability of failure.

4. FATIGUE OF POLYPROPYLENE FIBRE REINFORCED CONCRETE

4.1. Introduction

The use of polypropylene fibres has increased significantly in recent years due to their contribution to post-cracking strength and their inert, non-corrosive nature, particularly for those cases in which variations in the mechanical properties dependent on time are of paramount importance (e.g., sewerage buried pipelines and metro tunnels). Fatigue response of polypropylene fibre reinforced concrete (PFRC) under cyclic load has been studied in terms of fatigue load versus fatigue life (S-N curves) for constant and variable loading amplitudes at different frequencies, fatigue crack evolution, strain rate and accumulated damage. Nevertheless, limited information about post-cracking and post-fatigue residual response is available. Assumptions and conclusions obtained for SFRC cannot be directly generalized for PFRC due to the differences in the properties of these fibre (e.g. both lower elastic modulus and tensile strengths). Therefore, a good understanding of the post-cracking/fatigue behaviour of PFRC is of great importance for the satisfactory design of structures.

This chapter presents results of the experimental investigation on PFRC covering quasi-static and dynamic tests and the influence of the flexural load cycles on the mechanical performance of specimens. Experimental results provide a regression equation to predict the crack-opening evolution and the possibility to predict the remaining flexural strength. The

experimental campaign was carried out at Laboratorio de Estructuras Luis Agulló at the Universidad Polictécnica de Cataluña – BarcelonaTech.

4.1.1. Objectives

The main objective of this chapter is to analyse the mechanical behaviour of pre-cracked polypropylene fibre reinforced concrete subjected to load cycles. For this purpose, several specific objectives are defined:

- Assess the influence of the fibre type and fibre content on the mechanical response during dynamic loading and after the cycles;
- Evaluate the influence of the fatigue cycles on the remaining residual flexural strength and correlate with the quasi-static behaviour;
- Propose a regression equation that is able to predict the crack-opening of pre-cracked PFRC during fatigue cycles.

4.1.2. Outline of the chapter

The study encompasses an experimental investigation on PFRC with two types of polypropylene fibre and one PFRC with two fibre content to investigate the influence of the level of deflection-hardening on the mechanical behaviour after cycles. Also, specimens were subjected to a different maximum number of load cycles (N_{max}) applied during the fatigue test. Fresh- and hardened-state properties were assessed. The flexural fatigue response was evaluated in terms of the evolution of crack mouth opening displacement (CMOD) over the load cycles. Then, specimens were tested under quasi-static flexural configuration to evaluate the influence of the cyclic loading on the residual flexural strength. Thereafter, the cracked surface of PFRC samples and the fibre failure mode were examined with an optical microscope. Moreover, fibres were characterized through differential scanning calorimetry (DSC) and dynamic mechanical analysis (DMA).

This research provides knowledge, unique experimental results and proposes a conceptual model for the behaviour of PFRC under flexural dynamic cycles that can be used for generating specific fatigue models to be introduced in future FRC design codes and guidelines.

4.2. Experimental procedures

4.2.1. Mix design, casting and curing procedures

Table 14 shows the PFRC compositions used in the experimental program, which should satisfy the structural requirements for typical applications in heavy-duty pavements, industrial floors, tunnel segmental lining and precast elements in general. All mixes contained Portland cement CEM I-52.5 R, limestone aggregates, sodium polycarboxylate ether-based superplasticiser and water/cement ratio of 0.40. Two fibre contents were used to represent different levels of residual flexural strength. The first (5 kg/m^3 or 0.4% by volume) is expected to achieve an infracritical behaviour in bending according to the *fib* Model Code 2010 (Fib 2013), with limited stress recovery between f_{r1} and f_{r3} of a minimum of 50%. The second (10 kg/m^3 or 0.8% by volume) is expected to achieve a significant stress recovery between f_{r1} and f_{r3} in bending according to the *fib* Model Code 2010 (Fib 2013).

Table 14 – Mix proportions of PFRCs

Materials (kg/m3)	PF1_5	PF1_10	PF2_10
Cement	421	420	420
Water	168	168	168
Sand (0–4 mm)	862	860	860
Coarse aggregate (4–10 mm)	441	440	440
Coarse aggregate (10–20 mm)	491	490	490
Superplasticizer	4.2	4.2	4.2
Polypropylene fibres	5	10	10

To reduce the number of trials considering the long duration of each fatigue test, the influence of the fibre content was assessed only for PF1 by comparing PF1_5 and PF1_10 with 5 kg/m^3 and 10 kg/m^3, respectively. Likewise, the influence of the fibre type was only assessed for the highest fibre content by comparing PF1_10 with 10 kg/m^3 of PF1 and the analogous PF2_10 with 10 kg/m^3 of PF2. The reduction of the fibre content from 10 kg/m^3 to 5 kg/m^3 entailed an increase in the content of other materials, although their relative proportion was kept the same. The criteria adopted here was to maintain such relative proportion in all mixes, thus ensuring as much as possible identical matrices. This implies differences in the fresh-state rheology of mixes induced by the fibre type and content.

The mixing process took place in a vertical-axis mixer with a nominal capacity of 50 l. After homogenising all dry components (cement, sand and aggregates), water and superplasticizer were added to the mixer and, finally, fibres were added. Upon achieving a

homogeneous mix, the fresh-state properties were assessed and the following specimens were cast per composition: Ø150x300 mm^2 cylinders for compressive strength and elastic modulus, and 150×150×600 mm^3 and 75×75×275 mm^3 prismatic beams for residual flexural strength and fatigue tests. The second beam size was chosen pondering a reduction of material and ease of handling. After casting, the moulds were covered with a thin plastic sheet and left to cure at room temperature for 24 hours. Then, they were demoulded and stored in a climatic chamber at 20 °C and 95%-100% relative humidity until the date of the test.

4.2.2. Control tests

Slump, density and air content were characterised according to EN 12350-2:2009, EN 12350-6:2009 and EN 12350-7:2010, respectively. For each composition, compressive strength was measured in four cylinders in accordance to EN 12390-3:2009 and the elastic modulus was measured in three cylinders in accordance to the EN 12390-13:2014 using a universal compression testing machine IBERTEST MEH-3000 with a nominal maximum load capacity of 3,000 kN. The quasi-static flexural strength was measured following the EN 14651:2007 in three notched beams with a three-point bending test (3PBT) setup in an INSTRON hydraulic servo-controlled testing machine. A clip gauge placed at the notch controlled the CMOD during the 3PBT. All quasi-static tests were performed at 28 days.

4.2.3. Dynamic tests

Figure 25 shows the complete loading history of specimens subjected to the fatigue test. First, specimens were pre-cracked in 3PBT setup according to the procedure in EN 14651:2007. A constant CMOD rate of 0.05 mm/min was applied up to a total CMOD of 0.5 mm (considered the service limit value in *fib* Model Code 2010 (Fib 2013)). The force corresponding to this displacement was set as the maximum load in the fatigue test (P_{upp}). The minimum load (P_{low}) during the cycles was defined by considering an amplitude of 0.3 ($R = P_{low}/P_{upp} = 0.3$). Immediately after pre-cracking and without removing the specimen from the testing machine, a sinusoidal cyclic load with a frequency of 6 Hz ranging from P_{upp} to P_{low} was applied, and the evolution of CMOD was recorded at every 500 cycles. N_{max} was either 1,000,000 (de Andrade Silva et al. 2010; Breña et al. 2005; Chanvillard et al. 2004; Farhat et al. 2007; Nanni 1991; Tarifa et al. 2015) or 2,000,000 (Arora and Singh 2016; Johnston and Zemp 1991; Ramakrishnan et al.

1989; Zhang and Tian 2011), which are a common reference for the assessment of the endurance limit in the literature. Upon reaching N_{max}, the cyclic loading was interrupted, and the beams were immediately reloaded at a constant CMOD rate of 0.2 mm/min up to failure. Notice that the clip gage was kept in place throughout the whole process so that the 0 mm refers to the condition found before pre-cracking. After failure, specimens were removed from the frame and separated in 2 halves for the assessment of the failure cross-section and manual counting of fibres.

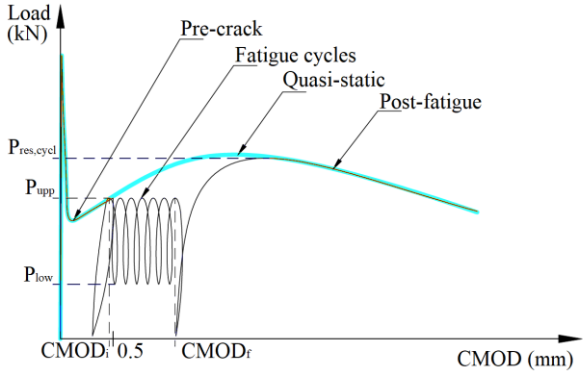

Figure 25 – Fatigue loading history

Table 15 shows the total number of specimens tested under fatigue. The election was based on the experimental programmes from other studies in the literature (Naaman and Hammoud 1998; Nagabhushanam et al. 1989; Parant et al. 2007; Ramakrishnan et al. 1989) about the residual resistant strength after application load cycles.

Table 15 – Total number of specimens subjected to cyclic loading

Mix	Specimen size (mm³)	Name	Number of specimen – fatigue test
PF1_5	150×150×600	PF1_5-1.1C	5
	75×75×275	PF1_5-1.0C	5
PF1_10	150×150×600	PF1_10-1.6E	5
	75×75×275	PF1_10-1.4E	5
PF2_10	150×150×600	PF2_10-1.5E	7
	75×75×275	PF2_10-1.9E	4

Owing to the limited availability of testing machines and the long duration of each test, the fatigue could not be assessed at the same age in all specimens. The specimens were tested in a period extending from 30 to 90 days since casting, alternating between mixes to minimise the influence of the age in the results. A variation of 5.5% in quasi-static flexural strength was expected between 30 and 90 days based on the formulations from the Eurocode 2-1 (EN 1992-

1-1). The temperature and relative humidity of testing room were 25 °C and 65%-70%, respectively.

4.3. Fibre properties

The fibre PF1 was 48-mm long and was made of virgin polypropylene with specific gravity of 0.89–0.91 g/cm^3. Fibre PF2 was 60-mm long and was made of polypropylene copolymer with specific gravity of 0.91 g/cm^3. Both had continuous embossing anchorage and were considered adequate for FRC with structural responsibility.

Polypropylene is a thermo-responsive polymer that shows a complex fatigue behaviour due to its viscous and elastic responses, which are affected by the loading frequency and dissipative heating phenomenon (Dao 1982; Matsumoto 2008). Failure can occur as a consequence of thermal fatigue (damage from material softening caused by melting) or mechanical fatigue (crack nucleation and growth, entanglement, scission, crazing, debonding and polymer network rearrangement (Dao 1982; Muliana 2014)).

The thermal properties of PF1 and PF2 were analysed through DSC in a JADE DSC from Perkin Elmer Inc. to evaluate their intrinsic differences. Scans were performed within the range from −40 to 280 °C, at a rate of 5 °C /min and under 20 mL.min^{-1} Nitrogen gas purge. Figure 26 shows cooling (a), and heating (b) scans of PF1 (continuous line) and PF2 (discontinuous line). The melting range of the polymer is visible as an endothermic peak. The figures also show the melting temperature (T_m), melting enthalpy (ΔH_m), crystallisation temperature (T_c) and crystallisation enthalpy (ΔH_c) of each fibre. The results of PF1 and PF2 are consistent with those reported by (Manchado et al. 2005; Samal et al. 2009) in the literature for pure polypropylene, which exhibits T_c of 116 °C and T_m of 162 °C.

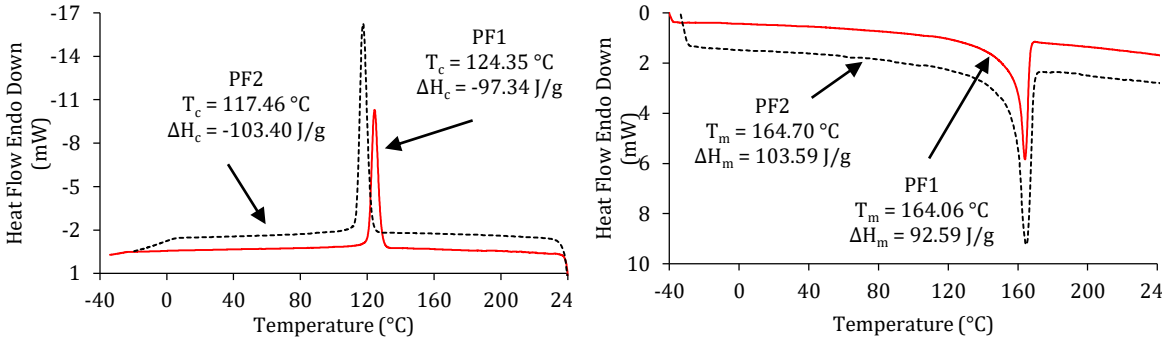

Figure 26 – DSC thermograms of PF1 and PF2: (a) cooling scan and (b) heating scan.

To characterise the effect of changes in temperature on the dynamic mechanical response of the fibres, DMA tests were performed on a TA Instruments Q800 machine operating at 1 Hz and with a heating ramp of 3 °C/min from 30 to 150 °C. The range of temperature was based on the DSC results and 1 Hz was fixed as the effect of frequency on the dynamic response of polypropylene can be considered negligible in the range from 1 to 10 Hz (López-Manchado and Arroyo 2000; Son et al. 2003). The dynamic response presents two parts: an elastic deformation or energy stored in the system given by the storage modulus (E') and the energy dissipated as heat given by the dynamic loss modulus (E''). The ratio between E'' and E' is known as the mechanical loss tangent (tan δ) (Samal et al. 2009; Tajvidi et al. 2006). The peak of the tan δ curve represents the glass transition temperature (T_g), which indicates the transition from a relatively brittle to a rubbery state.

Figure 27 shows the evolution of E', E'' and tan δ with the temperature and T_g for PF1 and PF2. In the range of temperature analysed, the stiffness and energy dissipation capacity were 15% bigger for PF1 than for PF2. The values of T_g confirm the results obtained with DSC analysis. Both polypropylene fibres show thermal stability. No change in the mechanical response nor phase transition are expected at room temperature.

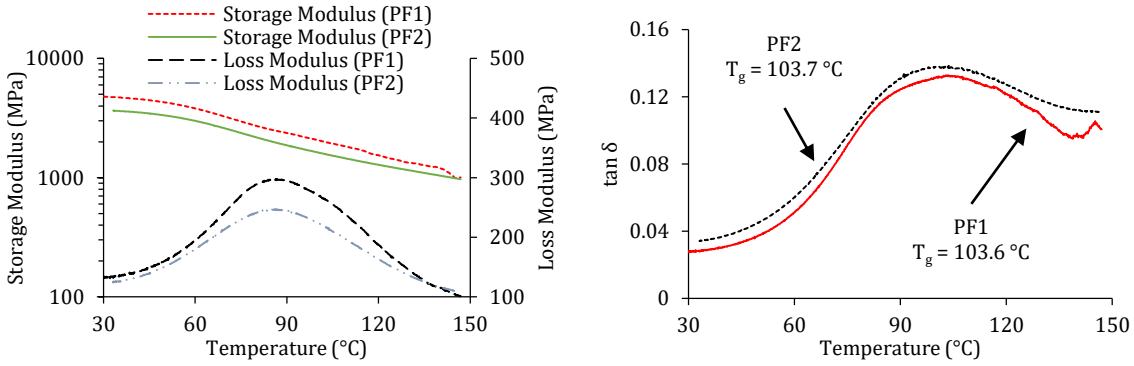

Figure 27 – DMA results for PF1 and PF2: (a) storage and loss moduli vs temperature; (b) tan δ vs. temperature

4.4. Results and discussion

4.4.1. Fresh state properties and mechanical characterization

Table 16 shows the average and the coefficient of variation (CV presented between parenthesis) for the slump, density, air content, compressive strength and elastic modulus of all mixes. The increase from 5 kg/m^3 of PF1 in PF1_5 to 10 kg/m^3 in PF1_10 did not have a statistically significant influence on the fresh-state properties, compressive strength and elastic

modulus of the PFRC. By contrast, the change in the type of fibre from PF1 in PF1_10 to PF2 in PF2_10 led to a 4-fold reduction in the slump and 50% increase in the air content, which might explain the 17% reduction observed in the compressive strength

Table 16 – Mix proportion, fresh state and control test results

		PF1_5	PF1_10	PF2_10
Fresh state results	Slump-test (cm)	9.5 (37.2%)	12.0 (23.6%)	3.0 (27.2%)
	Density (kg/m3)	2402 (0.4%)	2405 (0.0%)	2401 (0.3%)
	Air content (%)	2.2 (3.1%)	2.1 (17.3%)	3.0 (2.7%)
Control test results	Compressive strength (MPa)	64.5 (9.9%)	63.8 (2.8%)	53.6 (6.7%)
	Elastic modulus (MPa)	37.1 (4.4%)	37.0 (0.6%)	38.1 (4.2%)

Table 17 presents the average residual flexural strengths (f_{R1m}, f_{R2m}, f_{R3m}, f_{R4m} corresponding to CMOD values of 0.5, 1.5, 2.5 and 3.5 mm, respectively), limit of proportionality (f_{LOPm}), maximum post-cracking stress ($f_{PC,max}$) and the respective CMOD ($CMOD_{fPC,max}$) measured in the 3PBT. The table also includes the characteristic values of f_{LOP} (f_{LOPk}) and the flexural residual strengths f_{R1} (f_{R1k}) and f_{R3} (f_{R3k}) related respectively with the service and ultimate limit states (Fib 2013). Figure 28 gathers the 3PBT average (continuous line) and envelope (hatched area) curves for PF1_5-1.1C and PF1_10-1.6E (a), PF2_10-1.5E (b), PF1_5-1.0C and PF1_10-1.4E (c) and PF2_10-1.9E (d). All residual stresses presented were calculated considering an equivalent linear elastic non-cracked cross-section.

Table 17 – Average and characteristic 3PBT results and coefficient of variation in percentage and between parenthesis

Comp.	f_{LOPm} (MPa)	$f_{PC,max}$ (MPa)	$CMOD_{fPC,max}$ (mm)	f_{R1m} (MPa)	f_{R2m} (MPa)	f_{R3m} (MPa)	f_{R4m} (MPa)	f_{LOPk} (MPa)	f_{R1k} (MPa)	f_{R3k} (MPa)	f_{R3k}/f_{R1k}	f_{R1k}/f_{LOPk}
PF1_5-1.1C	5.21 (7.2)	2.22 (41.8)	3.059 (10.8)	1.45 (36.2)	1.92 (42.0)	2.17 (43.4)	2.17 (41.2)	4.76	0.59	0.62	1.1c*	0.1
PF1_10-1.6E	5.39 (12.2)	5.59 (10.5)	2.919 (4.9)	3.49 (9.7)	4.93 (11.9)	5.50 (10.7)	5.42 (9.0)	4.25	2.93	4.54	1.6e*	0.7
PF2_10-1.5E	5.14 (6.7)	3.47 (15.7)	3.994 (0.0)	2.05 (14.8)	2.73 (16.5)	3.18 (16.7)	3.40 (16.3)	4.61	1.55	2.31	1.5e*	0.3
PF1_5-1.0C	5.60 (8.7)	2.49 (32.2)	2.293 (26.6)	1.75 (23.4)	2.41 (28.6)	2.43 (33.6)	2.36 (37.4)	4.68	1.07	1.09	1.0c*	0.2
PF1_10-1.4E	6.90 (9.4)	7.29 (36.0)	2.746 (25.0)	4.63 (34.5)	6.53 (35.5)	7.24 (37.6)	6.96 (36.8)	5.96	2.00	2.76	1.4e*	0.3
PF2_10-1.9E	6.04 (4.9)	3.11 (12.4)	3.840 (7.0)	1.59 (20.0)	2.28 (17.2)	2.73 (15.8)	3.06 (13.9)	5.37	1.07	2.02	1.9e*	0.3

* Classification of the post-cracking strength based on Model Code 2010 (Fib 2013)

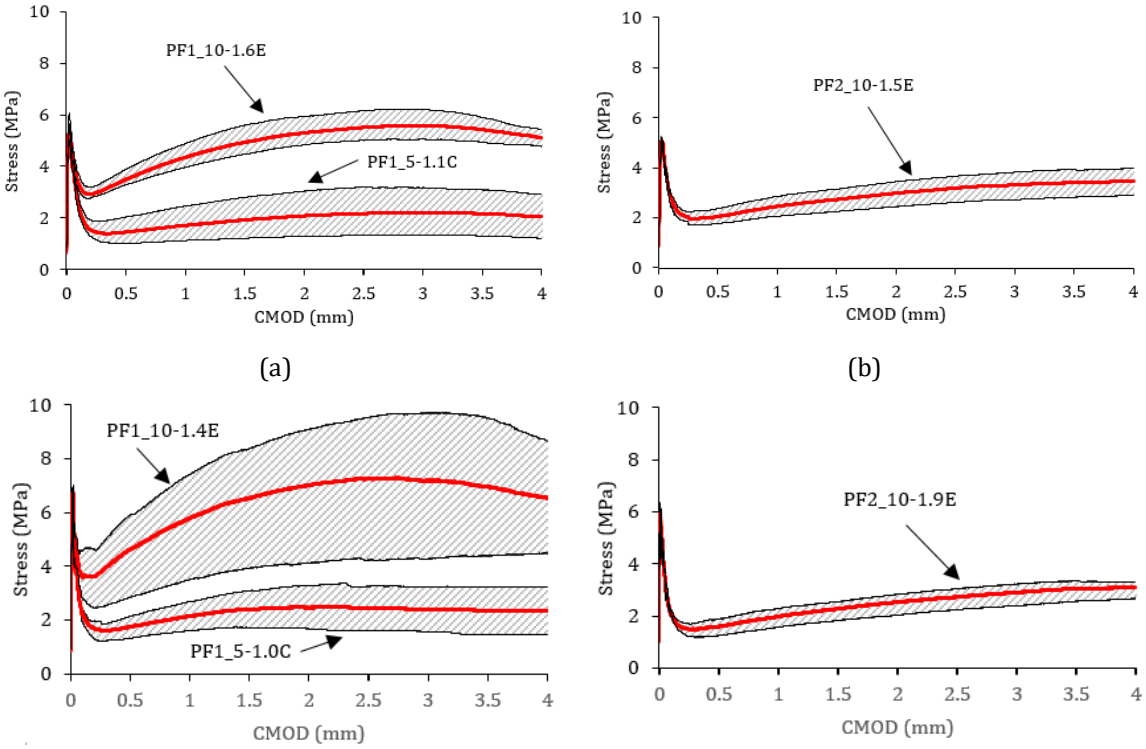

Figure 28 – Average and envelope of 3PBT results: PF1_5-1.1C and PF1_10-1.6E (a), PF2_10-1.5E (b), PF1_5-1.0C and PF1_10-1.4E (c) and PF2_10-1.9E (d)

The f_{LOPm} is not significantly affected by the fibre content and type. Differences between same composition within specimen size can be an effect of the fibre distribution and orientation, which has a stronger influence in smaller specimens. Immediately after cracking, PFRCs exhibited a sudden stress drop indicating loss of stiffness. The minimum residual stress observed just after cracking was approximately 66% (both PF1_5), 51% (both PF1_10), 57% (PF2_10-1.5E) and 48% (PF2_10-1.9E) of $f_{PC,max}$. The ductile behaviour and stress recovery are attributed to the contribution of the fibres (de Alencar Monteiro et al. 2018; Oh et al. 2007). PF1_5 showed a nearly stable post-cracking response while PF1_10 and PF2_10 showed an increase in stress when reaching higher CMOD values. Notice that the last part of the name of each mix represents their classification according to the Model Code 2010 (Fib 2013), which depends on the ration f_{R3k}/f_{R1k}. The further reduction of the strength after a maximum is reached arises from the progressive fibre debonding and slipping in the cross section. According to the classification proposed by the Model Code 2010 (Fib 2013) for the post-cracking strength, PF1_106E can be considered as a structural material ($f_{R1k}/f_{LOPk} > 0.4$ and $f_{R3k}/f_{R1k} > 0.5$).

4.4.2. Fatigue test: CMOD variation over cycles

Table 18 summarises for each specimen the maximum number of cycles (N_{max}), P_{upp}, CMOD for P_{upp} at the first, 1,000,000 and 2,000,000 cycles ($CMOD_1$, $CMOD_{1M}$ or $CMOD_{2M}$, respectively). The table also shows the difference between $CMOD_{1M}$ and $CMOD_1$ (ΔCMOD). To better illustrate the behaviour of the mixes, Figure 29 (a) to (f) show the evolution of the CMOD measured at different cycles for $P_{upp.}$ Figure 30 shows a typical specimen after fatigue test and cross section for fibre counting.

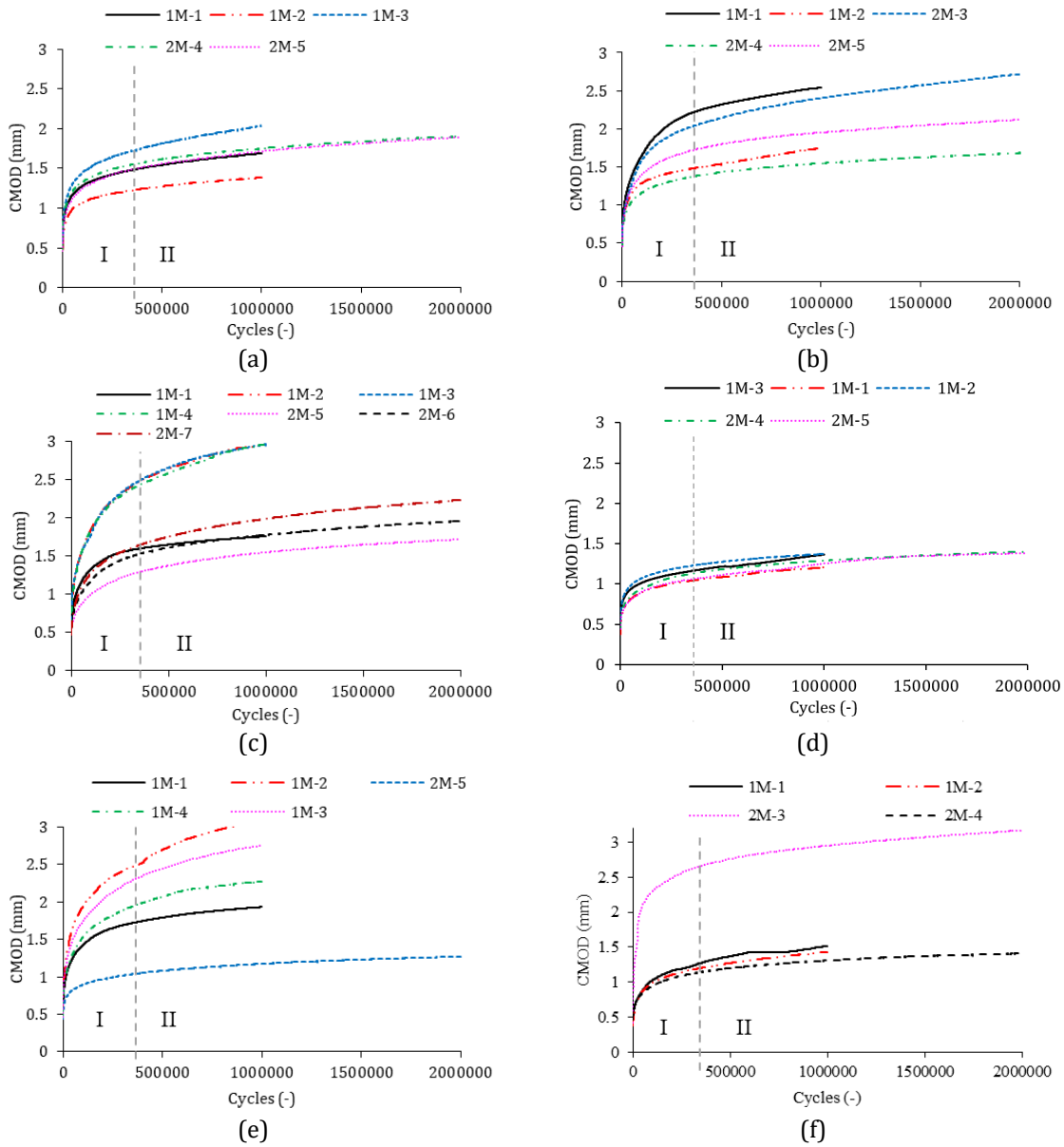

Figure 29 – CMOD evolution with cycles: PF1_5-1.1C (a), PF1_10-1.6E (b), PF2_10-1.5E (c), PF1_5-1.0C (d), PF1_10-1.4E (e) and PF2_10-1.9E (f)

Table 18 – Results of fatigue tests and post-fatigue quasi-static flexural strength

Reference	N_{max} (million cycles)	Fatigue test							Post-fatigue quasi static				
		P_{upp} (kN)	$CMOD_1$ (mm)	$CMOD_{1M}$ (mm)	$CMOD_{2M}$ (mm)	ΔCMOD (mm)	D_{1M}	D_{2M}	$f_{res,cycl}$ (MPa)	$CMOD_{fres,cycl}$ (mm)	$f_{res,cycl}/f_{PC,max}$	$S'_{fres,cycl}$	Fibre/cm²*
PF1_5-1.1C_1M-1	1	4.41	0.477	1.688	–	1.211	0.153	–	2.72	3.22	1.23	0.62	0.44 (83)
PF1_5-1.1C_1M-2	1	5.37	0.466	1.385	–	0.919	0.127	–	3.37	2.63	1.52	0.61	0.46 (87)
PF1_5-1.1C_1M-3	1	5.82	0.574	2.036	–	1.462	0.194	–	3.18	3.41	1.43	0.70	0.60 (113)
PF1_5-1.1C_2M-4	2	4.43	0.477	1.749	1.899	1.272	0.166	0.193	2.69	3.41	1.21	0.63	0.44 (83)
PF1_5-1.1C_2M-5	2	5.15	0.467	1.715	1.894	1.248	0.186	0.214	2.89	3.16	1.30	0.69	0.55 (104)
PF1_10-1.6E_1M-1	1	8.41	0.490	2.542	–	2.052	0.313	–	5.08	3.55	0.91	0.64	0.83 (156)
PF1_10-1.6E_1M-2	1	8.18	0.467	1.747	–	1.280	0.219	–	5.26	3.30	0.94	0.60	0.88 (165)
PF1_10-1.6E_2M-3	2	9.60	0.491	2.403	2.718	1.912	0.275	0.335	5.56	3.82	0.99	0.66	0.95 (179)
PF1_10-1.6E_2M-4	2	8.36	0.469	1.550	1.684	1.081	0.176	0.204	5.30	3.15	0.95	0.61	0.91 (170)
PF1_10-1.6E_2M-5	2	4.80	0.463	1.953	2.120	1.490	0.221	0.255	3.01	3.49	0.54	0.61	0.62 (116)
PF2_10-1.5E_1M-1	1	5.00	0.473	1.764	-	1.291	0.149	–	4.37	4.52	1.26	0.44	0.48 (91)
PF2_10-1.5E_1M-2	1	5.00	0.475	2.947	-	2.472	0.339	–	3.57	5.33	1.03	0.54	0.44 (83)
PF2_10-1.5E_1M-3	1	5.00	0.449	2.966	-	2.516	0.313	–	3.30	5.15	0.95	0.58	0.51 (96)
PF2_10-1.5E_1M-4	1	4.71	0.471	2.969	-	2.498	0.186	–	3.08	4.97	0.89	0.59	0.42 (79)
PF2_10-1.5E_2M-5	2	7.14	0.51	1.552	1.723	1.042	0.088	0.103	5.41	4.21	1.56	0.51	0.77 (145)
PF2_10-1.5E_2M-6	2	3.70	0.398	1.777	1.959	1.379	0.146	0.155	2.94	5.01	0.85	0.48	0.46 (86)
PF2_10-1.5E_2M-7	2	5.63	0.471	1.991	2.236	1.519	0.168	0.191	3.77	5.97	1.09	0.57	0.55 (104)
PF1_5-1.0C_1M-1	1	0.93	0.379	1.204	–	0.826	0.130	–	2.60	4.11	1.04	0.50	0.45 (21)
PF1_5-1.0C_1M-2	1	1.06	0.464	1.373	–	0.910	0.060	–	2.77	2.90	1.11	0.54	0.48 (23)
PF1_5-1.0C_1M-3	1	1.98	0.521	1.365	–	0.844	0.111	–	4.45	2.97	1.79	0.63	0.68 (32)
PF1_5-1.0C_2M-4	2	2.00	0.448	1.290	1.402	0.841	0.127	0.136	4.62	3.21	1.86	0.61	0.51 (24)
PF1_5-1.0C_2M-5	2	1.32	0.443	1.253	1.382	0.811	0.136	0.113	2.91	2.54	1.17	0.64	0.35 (17)
PF1_10-1.4E_1M-1	1	2.17	0.470	1.933	–	1.463	0.312	–	–	–	–	–	0.63 (30)
PF1_10-1.4E_1M-2	1	2.14	0.459	3.085	–	2.626	0.364	–	4.43	4.06	0.61	0.68	0.73 (34)
PF1_10-1.4E_1M-3	1	2.42	0.466	2.756	–	2.289	0.323	–	4.90	3.37	0.67	0.70	0.92 (43)
PF1_10-1.4E_1M-4	1	2.94	0.477	2.275	–	1.798	0.290	–	6.05	3.17	0.83	0.68	0.94 (44)
PF1_10-1.4E_2M-5	2	2.50	0.442	1.173	1.271	0.731	0.068	0.091	6.25	2.48	0.86	0.56	0.95 (45)
PF2_10-1.9E_1M-1	1	1.20	0.450	1.520	–	1.070	0.062	–	4.02	–	1.29	0.42	0.55 (26)
PF2_10-1.9E_1M-2	1	1.46	0.374	1.429	–	1.055	0.030	–	4.41	5.18	1.42	0.47	0.48 (23)
PF2_10-1.9E_2M-3	2	1.77	0.425	2.953	3.162	2.528	0.294	0.299	4.88	6.27	1.57	0.51	0.58 (27)
PF2_10-1.9E_2M-4	2	2.14	0.463	1.308	1.409	0.845	0.097	0.100	5.90	4.31	1.90	0.51	0.83 (39)

*Number in parenthesis is the number of fibres counted in the cross section

(a) (b)

Figure 30 - Specimen after fatigue test (a) and fibre counting of cross section (b)

Considering Figure 3 of section 2.3, the evolution of the CMOD during the fatigue test of all PFRC specimens in the experimental programme undergoes the 2 initial stages. In Stage I, the CMOD increases rapidly but with a decreasing rate up to approximately 350,000 cycles. Then, specimens show a linear relationship between the number of the cycle and the CMOD increment. Despite the high load value applied during the fatigue test (equal to the resistant capacity of the pre-cracked specimen for 0.5 mm CMOD), the absence of Stage III may be attributed to the hardening experienced by the PFRC in the post-cracking stage, which creates an additional barrier to the CMOD increment. Notice that the final CMOD after the fatigue test is smaller than the CMOD corresponding to the maximum residual flexural stress in the control quasi-static tests.

The pre-cracking process executed just before the fatigue test compromises the capacity of the matrix to transmit tensile forces in part of the cross-section. The difference in elastic modulus of fibre and matrix implies that an increment in the crack-opening is needed to activate the fibres that take over the transmission of tensile forces in such regions (Xu et al. 2018). This – combined with the high P_{upp} in comparison with the resistant capacity of the cross-section at the beginning of the fatigue test – favours crack propagation through the matrix and produces the rapid initial increment of CMOD in Stage I. Additional increases in CMOD further activate the fibres and elevate the cross-sectional resistant capacity that becomes progressively bigger than P_{upp}, thus leading to the reduction in the CMOD increment over the cycles at the end of Stage I. Additional microcracks develop in the fibre-matrix interface and merge into macrocracks (Malek et al. 2018) that facilitate fibre debonding and pull-out over the cycles. This gradual damage is responsible for the linear CMOD increase observed in Stage II. As mentioned before, 2,000,000 cycles were not enough to produce significant fibre pull-out in

the cross-section and accumulate damage to trigger Stage III in the mixes characterised in this experimental program.

The Welch's *t*-test was performed to determine whether the average CMOD or ΔCMOD of mixes and between different specimen sizes were statistically different. The analysis was conducted for each cycle recorded during the test. Results considering a level of significance (α) of 0.05 showed that the averages between 150×150×600 mm^3 and 75×75×275 mm^3 prismatic beams of PF1_10 and PF2_10 were not statistically different (p-value ≥ 0.163 (PF1_10) and ≥ 0.184 (PF2_10)). On the other hand, the average CMOD or ΔCMOD of different beam sizes of PF1_5 were statistically different (p-value ≤ 0.018). To avoid misinterpretation, only the beam size considered by EN 14651:2007 to compared the average CMOD or ΔCMOD of mixes with different fibre contents (PF1_5 and PF1_10). Results considering α of 0.05 showed that the averages were not statistically different despite doubling the fibre content (p-value ≥ 0.183 for all cycles). The differences in CMOD response for both compositions were probably eclipsed by the scatter due to fibre distribution and orientation, the production process of samples and associated to the precision of test equipment and set-up (Cavalaro and Aguado 2015). The same was found in the analysis of the influence of the fibre type through the comparison of PF1_10 and PF2_10. By using the same proportion of components and fixing P_{upp} in relation to the pre-cracking load, the behaviour in terms of the evolution of the CMOD during the fatigue cycles was not affected by the fibre type and content evaluated in this experimental program.

4.4.2.1. Damage evolution

The dissipated energy in the damaged zone due to cracking corresponds to the area enclosed by each unloading-reloading cycle, also known as hysteresis loop (Gylltoft 1984; Kolluru et al. 2000). Figure 31 (a) illustrates the hysteresis loops and Figure 31 (b) shows the evolution of the stiffness of the unloading branch and the hysteresis loop area for cycles 1, 500, 10,000, 50,000, 100,000, 500,000, 1,000,000 and 2,000,000 of specimen PF1_10-1.6E_2M-3 and Figure 31(c) illustrates the hysteresis loops and Figure 31(d) shows the evolution of the stiffness of the unloading branch and the hysteresis loop area for cycles 1, 500, 10,000, 50,000, 100,000, 500,000 and 1,000,000 of specimen PF1_10-1.4E_1M-2. Other specimens behaved similarly.

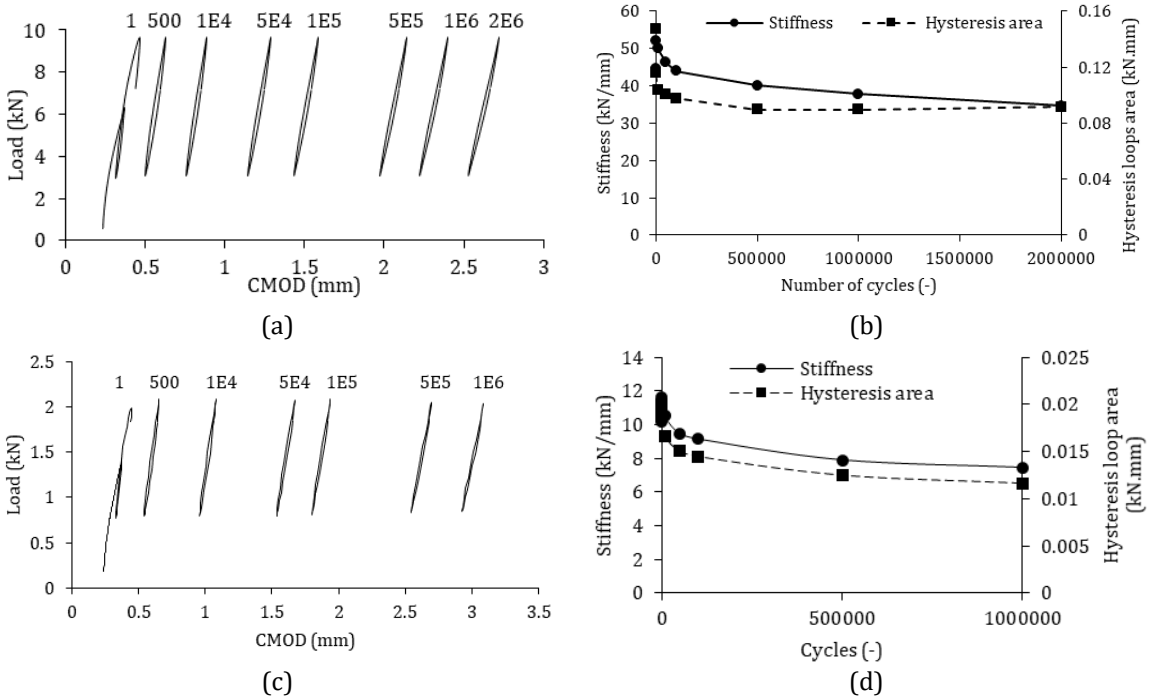

Figure 31 – Hysteresis loops over the cycles and stiffness and hysteresis loop area of specimen PF1-1.6E_2M-3 (a) (b) and specimen PF1_10-1.4E_1M-2 (c) (d)

Except for the first 1,000 cycles, the load-CMOD curve exhibits hysteresis loops with nearly the same area, suggesting a constant energy dissipation due to progressive cracking. The stiffness decreases, which reveals an increase in crack-opening for each load cycle and denotes stiffness degradation (Boulekbache et al. 2016; Carloni and Subramaniam 2013). The stiffness is used to assess the damage ratio (D) in Eq. (4.1), where k_{500} is the reference stiffness and k_n is the stiffness at a given cycle n. k_{500} was chosen as a reference to reduce inaccuracies caused by the initial flaws on the fibre-matrix interface on the assessment of the stiffness in the first cycles.

$$D = 1 - (k_n/k_{500}) \tag{4.1}$$

Figure 32 shows the total D after 1,000,000 (D_{1M}) and 2,000,000 (D_{2M}) cycles. Figure 32 shows the evolution of D for PF1_5-1.1C and PF1_10-1.6E (a), PF2_10-1.5E (b), PF1_5-1.0C and PF1_10-1.4E (c) and PF2_10-1.9E (d). The damage ratio increases rapidly, achieving 65% of D_{1M} in the first 100,000 cycles. After that, the degradation of the specimens becomes more gradual, increasing only by 15% from D_{1M} to D_{2M}.

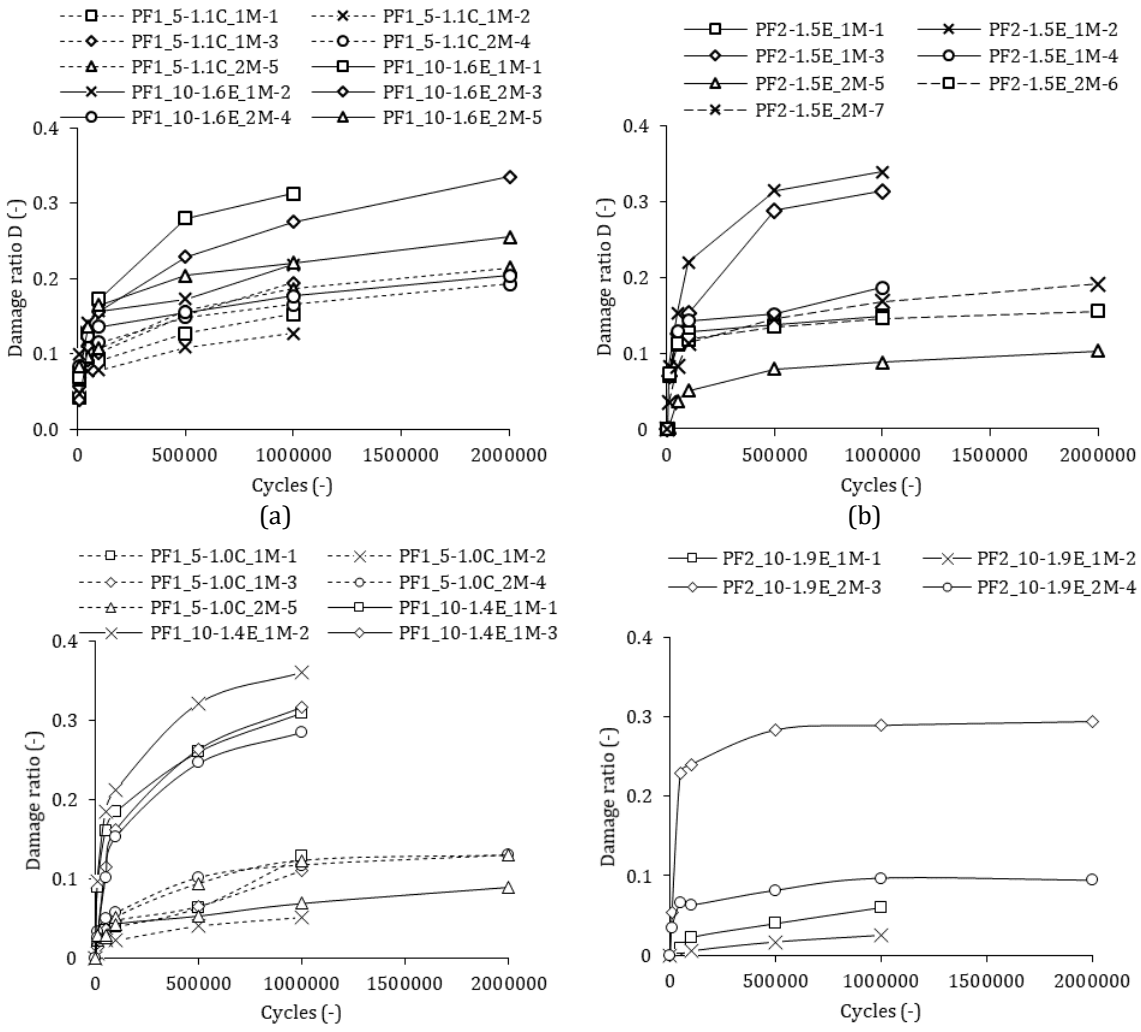

Figure 32 – Damage ratio versus cycles for PF1_5-1.1C and PF1_10-1.6E (a), PF2_10-1.5E (b), PF1_5-1.0C and PF1_10-1.4E (c) and PF2_10-1.9E (d)

The damage ratio of PF1_5 and PF1_10 (both beam sizes) were compared to verify if the fibre content influences the stiffness degradation of the specimens. The Welch's *t*-test (α equal to 0.05) reveals that the increase in fibre content produces statistically significant differences in the evolution of the average D over the cycles (p-value ≤ 0.038). Even though P_{upp} was defined in relation to the resistant capacity of each specimen, the bigger load-bearing capacity of PF1_10 leads to a proportionally bigger loss of stiffness during the cycles.

4.4.3. Remaining residual flexural strength after the fatigue test

Table 18 presents the maximum residual flexural strength after the fatigue cycles ($f_{res,cycl}$), the CMOD at $f_{res,cycl}$ ($CMOD_{Fres,cycl}$), the corresponding maximum measured in the control quasi-static test ($f_{PC,max}$ and $CMOD_{fPC,max}$) and the specific load level ($S'_{Fres,cycl}$) calculated as the ratio between P_{upp} and the maximum load reached after the fatigue test. $CMOD_{fres,cycl}$ is consistently bigger than the measured in the quasi-static control tests ($CMOD_{fPC,max}$), suggesting that the load cycles displaced the post-fatigue peak stress towards bigger CMOD values. PF1_5-1.1C and PF1_5-1.0C exhibited bigger post-fatigue maximum flexural residual strength (average of 34% and 39%, respectively) than the equivalent control quasi-static tests. By contrast, PF1_10-1.6E and PF1_10-1.4E showed smaller values (average of 13% and 26%, respectively) in comparison to the equivalent control quasi-static tests. PF2_10-1.5E presented $f_{res,cycl}$ 9% bigger than $f_{PC,max}$ and PF2_10-1.9E presented $f_{res,cycl}$ 54% bigger than $f_{PC,max}$.

Figure 33 shows the residual flexural strength curves for the specimens subjected to the fatigue test and the results for the control quasi-static tests of PF1_5-1.1C (a), PF1_10-1.6E (b), PF2_10-1.5E (c), PF1_5-1.0C (d), PF1_10-1.4E (e) and PF2_10-1.9E (f). The shape of the post-fatigue strength curve resembles and follows the trend found in the quasi-static control tests. Despite the difference expressed in the previous paragraph, notice that most of the stress-CMOD curves for specimens subjected to the fatigue test fall within the range of curves measured in the quasi-static control tests. This suggests that the CMOD increment observed after the load cycles led to a damage level similar to that found in the quasi-static control tests for the same CMOD increment.

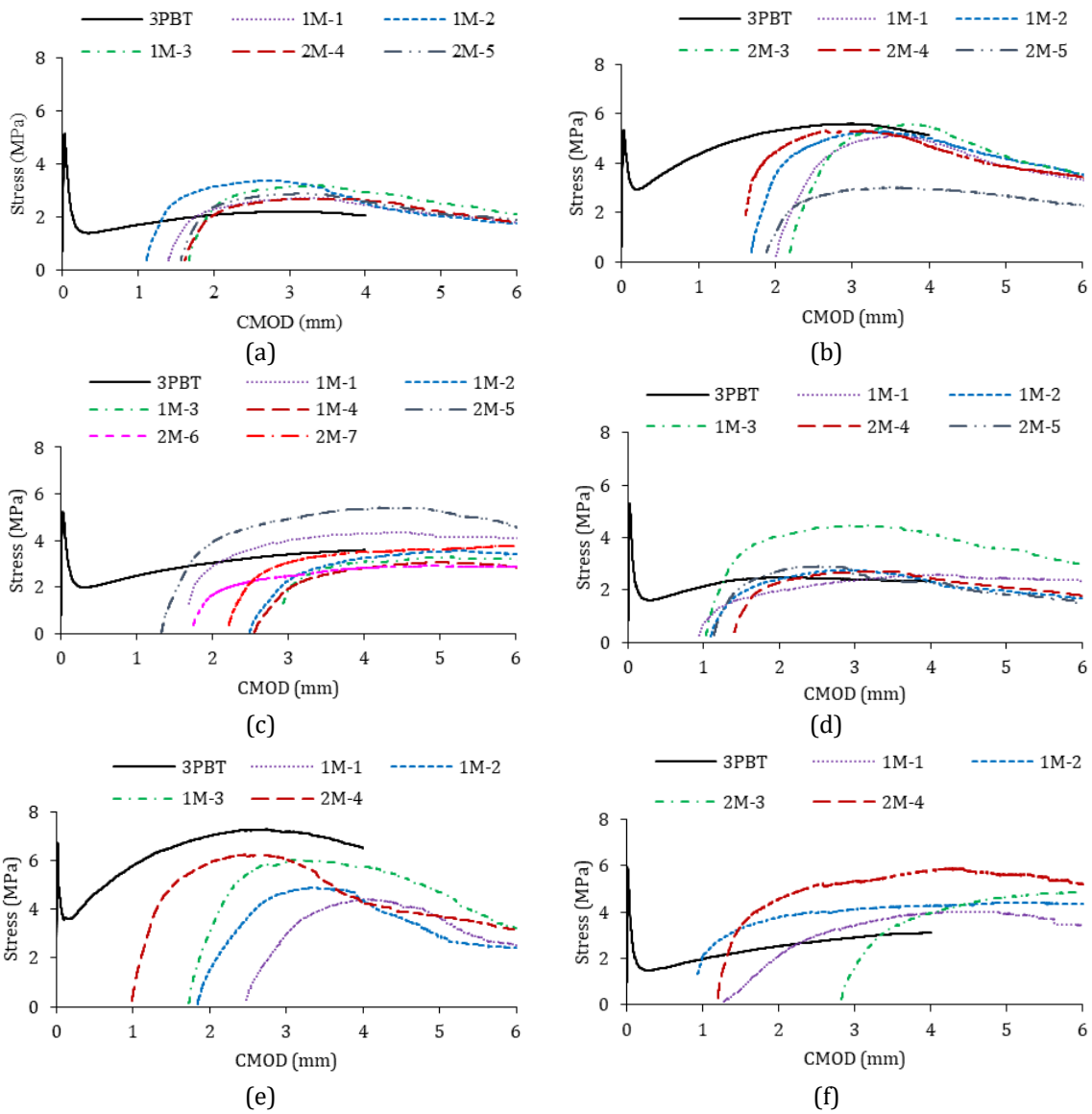

Figure 33 – Post-fatigue and control quasi-static strenth-CMOD curves of PF1_5-1.1C (a), PF1_10-1.6E (b), PF2_10-1.5E (c), PF1_5-1.0C (d), PF1_10-1.4E (e) and PF2_10-1.9E (f)

No significant difference in the post-fatigue maximum strength and the corresponding CMOD was observed between specimens subjected to a N_{max} of 1,000,000 or 2,000,000 cycles. The relatively small level of stiffness degradation between these cycles (only a 15% decrease in damage ratio) is eclipsed by the scatter observed in the tests. Studies in the literature report an increase in the maximum strength of specimens after load cycles in comparison with specimens subjected only to quasi-static tests (Nagabhushanam et al. 1989; Parant et al. 2007; Ramakrishnan et al. 1989). This increase is associated with the application of cyclic load below the endurance limit (Chanvillard et al. 2004; Naaman and Hammoud 1998; Parant et al. 2007;

Ramakrishnan et al. 2014) and depends on the stress ratio during the test (lower stress ratios promote higher post-fatigue strength) (Parant et al. 2007; Ramakrishnan and Sivakumar 1999). Such increase is attributed to the consolidation of microvoids at the beginning of the fatigue test (Zhang and Wu 1997), the relatively long duration of the tests (Federation Internacionale du beton 2000) and the stochastic nature of concrete (Fib 2013; Lohaus et al. 2012). The similar residual flexural strengths found in specimens characterised before and after the fatigue test do not support the findings by other studies in the literature.

To go deeper in this analysis, Figure 34 (a) and (c) show the relationship between f_{R1} and the corresponding maximum strength measured in the post-cracking stage ($f_{res,cycl}$ for specimens subjected to the fatigue test or $f_{PC,max}$ for specimens not subjected to the fatigue test) of 150×150×600 mm^3 and 75×75×275 mm^3 PFRC beams, respectively. Notice that f_{R1} was obtained before the fatigue test in all specimens, while the others were obtained either before or after the fatigue test depending on the procedure adopted for each specimen. Should the load cycles affect the resistant capacity of the specimen, the series subjected to the fatigue test would follow a different trendline from those not subjected to the fatigue test in Figure 34 (a/c). By contrast, no significant influence of the load cycle on the maximum post-fatigue resistant capacity would be expected if all specimens follow the same trendline. The analysis of Figure 34 (a) and (c) confirms this last conjecture, as no clear difference was found regardless of the application or not of the load cycles.

Specimens PF1_10-1.6E_2M-5, PF2_10-1.5E_2M-5 and PF1_5-1.0C_2M-3 are considered outliers in their respective series. The difference in behaviour is explained by the number of fibres crossing the fracture cross-section. PF1_10-1.6E_2M-5 has 26% fewer fibres than the specimen with the second-lowest number of fibres in the same series and 30% less than the average of the other specimens in the series. The number of fibres in PF1_10-1.6E_2M-5 is closer to the average found in PF1_5-1.1C than in PF1_10-1.6E, thus explaining why its residual strength after the fatigue test approximates more the former than the latter. The opposite happens with PF2_10-1.5E_2M-5, which has 39% more fibres in the fracture surface than the specimen with the second-highest number of fibres in the same series and 61% more than the average of the other specimens in the series. In this case, the number of fibres is closer to that of PF1_10-1.6E than to that of PF2_10-1.5E, thus explaining why the residual strength of PF2-1.5E_2M-5 approximates the former. The same assumption explains PF1_5-1.0C_2M-3 response, which has 52% more fibres than the average of the respective series. Figure 34 (b) and (d) shows the relationship between the number of fibres in the cross-section and $f_{res,cycl}$ of

150×150×600 mm³ and 75×75×275 mm³ specimens, respectively. The same figures show the linear regression for results obtained in mixes with PF1 and PF2. As expected, in all cases, there is a linear trend between $f_{res,cycl}$ and the number of fibres in the cross-section.

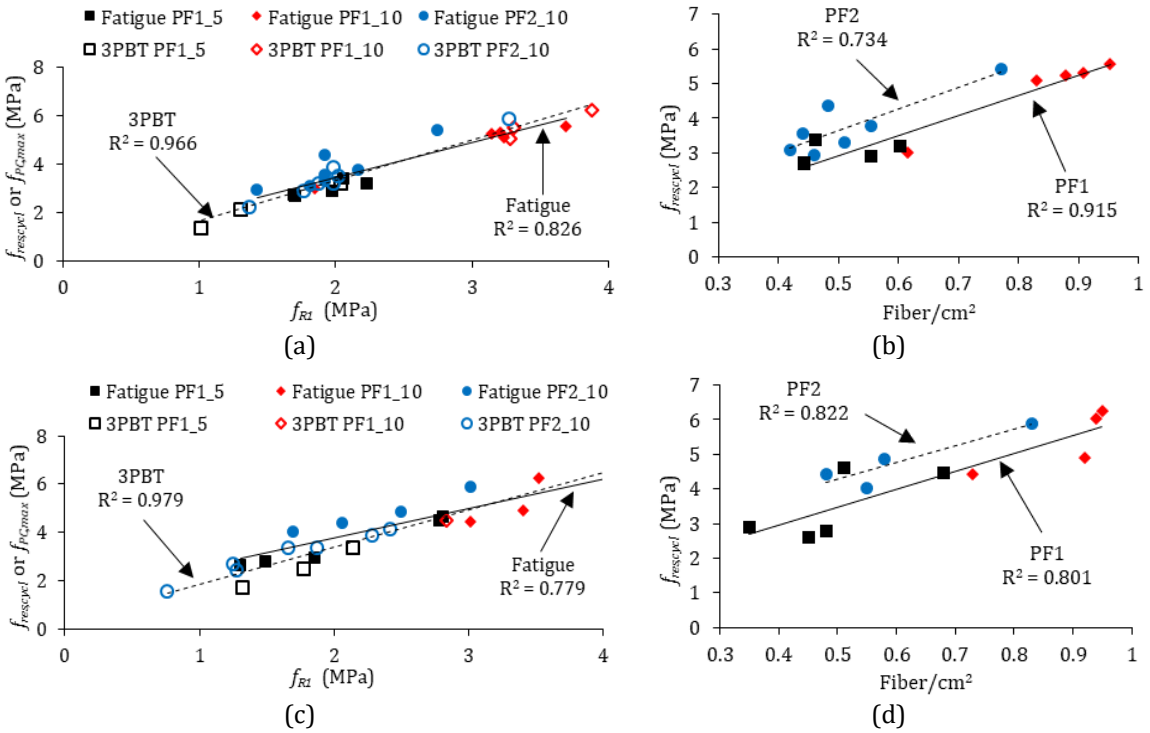

Figure 34 – Relationship between $f_{res,cycl}$ or $f_{PC,max}$ and f_{R1} for 150×150×600 mm³ (a) or 75×75×275 mm³ (c) specimens subjected to the control or fatigue tests and between $f_{res,cycl}$ and fibre/cm² for 150×150×600 mm³ (b) or 75×75×275 mm³ (d) specimens subjected to the fatigue test

4.4.4. Microscopic analysis of fractured surfaces

The inspection of the fracture surfaces revealed fibre with two failure modes. Some fibres were pulled out of the matrix and presented surface abrasion (Figure 35 a). The fibre tips were not sharpened, and loose particles of the cementitious matrix were attached to it (Figure 35 b), revealing the growth of microcracks and matrix damage (Müller and Mechtcherine 2017). Other fibres displayed damage characteristic of significant deformation, with fibrillation and cut tips, indicating that the surface layer was peeled off by the surrounding matrix (Figure 35 c and d) (Müller and Mechtcherine 2017; Qiu and Yang 2014). Both failure modes were found in all specimens without significant differences regardless of the fibre content, fibre type, maximum number of load cycles or application of load cycles. The lack of evident differences is consistent with the findings in terms of residual strength, which also showed no evident influence of the load cycles on the residual tensile strength.

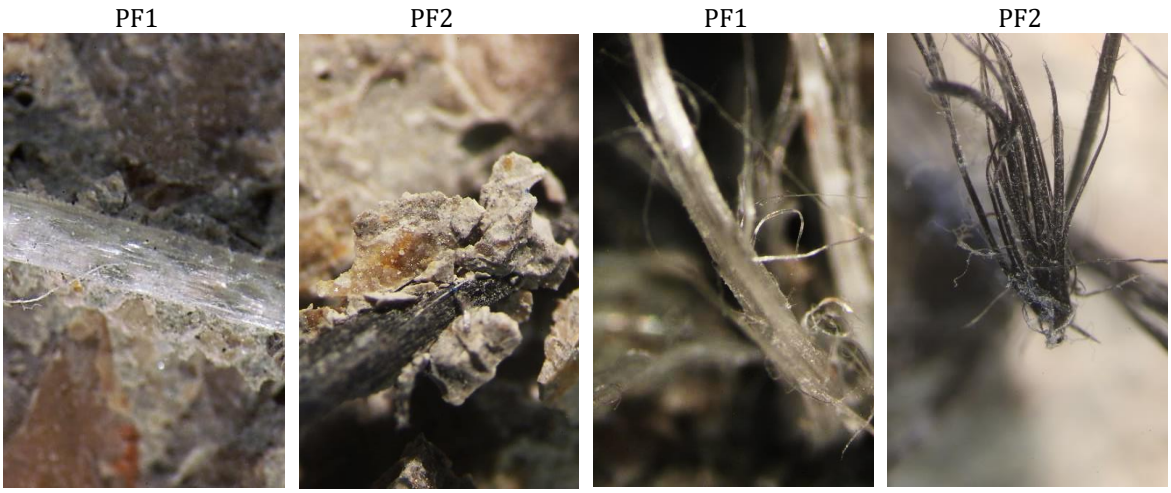

Figure 35 – Polypropylene fibres after residual strength test

4.4.5. Crack evolution equation

From a structural design point of view, is crucial to predict the crack opening after a fixed number of cycles have occurred. As the post-fatigue flexural strength is not affected by fatigue loading and it can be deduced from the equivalent flexural 3PBT load for a given CMOD, a constitutive relation to predict the fatigue crack opening in bending during service state for the investigated PFRC is proposed. The equation is derived from the fatigue flexural tests and can be used to design PFRC structures for which the crack width can be a governing parameter.

For each experimental curves of (Figure 29), the evolution of CMOD along fatigue cycles followed a power law function, defined by Eq. (4.2), where a and b an exponent parameters depending on the material properties. Table 19 presents the values of parameters a and b and the respective R^2 of 150×150×600 mm^3 beams (size considered by EN 14651:2007) (Figure 29 (a-c)). Both parameters are very similar regardless of fibre type and content.

$$CMOD(n) = a \cdot n^b \tag{4.2}$$

In order to understand the differences obtained within the experimental results, the Pearson product moment correlation (r_p) was taken into account (α of 0.05) to detect linear relationship between the values (variables) of the estimated parameters a and b and experimental results. Pearson correlation coefficient confirmed that the value of a is correlated to the applied load (r_p = -0.736, p-value = 0.015) and the value of b is correlated to the crack opening during phase II (r_p = 0.891, p-value = 0.005). This reveals that slope of the power function is correlated with the exponent b. Since parameter b is difficult to predict as b depends on the crack opening development, the value of b was fixed (b_P) considering the average values

of the experimental regression lines of the three investigated concretes (b_P = 0.16) and Eq. (4.2) rewritten to Eq. (4.3). The experimental equations were recalculated and the new values of parameter a (a_w) and the respective R^2 are presented in Table 19.

$$w(n) = a_w \cdot (n)^{0.16} \quad (4.3)$$

Table 19 – Calculated values of a_w and respective R^2

		Parameters from best-fit curve			*a(w)* recalculated by Eq. (2)	
	#	a	b	R^2	a_w	R^2
PF1_5-1.1C	PF1_5-1.1C_1M-1	0.309	0.123	0.991	0.192	0.900
	PF1_5-1.1C_1M-2	0.278	0.116	0.982	0.158	0.842
	PF1_5-1.1C_1M-3	0.274	0.144	0.986	0.224	0.974
	PF1_5-1.1C_2M-4	0.322	0.123	0.995	0.194	0.902
	PF1_5-1.1C_2M-5	0.251	0.139	0.994	0.189	0.972
PF1_10-1.6E	PF1_10-1.6E_1M-1	0.189	0.190	0.970	0.275	0.942
	PF1_10-1.6E_1M-2	0.274	0.133	0.980	0.193	0.939
	PF1_10-1.6E_2M-3	0.190	0.184	0.980	0.262	0.964
	PF1_10-1.6E_2M-4	0.277	0.124	0.991	0.173	0.907
	PF1_10-1.6E_2M-5	0.276	0.141	0.980	0.215	0.963
PF2_10-1.5E	PF2_10-1.5E_1M-1	0.265	0.139	0.960	0.204	0.935
	PF2_10-1.5E_1M-2	0.168	0.209	0.981	0.316	0.926
	PF2_10-1.5E_1M-3	0.163	0.212	0.979	0.317	0.920
	PF2_10-1.5E_1M-4	0.159	0.213	0.981	0.314	0.920
	PF2_10-1.5E_2M-5	0.138	0.175	0.981	0.168	0.973
	PF2_10-1.5E_2M-6	0.172	0.169	0.980	0.197	0.969
	PF2_10-1.5E_2M-7	0.145	0.189	0.985	0.216	0.961

Parameter a_w was correlated with the studied variables to assign a_w a physical meaning. Figure 36 shows the equation to predict the value of a_w as a function of the crack increment per cycle (dCMOD/dn) and respective R^2. The dCMOD/dn can be used to predict the fatigue life as the acceleration in the damage process close to the failure does not influence on the total number of cycles (Destrebecq 2013; Mu et al. 2004). Nonetheless, the relationship between the crack increment per cycle and fatigue life is independent of the load range (Kolluru et al. 2000; Mu et al. 2004).

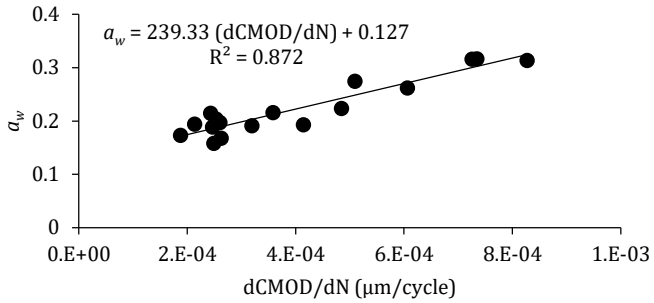

Figure 36 – Correlation between the crack increment per cycle and parameter a_w

The fitting parameter a_w can also be correlated with the ratio of damage, which expresses the stiffness degradation for a given stress amplitude and crack opening response. Figure 37 shows the equation to predict the value of a_w as a function of the damage ratio and respective R^2 for the studied PFRCs under service load.

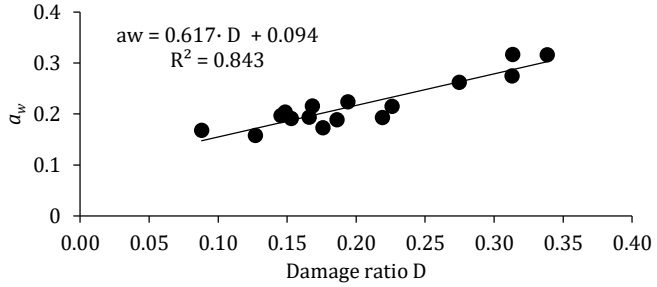

Figure 37 – Correlation between damage ratio and parameter a_w

To validate the application of Eq. (4.3), the characteristic crack opening displacement ($CMOD_k$) was compared to the best-fit line and the recalculated curve using Eq. (4.3) and shown in Figure 38 for PF1_5-1.1C (a), PF1_10-1.6E (b) and PF2_10-1.5E (c) with respective expressions and R^2. The $CMOD_k$ was calculated according to Student's *t*-distribution for a fractile of 5%, therefore 95% of the CMOD test results are expected to be comprised. Also, the $CMOD_k$ was calculated up to 1,000,000 cycles since the accumulated fatigue damage at 1,000,000 represents 85% of the damage at 2,000,000 cycles and follows a linear evolution.

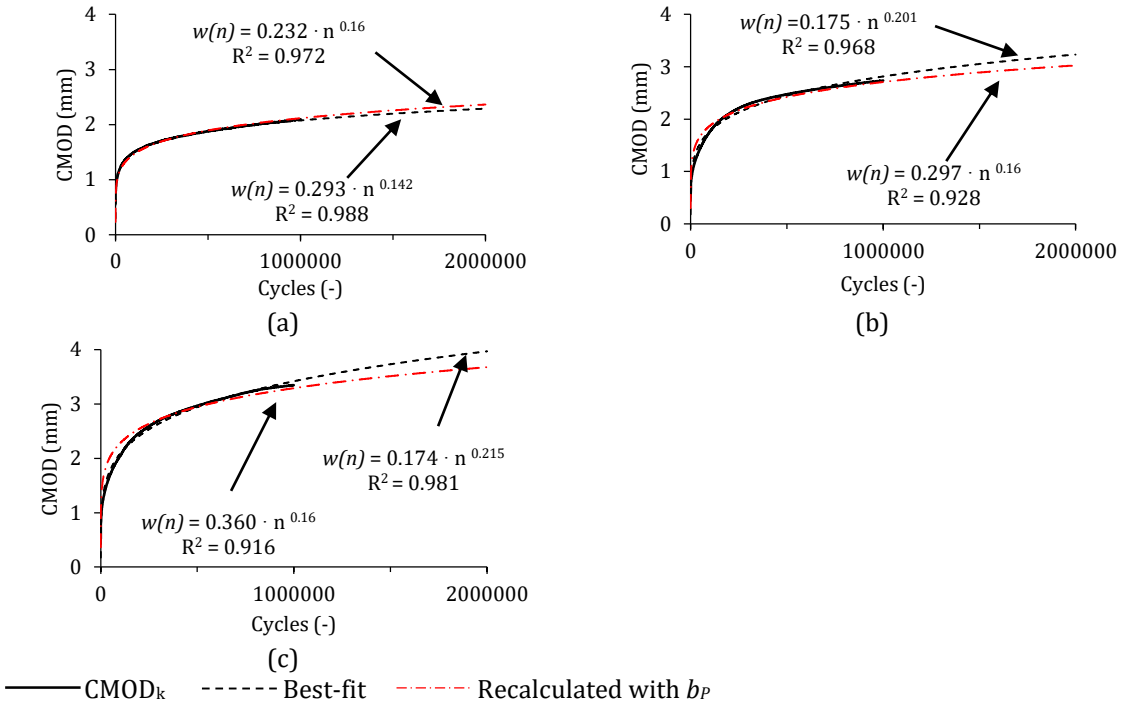

Figure 38 – Characteristic, regression line and recalculated curves for PF1_5-1.1C (a), PF1_10-1.6E (b) and PF2_10-1.5E (c)

From the expressions given by Eq. (4.3), considering the crack opening related to the ultimate limit state, PF1_5-1.1C, PF1_10-1.6E and PF2_10-1.5E would reach a maximum of 2,836,77, 605,895 and 182,068 cycles, respectively, at CMOD of 2.5 mm. In regards to the damage ratio, PF1_5-1.1C has D of 0.224, PF1_10-1.6E of 0.329 and PF2_10-1.5E the value of 0.431. The damage ratio of PF2_10-1.5E exceeds the limit of 0.4 which ensures safety (Destrebecq 2013; Federation Internacionale du beton 2000), therefore a maximum value of *a(w)* equal to 0.341 can be established. Nevertheless, the post-fatigue residual strength has to be taken into consideration for design purposes. The similarity between curves suggest that Eq. (4.3) can be used to predict the crack opening evolution a given number of cycle for the studied PFRCs.

4.5. Concluding remarks

The main findings of this research are outlined below.

- The mechanism of crack development during load cycles was independent of the adopted fibre content and determined by the distribution and orientation of fibre is

the cross section. The number of fibre existing into the pre-cracked cross section are responsible for determining P_{upp};

- Although the specimens were pre-cracked, the initial evolution of CMOD along dynamic cycles displayed a great increase attributable to the high elongation and deformation of the polypropylene fibres. From 350,000 cycles onwards, CMOD follows a continuous trend until the end of test without evidences of fatigue failure until 2,000,000 cycles;
- The stress-CMOD curve indicates that main loss of stiffness occurs during the initial cycle and the continuous decrease of the slope of the unloading stage denotes the degradation of the specimens. Hysteresis loops are similar along the 2,000,000 cycles, showing the constant energy dissipation due to progressive cracking;
- The post-fatigue response revealed that the bond strength between fibre-matrix interface of PFRCs was not affected by the previous dynamic cycles. Post-fatigue strength variations when compared to the quasi-static behaviour might be a consequence of the high variability found in flexural and fatigue tests and the orientation and distribution of fibre. The static load-CMOD curve might be used as a criterion to predict the residual strength;
- PFRC presented two different failure modes: (1) pulled out fibres, with surface abrasion and attached loose particles of cementitious matrix, and (2) damaged fibre with fibrillated sections, delamination and sharpened tip. Fatigue failure in PFRC vary from fibre-matrix bond degradation to a secondary damage process due to the accumulation of plastic deformations of the fibre;
- The proposed equation is able to predict the crack opening for a given number of cycle. This crack evolution conceptual mechanism has been found to be the first approach existing into the current literature and this can be considered in future revisions of the FRC structures design guidelines.

5. FATIGUE DESIGN

5.1. Introduction

The increasing amount of fibre reinforced concrete structures subjected to fatigue requires development of specific description of the material behaviour, testing standards and codes of design practice. Recommendations, technical reports and guidelines on fatigue in concrete are available, such as the Det Norske Veritas (DNV GL AS 2017), the Japan Recommendations for Design and Construction of High Performance Fiber Reinforced Cement Composites (Japan Society of Civil Engineers 2008), the ACI Considerations for Design of Concrete Structures Subjected to Fatigue Loading (ACI Committee 215 1974), the DNV GL standard (DNV GL AS 2016), the French standards (AFNOR 2016a; AFNOR 2016b), the draft of the German guideline (Schmidt et al. 2017), the European Committee for Standardization (EN1992-1-1 2005) and the *fib* Model Code 2010 (Fib 2013). Most of these publications report the fatigue behaviour of concrete without fibre reinforcement and under compression, just a few take into consideration the flexural tensile response. Nevertheless, those reports dealing with flexural tensile fatigue are valid for uncracked sections while only a few give recommendations for post-cracking fatigue response.

Another issue when considering fatigue load design requirements of fibre reinforced concrete structures is that different types and volumes of fibres have different responses and

generic conditions may lead to under or overestimations of reliable stress levels and fatigue life. Since post-cracking strength varies with increasing crack opening, at least two deformation values should be considered: (1) deformations that are significant for SLS verifications associated to f_{R1}, and (2) deformations that are significant for ULS verifications in respect to associated to f_{R3}.

Surrounding conditions and inherent quality of FRC element itself produce scatter of test results. The main sources of scatter can be classified into three groups (Cavalaro and Aguado 2015): the intrinsic scatter of the material, caused by random distribution and orientation of the fibres; the process of production of the samples; variations associated to the precision of the equipment and set-up used in the test. This variation becomes more pronounced when interpreting fatigue results, once the phenomenon itself is known for having considerable scatter (Fib 2013; Fib 2008). This characteristic leads to either the formulation of models that take into account logical basis for analysing design uncertainties to ensure the adequate evaluation of failure probability (Oh 1986); or introduce high safety coefficients to assess the imprecision in fatigue prescriptions within construction codes (Tarifa et al. 2018). Validation of the structural safety should consider values of crack opening correspondent to the expected fatigue life of the element during its service life (González et al. 2018). This chapter presents the design concepts provided by *fib* Model Code 2010 (Fib 2013), a proposal of fatigue design limitations for FRC and a conceptual model for the behaviour of the investigated FRCs under flexural load cycles that can inform future FRC design codes.

5.1.1. Objectives

The main objective of this chapter is to propose a conceptual model for the behaviour of the investigated FRCs under flexural load cycles. For this, specific objectives are defined:

- Describe the theoretical basis and requirements of design concepts guidelines of Model Code (Fib 2013);
- Propose design instructions based on the experimental results in terms of crack opening and applied fatigue load ratio;
- Validate the results of the experimental campaign into the proposed model of crack opening prediction.

5.1.2. Outline of the chapter

This chapter provides an overview of the fatigue design concept focusing on the verifications methods provided by *fib* Model Code 2010 (Fib 2013) in regards to the fatigue state limit. Also, results of the experimental campaign allowed to suggest FRC fatigue design limit conditions and to develop a semi-empirical model to predict the crack opening evolution and the remaining flexural strength.

5.2. Design concept

The primary target of current codes and standards is to guarantee the stability and serviceability of structures for economical compatibility and changing environmental conditions (Urban et al. 2014). Most fatigue procedures are based on the endurance of a structure, that is the structure can withstand cyclic loads during its service life. In practical design, limit states are related to structural response and further deterioration under a specific situation. Serviceability limit state (SLS) correspond to the inadequacy of the purpose (wide cracks, vibration, temporary large deformations etc.) or appearance of a structure or a structural component. Ultimate limit state (ULS) is associated with structural (near-)collapse, protection and life/environment safety (Fib 2013). In many cases, the risk of damage is indirectly excluded by ultimate limit state verifications. Fatigue limit state or resistance, corresponds to an ULS as loads below the static strengths may affect serviceability, durability and safety of a structure.

Model Code (Fib 2013) provides four fatigue design considerations according to level of sophistication: *level I approximation* is a qualitative verification that no variable action is able to produce fatigue; *level II approximation* establishes that the maximum design stress range in the steel, concrete compressive stress and tensile stress in plain concrete do not exceed determined design limit values; *level III approximation* considers a dominant fatigue load in the required service life associated with a maximum number of cycles to failure; and *level IV approximation* which consider the fatigue damage verification based on a spectrum of load levels. This verification considers uniaxial compression, tension, or reversed loads. Stress-life (S-N) curves are developed for normalized maximum compressive stresses, constant amplitude and for frequencies higher than 0.1 Hz for various concrete compressive strengths. The curves produced correspond to normalized minimum effective compressive stress levels with the compressive strength from 0 to 0.8.

Taking the characteristic compressive strength f_{ck} as a reference, the design fatigue strength $f_{cd,fat}$ in compression is given by Eq. (5.1).

$$f_{cd,fat} = 0.85 \cdot \beta_{cc}(t) \cdot \frac{f_{ck}}{\gamma_{c,fat}} \cdot \left(1 - \frac{f_{ck}}{400}\right) \quad (5.1)$$

where $\beta_{cc}(t)$ is the coefficient which depends on the age t of the concrete in days when fatigue loading starts and $\gamma_{c,fat}$ is a partial safety factor equal to 1.5. From Eq. (5.1), the first term ($0.85 \cdot \beta_{cc}(t) \cdot \frac{f_{ck}}{\gamma_{c,fat}}$) is related to the static compressive design strength (f_{cd}), while the second part $\left(1 - \frac{f_{ck}}{400}\right)$ is a strength-dependent term (α_{fat}) (Lohaus et al. 2012). The additional reduction due to α_{fat} increases with greater values of f_{ck}, which corresponds to a 0.88 reduction in term of α_{fat} for concretes of strength grades of C50, and, consequently, the design fatigue reference strength conceives 50% of the characteristic compressive strength. Figure 39 illustrates the comparison between characteristic compressive strength and design fatigue strength.

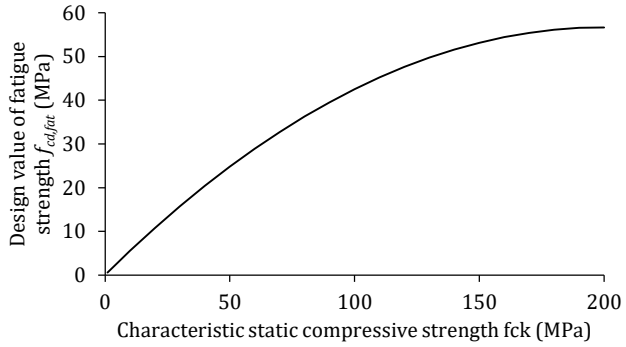

Figure 39 – Comparison between characteristic compressive strength fck and design fatigue strength $f_{cd,fat}$ according to Model Code (Fib 2013)

The fatigue life N is calculated according to the Model Code (Fib 2013) through Eq. (5.2) and (5.3):

$$\log N = \log N_1 \; if \; logN_1 \leq 8 \quad (5.2)$$

$$\log N = \log N_2 \; if \; logN_1 > 8 \quad (5.3)$$

where $\log N_1$ and $\log N_2$ can be expressed by Eq. (5.4) and (5.5) (Eq. 7.4-7a and Eq. 7.4-7b of Model Code, respectively):

$$\log N_1 = \frac{8}{(Y-1)} \cdot \left(S_{cd,max} - 1\right) \quad (5.4)$$

$$\log N_2 = 8 + \frac{8 \cdot \ln(10)}{(Y-1)} \cdot (Y - S_{cd,min}) \cdot log\left(\frac{S_{cd,max} - S_{cd,min}}{Y - S_{cd,min}}\right) \quad (5.5)$$

with Y expressed by Eq. (5.6):

$$Y = \frac{0.45+1.8 \cdot S_{cd,min}}{1+1.8 \cdot S_{cd,min}-0.3 \cdot S_{cd,min}^2} \quad (5.6)$$

where $S_{cd,max} = \gamma_{Ed} \cdot \sigma_{c,max} \cdot \eta_c / f_{cd,fat}$ and $S_{cd,min} = \gamma_{Ed} \cdot \sigma_{c,min} \cdot \eta_c / f_{cd,fat}$ are the respective maximum and minimum compressive stress level; $\sigma_{c,max}$ and $\sigma_{c,min}$ are the maximum and minimum compressive stress, respectively; η_c is an averaging factor considering the stress gradient; $f_{cd,fat}$ is the design fatigue reference strength for concrete in compression; and γ_{Ed} is the load factor assumed equal to 1.1 (or 1.0 if stress analysis is sufficiently accurate or conservative).

Lastly, level *IV approximation* ponders the fatigue damage for a spectrum of load levels and the expected damage D should not exceed the limit value of damage D_{lim} (Palmgren-Miner cumulative damage rule gibe by Eq. (5.7) (Eq. 7.4-10 of Model Code)).

$$D = \sum_{i=1}^{j} \frac{n_{Si}}{N_{Ri}} \leq D_{lim} = 1 \quad (5.7)$$

where D is fatigue damage, n_{Si} denotes the number of acting stress cycles associated with a given stress level and stress range and N_{Ri} denotes the number of cycles causing failure at the same stress level and stress range. The value of the Palmgren-Miner sum indicating failure is varying in various codes from 0.2 to 1.0. Consequently, the Palmgren-Miner rule is only a very rough approximation of the actual concrete behaviour. It may over- or underestimate the actual fatigue strength of concrete subjected to varying repeated loads. In any case, Model Code (Fib 2013) permits the use of characteristic S–N curves determined from fatigue tests results, considering type of concrete and fibre volume, purpose of the structure, environmental conditions, maintenance methods, etc. without any restriction (Fib 2013). Also, Model Code (Fib 2013) provides an equation to the progressive deflection under fatigue loading in the SLS. The cyclic effect can be calculated from Eq. (5.8) (Eq. 7.4-13 of Model Code).

$$a_n = a_1[1.5 - 0.5\, exp(-0.03n^{0.25})] \quad (5.8)$$

where a_n final deflection after n cycles, a_1 deflection in the first cycle due to the maximum load.

The fatigue design equations presented by Model Code consider reinforced and prestressed concrete members: reinforced concrete in tension is considered to be cracked and in the case of prestressed members if the relevant section is susceptible to cracking. Another issue related to fatigue design of FRC following the Model Code (Fib 2013) equations is that these equations consider the concrete compressive strength, however the structural design of

FRC elements is based on the post-cracking residual strength provided by fibre reinforcement. In compressive relations, where the benefits provided by the fibre are negligible, conditions that are valid for plain concrete are applicable to FRC. Therefore, due to the nature of FRC, optimized solutions and performance versus cost of FRC structures design are better sustained by experimental tests (Fib 2013).

5.3. Proposed limitations for fatigue design of FRC

Design procedures for the fatigue limit state consist of a comparison between design value of fatigue actions and fatigue strength. Two approaches can be adopted to assess the fatigue life: (1) the empirical fatigue life (S-N) curves and (2) the analysis of the crack propagation, both are described below. In view of that and from the results found in the conducted experimental campaign, some limitations are suggested in order to simplify the fatigue design of FRC elements under bending.

Accurate S-N curves demand an extensive experimental campaign to provide reliable relationships between maximum number of cycles for a given stress level before failure. Figure 40 illustrates fatigue life assessment through a S-N curve.

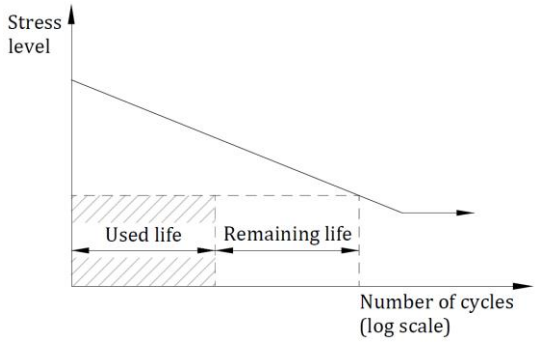

Figure 40 – Fatigue life evaluation based on S-N curve

Constitutive equations for HPFRC and SFRC presented in chapter 3 showed that both FRC displayed a fatigue endurance limit of 2,000,000 cycle of the order of 0.66 of f_{R1}. Also, results of post-fatigue quasi-static reload of HPFRC, SFRC and PFRC suggest that previous fatigue cycles under endurance limit do not affect the post-fatigue load bearing capacity. In view of that, the following statements are proposed: if applied cyclic loading ratio (Q_{fat}) is greater than 60% of the static f_{R1} ($Q_{f_{R1},stat}$), failure can be expected and the ultimate strength under fatigue loading is smaller than the ultimate strength obtained in quasi-static loading ($f_{R3,fat} <$

$f_{R3,stat}$). In contrast, if $Q_{fat} < 0.6\ Q_{f_{R1},stat}$ the ultimate strength under dynamic cyclic load can be assumed equal to the ultimate static strength ($f_{R3,fat} \cong f_{R3,stat}$). It is important to say that the improvement in f_{R3} post-fatigue compared to the static f_{R3} found should not be consider as there is not sufficient data to confirm this increase.

Crack propagation occur as a result of the progressive damage accumulation which induces a loss in the serviceability and may compromise the global stability of the structure. Fatigue cracks in concrete have no particular pattern, unlike fatigue cracks in steel (Comité Euro-international du Béton 1988). This is especially significant in tension, where differences in internal material structure of concrete affect the crack propagation. In the case of fibre reinforced concrete pre-cracked sections, the global fatigue response is greatly influenced by geometry, surface texture and mechanical properties of the fibres. Data presented in chapter 3 indicate that critical crack opening associated to failure for a given stress level can be estimated from the envelope curve (quasi-static response) (Figure 41 (a)). In the case that the expected maximum crack for a given stress level throughout service life do not reach the envelope curve, the remaining life can be estimated (Figure 41 (b)). The fatigue crack propagation evolution analysis also indicates if the applied dynamic load can affect service conditions, illustrated by Figure 41 (b). After the fatigue cycles, the final crack opening can surpass the maximum CMOD acceptable in serviceability state (> $CMOD_1$), however if the specimen is monotonically reloaded, remaining capacity of the section (f_{R3}) is not affected.

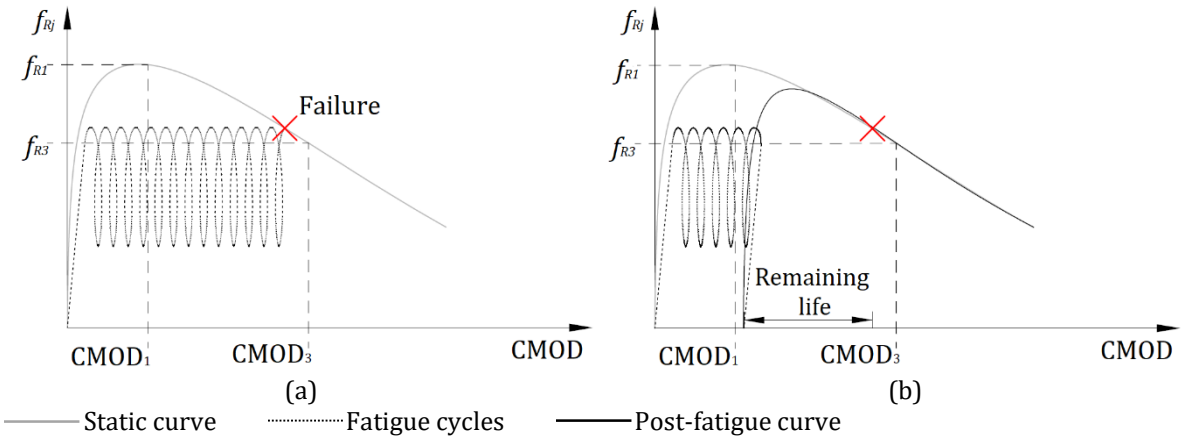

Figure 41 – Fatigue life assessment in terms of crack propagation: fatigue failure (a) and remaining life (b)

Another approach to estimate the critical crack opening is from the crack increment per cycle taken from cyclic creep curves. The secondary branch shows an stable crack increment per cycle and a linear ascent up to about 80% of the total number of cycles (Fib 2008). Just

before reaching failure, after the linear growth all curves presented “phase III” (rapid increase of deformations), therefore the value of 0.8 N can be set as a limit number of cycles where no damage in the post-fatigue residual strength is expected. Figure 42 illustrates the philosophy of fatigue life prediction based on an initial crack opening (w_0), expected crack opening after fatigue load (w_{exp}) or number of cycles (service life) (N_{exp}) and maximum crack opening considering failure of structure ($w_{failure}$). This purpose states that if the maximum crack opening expected during service life is smaller than the $w_{failure}$ as a function of 0.8 N, or the final number of cycles is less than 0.8 N, the residual strength after cycles may follow and can be predicted by the quasi-static monotonic load-displacement curve.

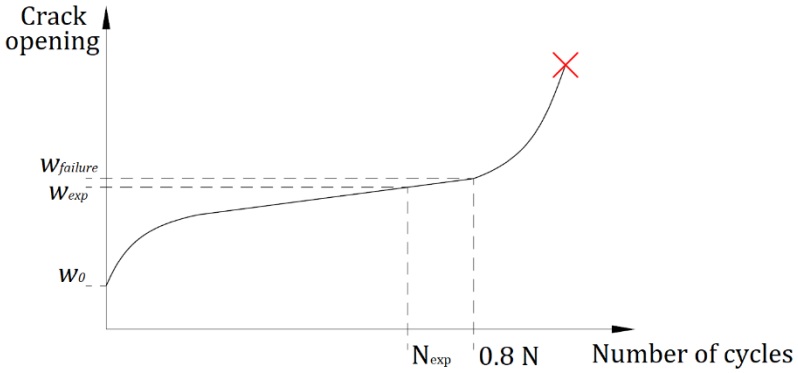

Figure 42 – Conceptual prediction of critical crack opening through cyclic creep curve

Assess the fatigue life through cyclic creep curve can provide valuable information about reliability with respect to the ultimate limit state and maintenance and repair considerations: as shown in chapter 3, HPFRC and SFRC specimens failed with applied load levels lower than the probable value of f_{R3} (considering the monotonic f_{R3}/f_{R1} relation) at lower CMOD than $CMOD_3$. Likewise, PFRC specimens (chapter 4) withstood cyclic dynamic loads at higher CMOD values than $CMOD_3$ with no effect in the residual post-fatigue strength.

5.4. Conceptual model for crack evolution

The procedure of verifying the fatigue life can be relatively complex and demand long-term experimental campaign in comparison with usual static analysis. Constitutive equations of HPFRC and SFRC were presented in chapter 3 and for PFRC in chapter 4. With the purpose developing a model that is able to predict the fatigue behaviour and, consequently, reducing the time of fatigue tests, a conceptual model was developed and compared to the experimental results comprised within this thesis.

Figure 43 ((a) – PFRC and (b) – HPFRC) shows the typical curve that relates the logarithm of the total number of load cycles and the logarithm of CMOD variation between cycles (*dCMOD/dN*), which is a proxy for the incremental damage induced by the load cycles. This last parameter was calculated for intervals of 1000 cycles to simplify the assessment and reduce the influence of the scatter in the measurements of CMOD. The respective CMOD-log (*N*) curves (Figure 43 (c) – PFRC and (d) – HPFRC) were included to elucidate the further explanation. All PFRC specimens tested here presented a similar general trend (Figure 43 (a)) regardless of the fibre type or content. Points tend to align following a straight line until bigger number of cycles are reached, when smaller increments in CMOD are observed (stage II, showed in Figure 43 (c)), and the scatter between cycles leads to more variability in the parameter log (*dCMOD/dN*). Despite that, the envelope of the points in this region still follows the linear trend observed initially

The typical curve of log (*dCMOD/dN*) versus log (*N*) of "run-out" specimens of HPFRC and SFRC (Figure 43(b)) exhibited dispersion of points, which increased when reaching higher number of cycles. The initial linear part is not present and the shape of the curve is similar to the shape found in "stage II" of PFRC. In fact, cyclic creep curves of pre-cracked HPFRC and SFRC did not show stage I, therefore only stage II is presented in log (*dCMOD/dN*) vs. log (*N*) curves.

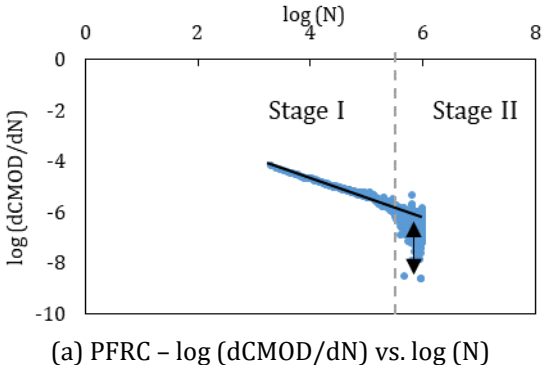

(a) PFRC – log (dCMOD/dN) vs. log (N)

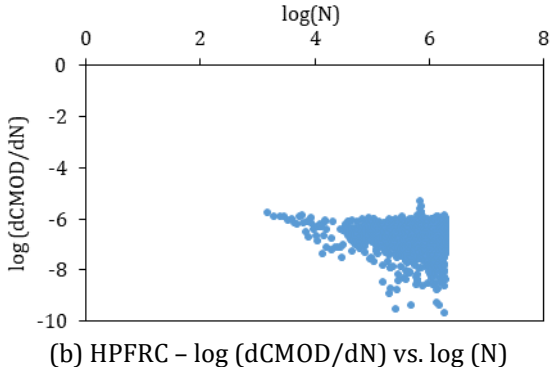

(b) HPFRC – log (dCMOD/dN) vs. log (N)

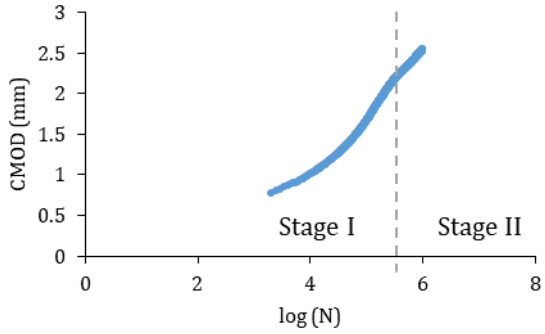

(c) PFRC – log (N) vs. CMOD

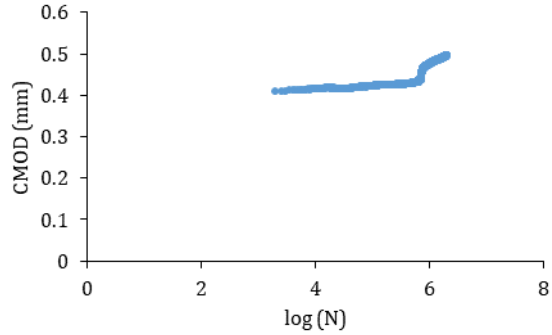

(d) HPFRC – log (N) vs. CMOD

Figure 43 – Typical relationship between log (*dCMOD/dN*) and log (*N*) and between CMOD and log (*N*) depicted by PFRC and HPFRC

Difference found between FRCs is attributable to fibre properties: lower elastic modulus, high elongation and deformation of the polypropylene fibres compared to the steel fibres leads to different fatigue failure modes. Steel fibres are activated after the first discontinuity of the static flexural strength curve (matrix crack), while PFRC shows a sudden stress drop after matrix crack and an increase stress when reaching higher CMOD values. Results suggest that stage I of PFRC can be associated to a "primary" fatigue led by accumulation of plastic deformations of fibres, which depends of fibre properties and stage II to a secondary damage process of fibre pull-out and cementitious matrix failure.

The stage I of the log ($dCMOD/dN$) vs. log (N) relationship in Figure 43 (a) is represented in Eq. (5.9). In this equation, v is related to the existing damage induced in the pre-cracking stage and u represents the increase in damage observed over the cycles. Parameters v and u are constants that may be determined experimentally by performing a limited number of cycles. The CMOD after N cycles (represented by $w(N)$) is calculated by integrating both sides of Eq. (5.9) in relation to dN, as shown in Eq. (5.10).

$$\log(dCMOD/dN) = u \cdot \log(N) + v \tag{5.9}$$

$$w(N) = \int_0^n dCMOD = \int_0^n 10^v \cdot N^u \cdot dn \tag{5.10}$$

The integration gives Eq. (5.11) for assessing the crack opening after the n cycles. The parameter w_o marks the initial damage taken as a reference in the test. Since the origin of CMOD was taken before pre-cracking in this experimental programme, w_o is 0. The parameters k_1 and k_2 are shown in Eq. (5.12) and (5.13), respectively.

$$w(N) = k_1 \cdot n^{k_2} + w_0 = k_1 \cdot n^{k_2} \tag{5.11}$$

$$k_2 = u + 1 \tag{5.12}$$

$$k_1 = 10^v / k_2 \tag{5.13}$$

The evolution of crack opening through the secondary damage ($CMOD_{II}$) is described by Eq. (5.14), which considers the final crack opening ($CMOD_I$) at the last cycle of stage I (n_{fI}) and α is the slope of the curve (Figure 44). Eq. (5.11) is rewritten to Eq. (5.15), thus allowing to predict the CMOD of the specimen subjected to the fatigue test.

$$CMOD_{II} = CMOD_I + \alpha \cdot (n - n_{fI}) \qquad n \geq n_{fI} \tag{5.14}$$

$$CMOD_I = k_1 \cdot n^{k_2} \qquad n < n_{fI} \tag{5.15}$$

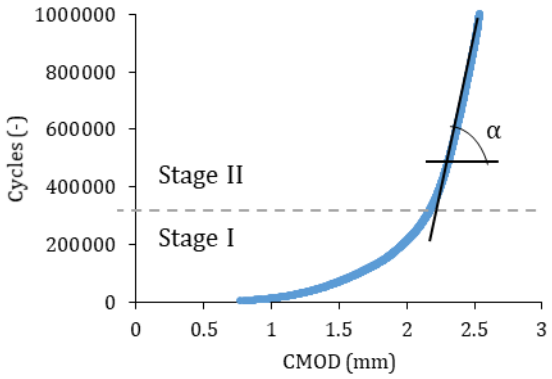

Figure 44 – Number of cycles versus CMOD curve highlighting stage I, stage II and parameter α

An optimisation procedure is proposed to determine when enough cycles have been applied to predict v and u so that the test can be interrupted and the values used to extrapolate the behaviour for a bigger number of cycles using Eq. (5.11). For a given intermediate cycle n bigger than 500 during the test of a particular specimen, it is possible to estimate u_n and v_n through the regression of the data up to n cycles using the relationship between *log(dCMOD/dN)* and *log(N)*. These parameters may be used in Eq. (5.12) and Eq. (5.13) to estimate $k_{1,n}$ and $k_{2,n}$, respectively. Both are used in Eq. (5.16) to estimate the average prediction error of the points obtained up to n cycles. Once the error reaches an acceptable value (0.1 mm in this study) or a clear minimum value, no more cycles are needed, and the test could be interrupted.

$$Error(n) = \frac{\sum_{N=500}^{n} \left| CMOD_{measured} - k_{1,n} \cdot N^{k_{2,n}} \right|}{n} \tag{5.16}$$

Figure 45 (a to f) shows the measured CMOD and the CMOD estimated with Eq. (5.14) and (5.15) using the optimisation procedure described above for a limited number of cycles in specimens from all polypropylene fibre reinforced compositions of the experimental campaign. All points are situated around the equivalence line with an R^2 bigger than 0.9508, which confirms that the model deducted here can adequately reproduce the overall fatigue behaviour of the PFRC even when a limited number of initial cycles are considered in the prediction.

To illustrate the potential of this approach to predict the flexural fatigue behaviour and shorten the fatigue test duration, Table 20 shows the minimum number of cycles (n) required to satisfy the maximum error condition in the optimisation procedure for the early interruption of the test and its proportion regarding the maximum number of cycles applied for each

specimen in this experimental program (N_{max}). The table shows the error of prediction expected supposing the early interruption of the test after n cycles and the use of parameter u_n and v_n to predict the CMOD expected at N_{max}. The average error for the whole curve considering the same u_n and v_n in Eq. (5.11) and the R^2 are also presented in Table 20.

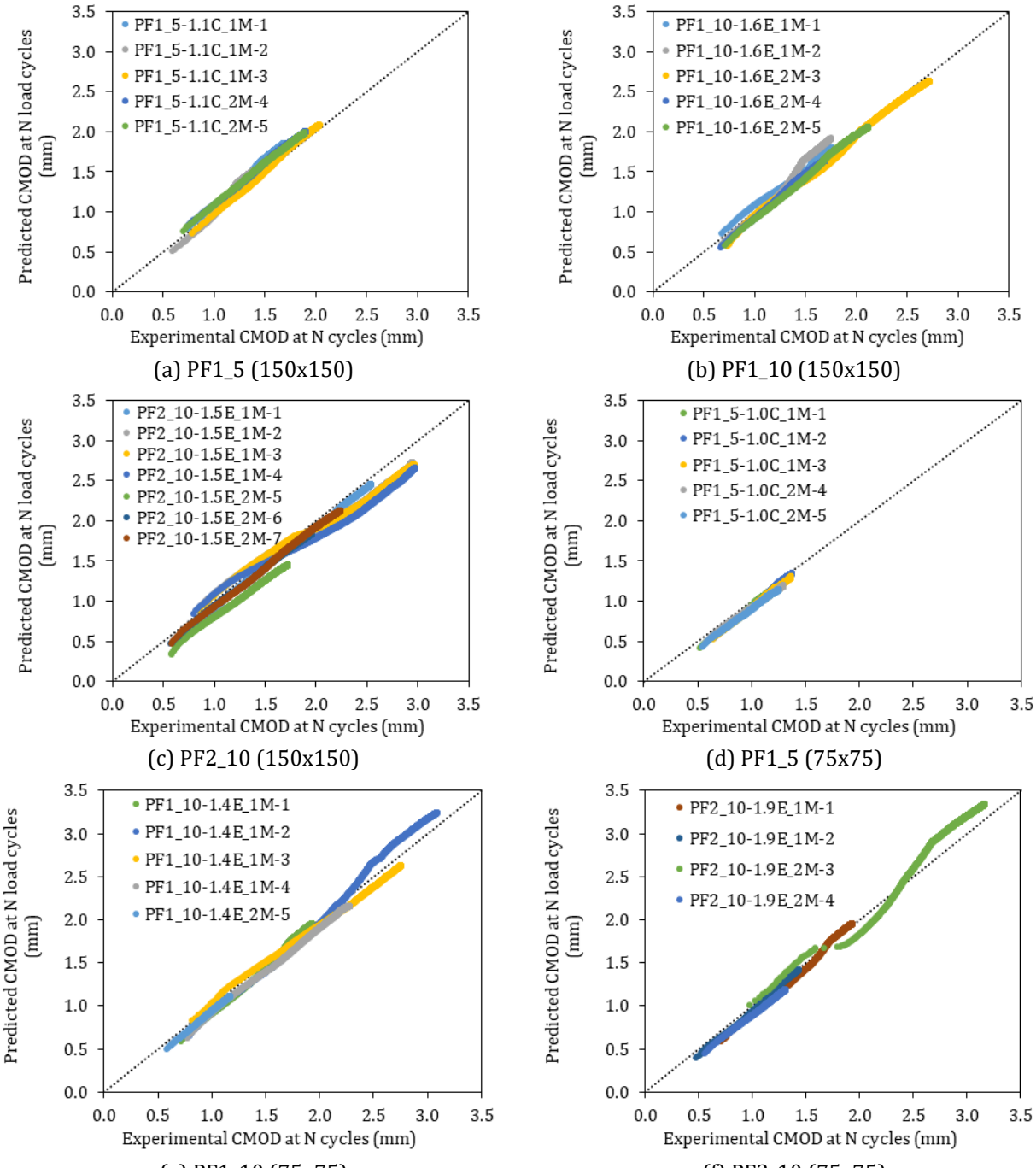

(a) PF1_5 (150x150)

(b) PF1_10 (150x150)

(c) PF2_10 (150x150)

(d) PF1_5 (75x75)

(e) PF1_10 (75x75)

(f) PF2_10 (75x75)

Figure 45 – Experimental versus predicted CMOD for all PFRC mixes ((150x150) stands for 150 x 150 x 600 mm beams and (75x75) for 75 x 75 x 275 mm beams)

Table 20 – Minimum number of cycles needed to predict u_n and v_n using optimisation procedure, error of CMOD prediction for the CMOD at N_{max} using Eq. (5.11), R^2 and average error of CMOD prediction for whole test

Specimen	Total number of cycles	Initial cycles used to estimate *u* and v		Error of prediction for maximum number of cycles (%)	Average error of prediction for whole curve (%)	R^2
		n	% of the total			
PF1_5-1.1C_1M-1	1000000	20000	2.0	13.9	10.33	0.9964
PF1_5-1.1C_1M-2	1000000	13500	1.4	19.4	8.64	0.9841
PF1_5-1.1C_1M-3	2000000	6000	0.3	4.6	2.64	0.9974
PF1_5-1.1C_2M-4	2000000	253500	12.7	11.0	6.80	0.9963
PF1_5-1.1C_2M-5	2000000	55000	2.8	8.4	6.63	0.9987
PF1_10-1.6E_1M-1	1000000	22000	2.2	10.3	2.88	0.9941
PF1_10-1.6E_1M-2	1000000	19500	2.0	15.5	8.64	0.9839
PF1_10-1.6E_2M-3	1000000	200500	20.1	12.8	2.41	0.9954
PF1_10-1.6E_2M-4	2000000	44000	2.2	8.5	2.20	0.9946
PF1_10-1.6E_2M-5	2000000	60500	3.0	15.1	2.22	0.9934
PF2_10-1.5E_1M-1	1000000	285000	28.5	8.5	4.03	0.9985
PF2_10-1.5E_1M-2	1000000	9000	0.9	7.8	7.68	0.9926
PF2_10-1.5E_1M-3	1000000	24500	2.5	8.3	7.92	0.9914
PF2_10-1.5E_1M-4	1000000	12500	1.3	14.8	11.38	0.9863
PF2_10-1.5E_2M-5	2000000	445500	22.3	9.6	16.35	0.9993
PF2_10-1.5E_2M-6	2000000	356000	17.8	8.4	5.45	0.9988
PF2_10-1.5E_2M-7	2000000	155500	7.8	6.1	4.41	0.9983
PF1_5-1.0C_1M-1	1000000	62500	6.25	0.75	5.12	0.9976
PF1_5-1.0C_1M-2	1000000	26500	2.65	3.12	3.00	0.9966
PF1_5-1.0C_1M-3	1000000	40500	4.05	6.40	5.73	0.9967
PF1_5-1.0C_2M-4	2000000	119500	5.98	4.52	7.75	0.9996
PF1_5-1.0C_2M-5	2000000	174500	8.73	8.12	8.76	0.9978
PF1_10-1.4E_1M-1	1000000	60000	6.00	12.21	2.52	0.9947
PF1_10-1.4E_1M-2	1000000	62500	6.25	12.97	5.48	0.9941
PF1_10-1.4E_1M-3	1000000	21500	2.15	3.84	3.99	0.9987
PF1_10-1.4E_1M-4	1000000	174500	17.45	0.95	4.98	0.9990
PF1_10-1.4E_2M-5	2000000	29500	1.48	2.79	5.40	0.9982
PF2_10-1.9E_1M-1	1000000	60000	6.00	36.99	2.52	0.9947
PF2_10-1.9E_1M-2	1000000	68500	6.85	5.12	1.95	0.9963
PF2_10-1.9E_2M-3	2000000	23000	1.15	26.70	6.63	0.9745
PF2_10-1.9E_2M-4	2000000	92000	4.60	3.04	9.72	0.9993

On average, the test can be interrupted after approximately 100,000 cycles, which equates to 5.0% of N_{max}. This represents an average reduction of 10 times on the total duration of the fatigue test. Such reduction and the application of the model from Eq. (5.11) would entail

an average error of prediction of CMOD for N_{max} of 10.0%. The average error of prediction for the whole curve would be 6.0%, which could be considered acceptable given the high scatter of the test and the significant reduction in the duration of the fatigue test.

In the case of both steel fibre reinforced concrete, only Eq. (5.14) is used (as cyclic creep curves of both FRC did not show stage I of damage) and $CMOD_1$ is the crack opening at the first cycle. Figure 46 (a) shows the measured CMOD and the estimated CMOD of "run-out" HPFRC specimens. Figure 46 (b) and (c) illustrate the application of the model on average values by stress level of measured CMOD and estimated CMOD of HPFRC and SFRC, respectively. Points that divert from the comparative line represent stage III. Correspondence between experimental and predicted CMODs suggests that the presented model is capable to appraise the CMOD variation over the load cycles.

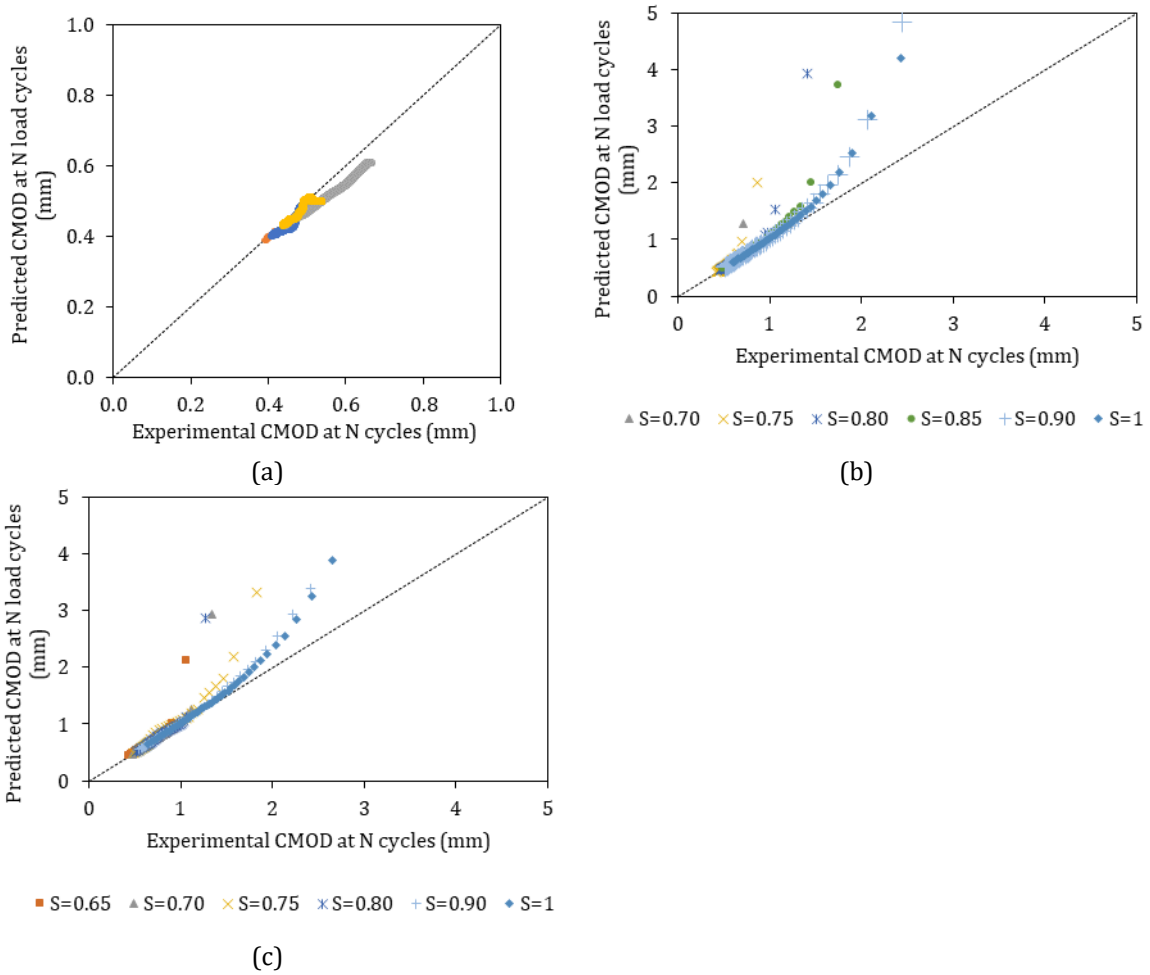

Figure 46 – Relationship between experimental versus predicted CMOD for "run-out" HPFRC specimens (a), average stress level value of CMOD development of HPFRC (b) and of SFRC (c)

5.5. Concluding remarks

The main findings of this research are outlined below.

- Differences in fatigue mode failure of investigated pre-cracked specimens of FRC are attributable to fibre properties. Stage I can be associated to a "primary" fatigue led by accumulation of plastic deformations of fibres, just found in PFRC, while stage II was observed in PFRC, HPFRC and SFRC and is related to a secondary damage process of fibre pull-out and cementitious matrix failure;
- From the experimental finding a fatigue life design limitation is proposed in terms of applied load: if $Q_{fat} \geq 0.6\, Q_{f_{R1},stat}$, failure is expected and $f_{R3,fat} < f_{R3,stat}$; if not $Q_{fat} < Q_{f_{R1},stat}$, $f_{R3,fat}$ can be assumed equal to $f_{R3,stat}$:
- Regarding crack opening, a fatigue life design limitation is suggested: if the maximum crack opening expected during service life is smaller than the $w_{failure}$ as a function of 0.8 N, or the total number of cycles < 0.8 N, the residual strength after cycles may follow and can be predicted by the quasi-static monotonic load-displacement curve;
- The numerical model to predict the fatigue behaviour is capable of predicting the CMOD variation over the load cycles of FRC. This model depends on parameters related with the initial damage due to pre-cracking (v) and the incremental damage induced by the cycles (u), which could vary depending on the loading regime, pre-cracking level and material characteristics. The optimising procedure proposed here to estimate v and u using a limited number of initial load cycles can enable a significant reduction in the duration of experimental programs about the fatigue of fibre reinforced concrete.

6. CONCLUSIONS

6.1. General conclusions

Fibre reinforced concrete has proven to be a suitable material for structural applications. On the other hand, the lack of studies on the flexural fatigue response showed that additional comprehension is needed. For this reason, the presented investigation intended to answer missing aspects by conducting an extensive experimental program together with theoretical studies on the cyclic and static behaviour of concrete reinforced with different types of fibre and volume. Together with the experimental results, a conceptual analysis and design limitations were proposed. In view of the general objectives presented in Chapter 1, general conclusions are drawn:

- The conducted experimental campaign was able to provide valuable information about FRC under flexural fatigue loading. The adopted method of pre-cracking and further application of percentages of f_{R1} allowed to compare results regardless differences in types of concrete, fibre nature or content;
- The post-fatigue response of all "run-out" specimens (despite type of concrete/fibre) showed that previous fatigue cycles does not seems to intervene in the post-fatigue quasi-static strength response and the load-displacement curve can be used as failure criterion under flexural fatigue loading;

- Depending of fibre type, different fatigue failure modes can be identified. Nonetheless, results exhibited similarities about CMOD evolution and critical width in terms of S and failure bond which were able to provide a basis for proposing design limitations;
- The numerical model to predict the fatigue behaviour is capable of accurately predicting the CMOD variation over the load cycles for the different fatigue failure modes identified within this experimental campaign. This model depends on parameters related with the initial damage due to pre-cracking and the incremental damage induced by the cycles, which could vary depending on the loading regime, pre-cracking level and material characteristics. The optimising procedure proposed here to estimate *v* and *u* using a limited number of initial load cycles can enable a significant reduction in the duration of experimental programs about the fatigue of fibre reinforced concrete.

6.2. Specific conclusions

In response to the specific objectives proposed in chapter 1, the specific conclusions of each subject addressed in the thesis are presented next:

Steel fibre reinforced concrete

- Considering the size of specimens adopted, static and dynamic tests indicate higher dispersion of SFRC results compared to HPFRC most likely due to considerable lower number of fibres bridging the damaged zone, consequently minor variations in fibre orientation and distribution can have great influence in the overall behaviour;
- Through cyclic creep curves, it is possible to see that the slope of the crack increment per cycle is influenced by the applied the load level which increases leading to growth of the crack opening displacement. Higher applied load level induces to a smoother curve at phase III at higher CMOD. This suggests that higher S could lead to failure through a continuous pull-out of the fibres, while smaller S can be responsible for the progressive weakening of the fibre-matrix interface through micro-cracks;

- Critical CMOD before fatigue failure concur with the strength bond provided by the quasi-static curve (envelope curve), suggesting that the monotonic load-CMOD curve might be used as failure criterion under flexural fatigue loading, at least for the adopted load levels and frequency;
- The S–N curve obtained supports that HPFRC and SFRC pre-cracked specimens have a fatigue endurance limit of 2,000,000 cycle of the order of 66% of $P_{0.5mm}$. Monotonic tests done on run-out specimens showed that the cyclic loads seem to act on the crack opening width, but not on the post-fatigue load capacity, regardless load level;
- Fatigue failure of HPFRC seems to occurs due to a pull-out of micro fibre. In addition, fatigue failure of SFRC seems to occurs due to fibre pull-out and fibre breakage more likely to longer fibre length;
- Probabilistic models were applied and can predict reasonably well the flexural fatigue strength of pre-cracked HPFRC and SFRC, for a desired probability of failure.

Plastic fibre reinforced concrete

- The adopted fatigue evaluation showed that the mechanism of crack evolution over the load cycles was similar in all compositions characterised here, regardless of the fibre type or content. The application of a bespoke fatigue loading regime based on the load achieved in the pre-cracking stage of each specimen is one of the factors responsible for this outcome;
- All specimens show a high initial CMOD increase rate over the load cycles, which gradually reduces, reaching an almost constant increase rate. Such behaviour is related to the crack opening required to activate the plastic fibres in the fracture surface. As more fibres become active with bigger CMOD, the sectional resistant capacity increases above the load applied in the fatigue test, thus leading to the reduction in the CMOD increase rate observed. This trend may change if CMOD values above the corresponding to the maximum post-cracking strength are reached. Above this limit, the sectional resistant capacity would be expected to decrease, approaching the fatigue load again and potentially leading to an increment in the CMOD increase rate. This conjecture could not be confirmed in this study as no specimen reached such CMOD values;

- The residual flexural strength of specimens subjected to the fatigue test follows the curve obtained in the quasi-static control tests of equivalent specimens not subjected to the fatigue test. No clear difference was observed in terms of the fracture and fibre pull-out of specimens subjected to 3PBT flexural tests before and after the load cycles. Both findings indicate that the damage induced by the load cycles is equivalent to that observed in the quasi-static control test for the same CMOD increment, which has important repercussions from the design standpoint. Supposing that the same applies to bigger elements, the resistant capacity of a structure subjected to load cycles could be estimated by assessing numerically the quasi-static flexural response for the same total CMOD. In other words, the designer would only have to estimate the CMOD expected after the load cycles and apply it in a traditional sectional analysis to assess the remaining resistant capacity.

Fatigue conceptual model for crack evolution

- Differences in fatigue mode failure of investigated pre-cracked specimens of FRC are attributable to fibre properties. Stage I can be associated to a "primary" fatigue led by accumulation of plastic deformations of fibres, just found in PFRC, while stage II was observed in PFRC, HPFRC and SFRC and is related to a secondary damage process of fibre pull-out and cementitious matrix failure;
- A fatigue life design limitation is proposed based on applied load: fatigue failure can be expected when the applied load is higher than 60% of f_{r1}. If applied fatigue load is smaller than 60%, the residual strength after cyclic loading can be assumed equal to f_{r3} of the quasi-static curve. Regarding crack opening, if the maximum crack opening expected during service life is smaller than the equivalent CMOD at 80% of total number of cycles the residual strength after cycles can be predicted by the quasi-static monotonic load-displacement curve;
- The numerical model to predict the fatigue behaviour is capable of predicting the CMOD variation over the load cycles of FRC. This model depends on parameters related with the initial damage due to pre-cracking and the incremental damage induced by the cycles, which could vary depending on the loading regime, pre-cracking level and material characteristics. The optimising procedure proposed

using a limited number of initial load cycles can enable a significant reduction in the duration of experimental programs about the fatigue of fibre reinforced concrete.

6.3. Future perspectives

- The investigation conducted in the presented doctoral thesis elucidated significant aspects and allowed to develop a model to predict the fatigue behaviour of fibre reinforced concrete. The investigated concretes respond to applications with relevant structural responsibility. For this reason, other studies are here proposed in order to ensure reliability for predictive capabilities with regard to structural applications. Here, only small beams without traditional reinforcement were investigated, in this regard, real scale specimens and the combination of fibres and rebars are points of further research.

Steel fibre reinforced concrete

- The results obtained in this investigation were based on the small sized specimens, therefore flexural tests on larger and real scale specimens should be carried out in order to evaluate scale effects;
- To ensure reliability of predictive models to be considered in future design codes, other studies performing variable and reversible loading patterns are needed;
- The fatigue evaluation of both SFRC and HPFRC should be extended to other fibre contents and geometry in order analyse the particularities and influence of these variables. Also, a mixture optimization to improve the bond between cementitious matrix and fibres.

Plastic fibre reinforced concrete

- Reversible loading regimes and fatigue tests up to failure providing S-N curves should be performed in order to achieve robust recommendations and parameters to account for the effect of fatigue in the design of PFRC structures;
- Investigate the fatigue response of PFRC considering other fibre types, geometry and volumes to account the effects and influence of these variables. Quasi-static and

cyclic fibre pull-out tests could provide further insight about fibre crack bridging, damage mechanism and stress transfer;

Fatigue conceptual model for crack evolution

- The proposed design limitations and conceptual model considered the investigated concretes, therefore both should be checked for other types of concretes/fibre/fibre content to confirm their consistency;
- Although Model Code 2010 (Fib 2013) provides fatigue design under compression, further research on the flexural response should be done in order to provide reliable models. Also, the provided target reliability index and probability of failure should be calibrated for new peculiarities proposed before.

7. REFERENCES

ACI Committee 215: Considerations for Design of Concrete Structures Subjected To Fatigue Loading. (1974)

AFNOR: No TitleNF P18-710 Avril 2016 Complément national à l'Eurocode 2 - Calcul des structures en béton : règles spécifiques pour les bétons fibrés à ultra-hautes performances (BFUP). (2016)(a)

AFNOR: NF P 18-470 Juillet 2016 - Bétons - Bétons fibrés à ultra hautes performances - Spécification, performance, production et conformité. , Paris (2016)(b)

de Alencar Monteiro, V.M., Lima, L.R., de Andrade Silva, F.: On the mechanical behavior of polypropylene, steel and hybrid fiber reinforced self-consolidating concrete. Constr. Build. Mater. 188, 280–291 (2018). https://doi.org/10.1016/j.conbuildmat.2018.08.103

de Andrade Silva, F., Mobasher, B., Filho, R.D.T.: Fatigue behavior of sisal fiber reinforced cement composites. Mater. Sci. Eng. A. 527, 5507–5513 (2010). https://doi.org/10.1016/j.msea.2010.05.007

Arora, S., Singh, S.P.: Analysis of flexural fatigue failure of concrete made with 100% Coarse Recycled Concrete Aggregates. Constr. Build. Mater. 102, 782–791 (2016). https://doi.org/10.1016/j.conbuildmat.2015.10.098

Banjara, N.K., Ramanjaneyulu, K.: Experimental Investigations and Numerical Simulations on the Flexural Fatigue Behavior of Plain and Fiber-Reinforced Concrete. J. Mater. Civ. Eng. 30, 04018151 (2018). https://doi.org/10.1061/(ASCE)MT.1943-5533.0002351

Bazant, Z., Schell, W.F.: Fatigue Fracture of High-Strength Concrete and Size Effect. ACI Mater. J. 90, 472–478 (1993). https://doi.org/10.14359/3880

Bedi, R., Singh, S.P., Chandra, R.: Design Fatigue Lives of Polypropylene Fibre Reinforced Polymer Concrete Composites. J. Mater. Eng. Struct. 1, 99–109 (2014)

Behfarnia, K., Behravan, A.: Application of high performance polypropylene fibers in concrete lining of water tunnels. Mater. Des. 55, 274–279 (2014). https://doi.org/10.1016/j.matdes.2013.09.075

Belletti, B., Cerioni, R., Meda, A., Plizzari, G.: Design aspects on steel fiber-reinforced concrete pavements. J. Mater. Civ. Eng. 20, 599–607 (2008). https://doi.org/Doi 10.1061/(Asce)0899-1561(2008)20:9(599)

Bentur, A., Mindess, S.: Fibre Reinforced Cementitious Composites. (2007)

Blasón, S., Poveda, E., Ruiz, G., Cifuentes, H., Fernández Canteli, A.: Twofold normalization of the cyclic creep curve of plain and steel-fiber reinforced concrete and its application to predict fatigue failure. Int. J. Fatigue. 120, 215–227 (2019). https://doi.org/10.1016/j.ijfatigue.2018.11.021

Boulekbache, B., Hamrat, M., Chemrouk, M., Amziane, S.: Flexural behaviour of steel fibre-reinforced concrete under cyclic loading. Constr. Build. Mater. 126, 253–262 (2016). https://doi.org/10.1016/j.conbuildmat.2016.09.035

Breña, S.F., Benouaich, M.A., Kreger, M.E., Wood, S.L.: Fatigue tests of reinforced concrete beams strengthened using carbon fiber-reinforced polymer composites. ACI Struct. J. 102, 305–313 (2005). https://doi.org/10.14359/14282

Brugeaud, Y.: Express bridge deck and light duty bridge. In: Toutlemonde, F. and Resplendino, J. (eds.) RILEM-fib-AFGC International Symposium on Ultra-High Performance Fibre-Reinforced Concrete. pp. 389–394. , Marseille, France (2013)

Cachim, P.B., Figueiras, J.A., Pereira, P.A.A.: Fatigue behavior of fiber-reinforced concrete in compression. Cem. Concr. Compos. 24, 211–217 (2002)

Cangiano, S., Plizzari, G.A., Slowik, V.: Experimental investigation into the fatigue crack growth in concrete. In: Fracture Mechanics of Concrete Structures Proceedings FRAMCOS-3. pp. 645–654 (1996)

Carlesso, D.M., de la Fuente, A., Cavalaro, S.H.P.: Fatigue of cracked high performance fiber reinforced concrete subjected to bending. Constr. Build. Mater. 220, 444–455 (2019). https://doi.org/10.1016/j.conbuildmat.2019.06.038

Carloni, C., Subramaniam, K. V.: Investigation of sub-critical fatigue crack growth in FRP/concrete cohesive interface using digital image analysis. Compos. Part B Eng. 51, 35–43 (2013). https://doi.org/10.1016/j.compositesb.2013.02.015

Cavalaro, S.H.P., Aguado, A.: Intrinsic scatter of FRC: an alternative philosophy to estimate characteristic values. Mater. Struct. Constr. 48, 3537–3555 (2015). https://doi.org/10.1617/s11527-014-0420-6

Chanvillard, G., Pimienta, P., Pineaud, A., Rivillon, P.: Fatigue flexural behaviour of pre-cracked specimens of Ductal® UHPFRC. In: Di Prisco, M., Felicetti, R., and Plizzari, G.A. (eds.) 6th International RILEM Symposium on Fibre-Reinforced Concretes (BEFIB'2004). p. 16 (2004)

Cifuentes, H., García, F., Maeso, O., Medina, F.: Influence of the properties of polypropylene fibres on the fracture behaviour of low-, normal- and high-strength FRC. Constr. Build. Mater. 45, 130–137 (2013). https://doi.org/10.1016/j.conbuildmat.2013.03.098

Comité Euro-international du Béton, C.: Fatigue of Concrete Structures: State of the Art Report. Bull. d'information / Com. Euro-international du Beton, CEB. 300 (1988)

Conforti, A., Tiberti, G., Plizzari, G.A., Caratelli, A., Meda, A.: Precast tunnel segments

reinforced by macro-synthetic fibers. Tunn. Undergr. Sp. Technol. 63, 1–11 (2017). https://doi.org/10.1016/j.tust.2016.12.005

Dao, K.C.: Fatigue failure mechanisms in polymer composites. Polym. Compos. 3, 12–17 (1982). https://doi.org/10.1002/pc.750030104

Destrebecq, J.-F.: Cyclic and Dynamic Loading Fatigue of Structural Concrete. In: Mechanical Behavior of Concrete. pp. 185–224. John Wiley & Sons, Inc., Hoboken, NJ USA (2013)

DNV GL AS: Standard DNVGL-ST-0126 - Support structures for wind turbines. (2016)

DNV GL AS: Standard DNVGL-ST-C502 - Offshore concrete structures. (2017)

Do, M.-T., Chaallal, O., Aïtcin, P.-C.: Fatigue Behavior of High-Performance Concrete. J. Mater. Civ. Eng. 5, 96–111 (1993). https://doi.org/10.1061/(ASCE)0899-1561(1993)5:1(96)

EN1992-1-1: Eurocode 2: Design of concrete structures - Part 1-1 : General rules and rules for buildings Eurocode. (2005)

Farhat, F.A., Nicolaides, D., Kanellopoulos, A., Karihaloo, B.L.: High performance fibre-reinforced cementitious composite (CARDIFRC) - Performance and application to retrofitting. Eng. Fract. Mech. 74, 151–167 (2007). https://doi.org/10.1016/j.engfracmech.2006.01.023

Federation Internacionale du beton, fib: Bond of reinforcement in concrete - State-of-the-art report. (2000)

Fib: International Federation for Structural Concrete. Constitutive modelling of high strength/high performance concrete. , Germany (2008)

Fib: International Federation for Structural Concrete fib Model Code for Concrete Structures 2010. , Germany (2013)

Freudenthal, A.M., Gumbel, E.J.: On the Statistical Interpretation of Fatigue Tests. Proc. R. Soc. A Math. Phys. Eng. Sci. 216, 309–332 (1953). https://doi.org/10.1098/rspa.1953.0024

Ganesan, N., Bharati Raj, J., Shashikala, A.P.: Flexural fatigue behavior of self compacting rubberized concrete. Constr. Build. Mater. 44, 7–14 (2013). https://doi.org/10.1016/j.conbuildmat.2013.02.077

Germano, F., Tiberti, G., Plizzari, G.: Post-peak fatigue performance of steel fiber reinforced concrete under flexure. Mater. Struct. 49, 4229–4245 (2016). https://doi.org/10.1617/s11527-015-0783-3

Goel, S., Singh, S.P., Singh, P.: Fatigue analysis of plain and fiber-reinforced self-consolidating concrete. ACI Mater. J. 109, 573–582 (2012)(a)

Goel, S., Singh, S.P., Singh, P.: Flexural fatigue strength and failure probability of Self Compacting Fibre Reinforced Concrete beams. Eng. Struct. 40, 131–140 (2012)(b). https://doi.org/10.1016/j.engstruct.2012.02.035

González, D.C., Moradillo, R., Mínguez, J., Martínez, J.A., Vicente, M.A.: Postcracking residual strengths of fiber-reinforced high-performance concrete after cyclic loading. Struct. Concr. 19, 340–351 (2018). https://doi.org/10.1002/suco.201600102

Graeff, A.G., Pilakoutas, K., Neocleous, K., Peres, M.V.N.N.: Fatigue resistance and cracking mechanism of concrete pavements reinforced with recycled steel fibres recovered from post-consumer tyres. Eng. Struct. 45, 385–395 (2012). https://doi.org/10.1016/j.engstruct.2012.06.030

Graybeal, B.: UHPC in the US Highway Infrastructure: experience and outlook. In:

Toutlemonde, F. and Resplendino, J. (eds.) RILEM-fib-AFGC International Symposium on Ultra-High Performance Fibre-Reinforced Concrete. pp. 361–370. , Marseille, France (2013)

Gylltoft, K.: A fracture mechanics model for fatigue in concrete. Matériaux Constr. 17, 55–58 (1984). https://doi.org/10.1007/BF02474057

Holmen, J.O.: Fatigue design evaluation of offshore concrete structures. Matériaux Constr. 17, 39–42 (1984). https://doi.org/10.1007/BF02474054

Huang, B.T., Li, Q.H., Xu, S.L., Liu, W., Wang, H.T.: Fatigue deformation behavior and fiber failure mechanism of ultra-high toughness cementitious composites in compression. Mater. Des. 157, 457–468 (2018). https://doi.org/10.1016/j.matdes.2018.08.002

Isojeh, B.: Fatigue Damage Analysis of Reinforced. (2017)

Isojeh, B., El-Zeghayar, M., Vecchio, F.J.: Concrete Damage under Fatigue Loading in Uniaxial Compression. ACI Mater. J. 114, (2017). https://doi.org/10.14359/51689477

Japan Society of Civil Engineers: Recommendations for Design and Construction of High Performance Fiber Reinforced Cement Composites with Multiple Fine Cracks (HPFRCC). Concr. Eng. Ser. 82, Testing Method 6-10 (2008)

Johnston, C.D., Zemp, R.W.: Flexural Fatigue Performance of Steel Fiber Reinforced Concrete--Influence of Fiber Content, Aspect Ratio, and Type. ACI Mater. J. 88, 374–383 (1991). https://doi.org/10.14359/1875

Kessler-Kramer, C., Mechtcherine, V., Müller, H.S.: Fatigue behaviour of concrete in tension. In: de Borst, R., Mazars, J., Pijaudier-Cabot, G., and van Mier, J.G.M. (eds.) Proceedings of the fourth international confere on fracture mechanics of concrete and concrete structures. pp. 573–578. , Cachan, France (2001)

Kim, J.-K., Kim, Y.-Y.: Experimental study of the fatigue behavior of high strength concrete. Cem. Concr. Res. 26, 1513–1523 (1996). https://doi.org/10.1016/0008-8846(96)00151-2

Kolluru, S. V., O'Neil, E.F., Popovics, J.S., Shah, S.P.: Crack Propagation in Flexural Fatigue of Concrete. J. Eng. Mech. 126, 891–898 (2000). https://doi.org/10.1061/(ASCE)0733-9399(2000)126:9(891)

Korte, S., Boel, V., De Corte, W., De Schutter, G.: Static and fatigue fracture mechanics properties of self-compacting concrete using three-point bending tests and wedge-splitting tests. Constr. Build. Mater. 57, 1–8 (2014). https://doi.org/10.1016/j.conbuildmat.2014.01.090

de la Fuente, A., Blanco, A., Armengou, J., Aguado, A.: Sustainability based-approach to determine the concrete type and reinforcement configuration of TBM tunnels linings. Case study: Extension line to Barcelona Airport T1. Tunn. Undergr. Sp. Technol. 61, 179–188 (2017). https://doi.org/10.1016/j.tust.2016.10.008

De La Fuente, A., Escariz, R.C., De Figueiredo, A.D., Aguado, A.: Design of macro-synthetic fibre reinforced concrete pipes. Constr. Build. Mater. 43, 523–532 (2013). https://doi.org/10.1016/j.conbuildmat.2013.02.036

De La Fuente, A., Pons, O., Josa, A., Aguado, A.: Multi-criteria decision making in the sustainability assessment of sewerage pipe systems. J. Clean. Prod. 112, 4762–4770 (2016). https://doi.org/10.1016/j.jclepro.2015.07.002

Lappa, E.: High Strength Fibre Reinforced Concrete Static and fatigue behaviour in

bending, (2007)

Lappa, E., Braam, R., Walraven, J.: Fatigue Failure Properties of High and Ultra High Strength Fibre Reinforced Concrete. In: Fischer, G. and Li, V.C. (eds.) 6th International PhD Symposium in Civil Engineering. pp. 86–87 (2006)

Lee, M.K., Barr, B.I.G.: An overview of the fatigue behaviour of plain and fibre reinforced concrete. Cem. Concr. Compos. 26, 299–305 (2004). https://doi.org/10.1016/S0958-9465(02)00139-7

Lenschow, R.: Long term random dynamic loading of concrete structures. Matériaux Constr. 17, 1–28 (1984). https://doi.org/10.1007/BF02474050

Leung, C.K.Y., Cheung, Y.N., Zhang, J.: Fatigue enhancement of concrete beam with ECC layer. Cem. Concr. Res. 37, 743–750 (2007). https://doi.org/10.1016/j.cemconres.2007.01.015

Li, D., Huang, P., Guo, X., Zheng, X., Lin, J., Chen, Z.: Fatigue crack propagation behavior of RC beams strengthened with CFRP under cyclic bending loads. Fatigue Fract. Eng. Mater. Struct. 41, 212–222 (2018). https://doi.org/10.1111/ffe.12673

Li, H., Zhang, M. hua, Ou, J. ping: Flexural fatigue performance of concrete containing nano-particles for pavement. Int. J. Fatigue. 29, 1292–1301 (2007). https://doi.org/10.1016/j.ijfatigue.2006.10.004

Li, V.C., Matsumoto, T.: Fatigue crack growth analysis of fiber reinforced concrete with effect of interfacial bond degradation. Cem. Concr. Compos. 20, 339–351 (1998). https://doi.org/10.1016/S0958-9465(98)00010-9

Lohaus, L., Oneschkow, N., Wefer, M.: Design model for the fatigue behaviour of normal-strength, high-strength and ultra-high-strength concrete. Struct. Concr. 13, 182–192 (2012). https://doi.org/10.1002/suco.201100054

López-Manchado, M.A., Arroyo, M.: Thermal and dynamic mechanical properties of polypropylene and short organic fiber composites. Polymer (Guildf). 41, 7761–7767 (2000). https://doi.org/10.1016/S0032-3861(00)00152-X

Makita, T., Brühwiler, E.: Tensile fatigue behaviour of ultra-high performance fibre reinforced concrete (UHPFRC). Mater. Struct. 47, 475–491 (2014). https://doi.org/10.1617/s11527-013-0073-x

Malek, A., Scott, A., Pampanin, S., MacRae, G., Marx, S.: Residual Capacity and Permeability-Based Damage Assessment of Concrete under Low-Cycle Fatigue. J. Mater. Civ. Eng. 30, 04018081 (2018). https://doi.org/10.1061/(ASCE)MT.1943-5533.0002248

Manchado, M.A.L., Valentini, L., Biagiotti, J., Kenny, J.M.: Thermal and mechanical properties of single-walled carbon nanotubes-polypropylene composites prepared by melt processing. Carbon N. Y. 43, 1499–1505 (2005). https://doi.org/10.1016/j.carbon.2005.01.031

Matsumoto, T.: Effect of fiber fatigue rupture on monotonic and cyclic crack bridging laws in discontinuous fiber reinforced composites. J. Appl. Mech. 11, 891–902 (2008). https://doi.org/10.2208/journalam.11.891

McCall, J.T.: Probability of fatigue failure of plain concrete. J. Proc. 55, 233–244 (1958)

Medeiros, A., Zhang, X., Ruiz, G., Yu, R.C., Velasco, M.D.S.L.: Effect of the loading frequency on the compressive fatigue behavior of plain and fiber reinforced concrete. Int. J. Fatigue. 70, 342–350 (2015). https://doi.org/10.1016/j.ijfatigue.2014.08.005

Mohamadi, M.R., Mohandesi, J.A., Homayonifar, M.: Fatigue behavior of polypropylene fiber reinforced concrete under constant and variable amplitude loading. J. Compos. Mater. 47, 3331–3342 (2013). https://doi.org/10.1177/0021998312464083

Mohammadi, Y., Kaushik, S.K.: Flexural Fatigue-Life Distributions of Plain and Fibrous Concrete at Various Stress Levels. J. Mater. Civ. Eng. 17, 650–658 (2005). https://doi.org/10.1061/(ASCE)0899-1561(2005)17:6(650)

Morris, A.D., Garrett, G.G.: A comparative study of the static and fatigue behaviour of plain and steel fibre reinforced mortar in compression and direct tension. Int. J. Cem. Compos. Light. Concr. 3, 73–91 (1981). https://doi.org/10.1016/0262-5075(81)90002-6

Mu, B., Subramaniam, K. V., Shah, S.P.: Failure Mechanism of Concrete under Fatigue Compressive Load. J. Mater. Civ. Eng. 16, 566–572 (2004). https://doi.org/10.1061/(asce)0899-1561(2004)16:6(566)

Muliana, A.: Nonlinear viscoelastic-degradation model for polymeric based materials. Int. J. Solids Struct. 51, 122–132 (2014). https://doi.org/10.1016/j.ijsolstr.2013.09.016

Müller, S., Mechtcherine, V.: Fatigue behaviour of strain-hardening cement-based composites (SHCC). Cem. Concr. Res. 92, 75–83 (2017). https://doi.org/10.1016/j.cemconres.2016.11.003

Naaman, A.E., Hammoud, H.: Fatigue characteristics of high performance fiber-reinforced concrete. Cem. Concr. Compos. 20, 353–363 (1998). https://doi.org/10.1016/S0958-9465(98)00004-3

Naaman, A.E., Reinhardt, H.W.: Proposed classification of HPFRC composites based on their tensile response. Mater. Struct. 39, 547–555 (2007). https://doi.org/10.1617/s11527-006-9103-2

Nagabhushanam, M., Ramakrishnan, V., Vondran, G.: Fatigue Strength of Fibrillated Polypropylene Fiber Reinforced Concretes. Transp. Res. Rec. 1226, 36–47 (1989)

Nanni, A.: Fatigue behaviour of steel fiber reinforced concrete. Cem. Concr. Compos. 13, 239–245 (1991). https://doi.org/10.1016/0958-9465(91)90029-H

Nussbaumer, A., Borges, L., Davaine, L.: Fatigue Design of Steel and Composite Structures. Wiley-VCH Verlag GmbH & Co. KGaA, Weinheim, Germany (2018)

Oh, B.H.: Fatigue Analysis of Plain Concrete in Flexure. J. Struct. Eng. 112, 273–288 (1986). https://doi.org/10.1061/(ASCE)0733-9445(1986)112:2(273)

Oh, B.H., Kim, J.C., Choi, Y.C.: Fracture behavior of concrete members reinforced with structural synthetic fibers. Eng. Fract. Mech. 74, 243–257 (2007). https://doi.org/10.1016/j.engfracmech.2006.01.032

Pająk, M., Ponikiewski, T.: Flexural behavior of self-compacting concrete reinforced with different types of steel fibers. Constr. Build. Mater. 47, 397–408 (2013). https://doi.org/10.1016/j.conbuildmat.2013.05.072

Parant, E., Rossi, P., Boulay, C.: Fatigue behavior of a multi-scale cement composite. Cem. Concr. Res. 37, 264–269 (2007). https://doi.org/10.1016/j.cemconres.2006.04.006

Plizzari, G.A., Cangiano, S., Alleruzzo, S.: The fatigue behaviour of cracked concrete. Fatigue Fract. Eng. Mater. Struct. 20, 1195–1206 (1997). https://doi.org/10.1111/j.1460-2695.1997.tb00323.x

di Prisco, M., Plizzari, G., Vandewalle, L.: Fibre reinforced concrete: new design perspectives. Mater. Struct. 42, 1261–1281 (2009). https://doi.org/10.1617/s11527-009-9529-4

Di Prisco, M., Plizzari, G.A.: Preface. In: Di Prisco, M., Felicetti, R., and Plizzari, G.A. (eds.) 6th International RILEM Symposium on Fibre-Reinforced Concretes (BEFIB'2004). p. 1544 (2004)

Qiu, J., Yang, E.-H.: Study on fatigue failure of polymeric fiber-reinforced strain-hardening cementitious composites. In: 3rd International Rilem Conference on Strain Hardening Cementitious CompositesAt: Dordrecht, Netherlands. pp. 145–153 (2014)

Ramakrishnan, V., Mayer, C., Naaman, A.E.: Cyclic behaviour, fatigue strength, endurance limit and models for fatigue behavior of FRC. Chapter. 4, 101–148 (2014)

Ramakrishnan, V., Sivakumar, C.: Constitutive model for prediction of flexural fatigue life and performance characteristics of polyolefin fiber reinforced concrete. In: Reinhardt, H.W. and Naaman, A.E. (eds.) International RILEM Conference on High Performance Fiber Reinforced Cement Composites (HPFRCC 3). pp. 299–320. , Mainz (1999)

Ramakrishnan, V., Wu, G.Y., Hosalli, G.: Flexural Fatigue Strength, Endurance Limit, and Impact Strength of Fiber Reinforced Concretes. Transp. Res. Rec. J. Transp. Res. Board. 1226, 17–24 (1989)

Reinhardt, H.W., Cornelissen, H.A.W.: Post-peak cyclic behaviour of concrete in uniaxial tensile and alternating tensile and compressive loading. Cem. Concr. Res. 14, 263–270 (1984). https://doi.org/10.1016/0008-8846(84)90113-3

Russell, H.G., Graybeal, B.A.: Ultra-High Performance Concrete: A State-of-the-Art Report for the Bridge Community. (2013)

Samal, S.K., Mohanty, S., Nayak, S.K.: Polypropylene—Bamboo/Glass Fiber Hybrid Composites: Fabrication and Analysis of Mechanical, Morphological, Thermal, and Dynamic Mechanical Behavior. J. Reinf. Plast. Compos. 28, 2729–2747 (2009). https://doi.org/10.1177/0731684408093451

Schmidt, M., Leutbecher, T., Piotrowski, S., Wiens, U.: The German Guideline for Ultra-High Performance. In: Toutlemonde, F. and Resplendino, J. (eds.) UHPFRC 2017 Designing and Building with UHPFRC: New large-scale implementations, recent technical advances, experience and standards. pp. 545–554. , Montpellier, France (2017)

Shah, S.P.: Predictions of comulative damage for concrete and reinforced concrete. Matériaux Constr. 17, 65–68 (1984). https://doi.org/10.1007/BF02474059

Shen, S., Carpenter, S.: Application of the Dissipated Energy Concept in Fatigue Endurance Limit Testing. Transp. Res. Rec. J. Transp. Res. Board. 1929, 165–173 (2007). https://doi.org/10.3141/1929-20

Singh, H.: Design of SFRC Flexural Members. In: International Conference on Structural Engineering and Construction Management (ICSECM). pp. 59–108 (2017)

Singh, S.P., Kaushik, S.K.: Flexural Fatigue Life Distributions and Failure Probability of Steel Fibrous Concrete. ACI Mater. J. 97, 658–667 (2000)

Singh, S.P., Kaushik, S.K.: Flexural Fatigue Analysis of Steel Fiber-Reinforced Concrete. ACI Mater. J. 98, 306–312 (2001)

Singh, S.P., Kaushik, S.K.: Fatigue strength of steel fibre reinforced concrete in flexure.

Cem. Concr. Compos. 25, 779–786 (2003). https://doi.org/10.1016/S0958-9465(02)00102-6

Singh, S.P., Mohammadi, Y., Madan, S.K.: Flexural fatigue strength of steel fibrous concrete containing mixed steel fibres. J. Zhejiang Univ. A. 7, 1329–1335 (2006). https://doi.org/10.1631/jzus.2006.A1329

Singh, S.P., Singh, B., Kaushik, S.K.: Probability of fatigue failure of steel fibrous concrete. Mag. Concr. Res. 57, 65–72 (2005). https://doi.org/10.1680/macr.2005.57.2.65

Sohel, K.M.A., Al-Jabri, K., Zhang, M.H., Liew, J.Y.R.: Flexural fatigue behavior of ultra-lightweight cement composite and high strength lightweight aggregate concrete. Constr. Build. Mater. 173, 90–100 (2018). https://doi.org/10.1016/j.conbuildmat.2018.03.276

Son, J., Gardner, D.J., O'Neill, S., Metaxas, C.: Understanding the viscoelastic properties of extruded polypropylene wood plastic composites. J. Appl. Polym. Sci. 89, 1638–1644 (2003). https://doi.org/10.1002/app.12372

Spadea, G., Bencardino, F.: Behavior of Fiber-Reinforced Concrete Beams. J. Struct. Eng. 123, 660–668 (1997)

Sparks, P.R., Menzies, J.B.: The effect of rate of loading upon the static and fatigue strengths of plain concrete in compression. Mag. Concr. Res. 25, 73–80 (1973). https://doi.org/10.1680/macr.1973.25.83.73

Sritharan, S., Schmitz, G.M.: Design of Tall Wind Turbine Towers Utilizing UHPC. In: Toutlemonde, F. and Resplendino, J. (eds.) RILEM-fib-AFGC International Symposium on Ultra-High Performance Fibre-Reinforced Concrete. pp. 433–442. , Marseille, France (2013)

Standard, E.: Eurocode - Basis of structural design - EN 1990:2002+A1 European Standards, (2008)

Suthiwarapirak, P., Matsumoto, T., Kanda, T.: Flexural fatigue failure characteristics of an engineered cementitious composite and polymer cement mortars. Doboku Gakkai Ronbunshu. 718, 121–134 (2002). https://doi.org/10.2208/jscej.2002.718_121

Tajvidi, M., Falk, R.H., Hermanson, J.C.: Effect of natural fibers on thermal and mechanical properties of natural fiber polypropylene composites studied by dynamic mechanical analysis. J. Appl. Polym. Sci. 101, 4341–4349 (2006). https://doi.org/10.1002/app.24289

Tanaka, S., Ichikawa, M.: Approximate formula of coefficient of variation for Weibull distribution. Reliab. Eng. 4, 141–143 (1983). https://doi.org/10.1016/0143-8174(83)90047-1

Tapsoba, N., Citek, D., Dobrusky, S., Kolisko, J.: Fatigue Behavior of Ultra-High Performance Concrete (UHPC) Under Compressive Loading. In: Toutlemonde, F. and Resplendino, J. (eds.) HPFRC 2017 Designing and Building with UHPFRC: New large-scale implementations, recent technical advances, experience and standards. pp. 291–300. , Montpellier, France (2017)

Tarifa, M., Ruiz, G., Poveda, E., Zhang, X., Vicente, M.A., González, D.C.: Effect of uncertainty on load position in the fatigue life of steel-fiber reinforced concrete under compression. Mater. Struct. 51, 31 (2018). https://doi.org/10.1617/s11527-018-1155-6

Tarifa, M., Zhang, X., Ruiz, G., Poveda, E.: Full-scale fatigue tests of precast reinforced concrete slabs for railway tracks. Eng. Struct. 100, 610–621 (2015). https://doi.org/10.1016/j.engstruct.2015.06.016

Urban, S., Strauss, A., Schütz, R., Bergmeister, K., Dehlinger, C.: Dynamically loaded concrete structures - monitoring-based assessment of the real degree of fatigue deterioration. Struct. Concr. 15, 530–542 (2014). https://doi.org/10.1002/suco.201300095

Waagaard, K.: Fatigue strength evaluation of offshore concrete structures. IABSE Proc. 6, 97–115 (1982). https://doi.org/http://doi.org/10.5169/seals-36662 Nutzungsbedingungen

Xu, L., Li, B., Ding, X., Chi, Y., Li, C., Huang, B., Shi, Y.: Experimental Investigation on Damage Behavior of Polypropylene Fiber Reinforced Concrete under Compression. Int. J. Concr. Struct. Mater. 12, 68 (2018). https://doi.org/10.1186/s40069-018-0302-3

Yoo, D.Y., Banthia, N.: Mechanical and structural behaviors of ultra-high-performance fiber-reinforced concrete subjected to impact and blast. Constr. Build. Mater. 149, 416–431 (2017). https://doi.org/10.1016/j.conbuildmat.2017.05.136

Zhang, B., Phillips, D. V., Wu, K.: Effects of loading frequency and stress reversal on fatigue life of plain concrete. Mag. Concr. Res. 48, 361–375 (1996). https://doi.org/10.1680/macr.1996.48.177.361

Zhang, B., Wu, K.: Residual fatigue strength and stiffness of ordinary concrete under bending. Cem. Concr. Res. 27, 115–126 (1997). https://doi.org/10.1016/S0008-8846(96)00183-4

Zhang, H., Tian, K.: Properties and mechanism on flexural fatigue of polypropylene fiber reinforced concrete containing slag. J. Wuhan Univ. Technol. Mater. Sci. Ed. 26, 533–540 (2011). https://doi.org/10.1007/s11595-011-0263-8

Zhang, J., Stang, H., Li, V.C.: Fatigue life prediction of fiber reinforced concrete under flexural load. Int. J. Fatigue. 21, 1033–1049 (1999). https://doi.org/10.1016/S0142-1123(99)00093-6

Zhang, J., Stang, H., Li, V.C.: Experimental Study on Crack Bridging in FRC under Uniaxial Fatigue Tension. J. Mater. Civ. Eng. 12, 66–73 (2000). https://doi.org/10.1061/(ASCE)0899-1561(2000)12:1(66)

8. PUBLICATIONS

CARLESSO, D. M.; CAVALARO, S. H. P.; ANTEQUERA, A. F.; REPETTE, W. L.. Estudo do comportamento de concreto de ultra-alto desempenho reforçado com fibras à fadiga por flexão. In: 59º Congresso Brasileiro do Concreto, 2017, Bento Gonçalves. Anais do 59º Congresso Brasileiro do Concreto, 2017.

CARLESSO, D. M.; ANTEQUERA, A. F.; CAVALARO, S. H. P.; REPETTE, W. L.. Flexural fatigue performance of plastic fiber and steel microfiber in reinforced concrete. In: 3rd FRC International Workshop: Fibre Reinforced Concrete: from Design to Structural Applications, 2018, Desenzano del Garda. ACI - *fib* - RILEM Joint Workshop: Fibre Reinforced Concrete: from Design to Structural Applications Joint ACI-fib-RILEM International Workshop, 2018.

CARLESSO, D. M.; DE LA FUENTE, A.; CAVALARO, S. H. P. Fatigue of cracked high performance fiber reinforced concrete subjected to bending. CONSTRUCTION AND BUILDING MATERIALS, v. 220, p. 444-455, 2019.